

DETERMINATION OF SNOW WATER EQUIVALENT OVER EASTERN  
PART OF TURKEY USING PASSIVE MICROWAVE DATA

A THESIS SUBMITTED TO  
THE GRADUATE SCHOOL OF NATURAL AND APPLIED SCIENCES  
OF  
MIDDLE EAST TECHNICAL UNIVERSITY

BY

ÖZGÜR BEŞER

IN PARTIAL FULFILLMENT OF THE REQUIREMENTS  
FOR  
THE DEGREE OF DOCTOR OF PHILOSOPHY  
IN  
CIVIL ENGINEERING

AUGUST 2011

Approval of the thesis:

**DETERMINATION OF SNOW WATER EQUIVALENT OVER EASTERN PART  
OF TURKEY USING PASSIVE MICROWAVE DATA**

submitted by **ÖZGÜR BEŞER** in partial fulfillment of the requirements for the degree of **Doctor of Philosophy in Civil Engineering Department, Middle East Technical University** by,

Prof. Dr. Canan Özgen \_\_\_\_\_  
Dean, Graduate School of **Natural and Applied Sciences**

Prof. Dr. Güney Özcebe \_\_\_\_\_  
Head of Department, **Civil Engineering Dept., METU**

Prof. Dr. Ali Ünal Şorman \_\_\_\_\_  
Supervisor, **Civil Engineering Dept., METU**

**Examining Committee Members:**

Prof. Dr. Vedat Toprak \_\_\_\_\_  
Geological Engineering Dept., METU

Prof. Dr. Ali Ünal Şorman \_\_\_\_\_  
Civil Engineering Dept., METU

Prof. Dr. İbrahim Gürer \_\_\_\_\_  
Civil Engineering Dept., Gazi University

Assoc. Prof. Dr. İsmail Yücel \_\_\_\_\_  
Civil Engineering Dept., METU

Assoc. Prof. Dr. Sevda Zuhale Akyurek \_\_\_\_\_  
Civil Engineering Dept., METU

**Date:** 02.08.2011

**I hereby declare that all information in this document has been obtained and presented in accordance with academic rules and ethical conduct. I also declare that, as required by these rules and conduct, I have fully cited and referenced all material and results that are not original to this work.**

Name, Last Name : Özgür Beşer

Signature :

## **ABSTRACT**

### **DETERMINATION OF SNOW WATER EQUIVALENT OVER EASTERN PART OF TURKEY USING PASSIVE MICROWAVE DATA**

Beşer, Özgür

Ph.D., Department of Civil Engineering

Supervisor: Prof. Dr. A. Ünal Şorman

August 2011, 100 pages

The assimilation process to produce daily Snow Water Equivalent (SWE) maps is modified by using Helsinki University of Technology (HUT) snow emission model and AMSR-E passive microwave data. The characteristics of HUT emission model is analyzed in-depth and discussed with respects to the extinction coefficient function. A new extinction coefficient function for the HUT model is proposed for snow over mountainous areas. Performance of the modified model is checked against original and other modified cases against ground truth data covering 2003-2007 winter periods. A new approach to calculate grain size and density is integrated inside the developed data assimilation process. An extensive validation is successfully carried out by means of snow data measured at ground stations during 2008-2010 winter periods. Validation results were less satisfactory for SWE smaller than 75.0 mm and greater than 200.0 mm. Overestimation is especially observed for stations located below 1750.0 m elevation where SWE is less than 75.0 mm. Applied methodology is fine tuned to improve its performance for shallow snow depths observed below 1750 m elevation using a relationship that integrates 10.7 GHz channel data. But an underestimation for SWE greater than 150 mm could not be

resolved due to microwave signal saturation that is expected in dense snowpack.

**Keywords:** Snow water equivalent, HUT, AMSR-E, microwave, remote sensing

## ÖZ

### TÜRKİYE'NİN DOĞUSUNDA KAR-SU EŞDEĞERİNİN PASİF MİKRODALGA UYDU VERİLERİ İLE HESAPLANMASI

Beşer, Özgür

Doktora, İnşaat Mühendisliği Bölümü

Tez Yöneticisi: Prof. Dr. A. Ünal Şorman

Ağustos 2011, 100 sayfa

Günlük Kar-su eşdeğeri (KSE) haritalarının üretimi için HUT modeli ve AMSR-E pasif mikrodalga verilerini kullanan bir asimilasyon yöntemi geliştirilmiştir. HUT modeli derinlemesine analiz edilmiş ve tükenme katsayısı fonksiyonu özelinde tartışılmıştır. Dağlık alanlarda gözlenen kar örtüsünü daha iyi modelleyebilmek adına HUT modeli için yeni bir tükenme katsayısı fonksiyonu önerilmiştir. Önerilen değişiklik ile model performansı orijinal ve diğer değiştirilmiş durumlara karşı 2003-2007 kış dönemlerine ait yer kar ölçümleri kullanılarak kontrol edilmiştir. Geliştirilen asimilasyon yöntemine kar dane boyutu ve kar yoğunluğu hesaplamaları ile ilgili yeni bir yaklaşım tümelştirilmiştir. Hesaplanan KSE nin geçerliliği 2008-2010 kış sezonunda yapılmış yersel kar ölçümleri ile kontrol edilmiştir. KSE nin 75.0 mm den küçük ve 200.0 mm den büyük olduğu durumlar için elde edilen geçerlilik sonuçları tatmin edici olmamıştır. Özellikle 1750.0 m kotunun altında yer alan istasyonlarda KSE genellikle 75.0 mm den düşüktür ve bu istasyonlar için daha yüksek değerlerin hesaplandığı gözlenmiştir. Geliştirilen yöntem özellikle 1750.0 m kotunun altında gözlenen sığ kar derinliklerini daha iyi modelleyebilmek için 10.7 GHz kanal verilerini de içeren yeni bir ilişki ile iyileştirilmiştir. Fakat KSE nin 150 mm den daha

büyük olduđu durumlar için herhangi bir iyileştirme pasif mikrodalga verilerinin yüksek kar derinliklerinde doygunlaşması nedeni ile sağlanamamıştır.

**Anahtar Kelimeler:** Kar-su eşdeđeri, HUT, AMSR-E, mikrodalga, uzaktan algılama

To my lovely family Sibel and Can



## ACKNOWLEDGEMENT

I would like to express my endless gratitude to Prof. Dr. A. Ünal Şorman who helped me in selecting this topic, for supervising me throughout the study, for his innovative approach to each detail in this thesis and for his friendship throughout the study.

My deepest thanks go to Assoc. Prof. Dr. Zuhale Akyürek for the valuable hours she has spent for advising, encouraging and guiding me. She is not only a perfect scientist but also a sage for me and for my family in our social life.

I would like to thank to Prof. Dr. Jouni Pulliainen for providing original HUT model source code.

I would also like to thank to my partner Dr. Orhan Gökdemir for his patience and his never-ending support throughout all this study.

I also wish to express my gratuities to my friend Serdar Sürer for his modesty to my all attitudes during his help.

At last but not least I would like to thank my beloved father, mother and sisters who shaped my life and who never gave up believing me and my work.

# TABLE OF CONTENTS

<b>ABSTRACT .....</b>	<b>iv</b>
<b>ÖZ .....</b>	<b>vi</b>
<b>ACKNOWLEDGEMENTS .....</b>	<b>ix</b>
<b>TABLE OF CONTENTS .....</b>	<b>x</b>
<b>LIST OF FIGURES .....</b>	<b>xii</b>
<b>LIST OF TABLES.....</b>	<b>xvi</b>

## CHAPTERS

<b>1. INTRODUCTION .....</b>	<b>1</b>
<b>1.1 General .....</b>	<b>1</b>
<b>1.2 Objective .....</b>	<b>3</b>
<b>1.3 Thesis Outline.....</b>	<b>4</b>
<b>2. USING PASSIVE MICROWAVE REMOTE SENSING TO MONITOR     SWE .....</b>	<b>6</b>
<b>2.1. Microwave Radiation From Natural Surfaces.....</b>	<b>6</b>
<b>2.2. Emission Behavior of Snow .....</b>	<b>8</b>
<b>2.3. Passive Microwave Systems .....</b>	<b>18</b>
<b>2.4. Microwave Emission Models .....</b>	<b>22</b>
<b>3. HUT SNOW EMISSION MODEL.....</b>	<b>27</b>
<b>3.1. Description of HUT Model.....</b>	<b>27</b>
3.1.1. Emission from a Homogenous Snowpack.....	27
3.1.2 Spaceborne Observed Scene Brightness Temperature .....	30
<b>3.2. Sensitivity Analysis of HUT Model.....</b>	<b>34</b>
<b>3.3. Improvement of HUT Model .....</b>	<b>43</b>
<b>3.4. Performance of Modified HUT Model .....</b>	<b>49</b>
3.4.1 Ground Snow Data Description.....	49

3.4.2 Satellite Data Description .....	50
3.4.3 Comparison Results of Original and Improved Models .....	51
<b>4. DEVELOPMENT OF SNOW WATER EQUIVALENT RETRIEVAL</b>	
<b>METHODOLOGY .....</b>	<b>55</b>
<b>4.1 Density and Grain Size Retrieval Approach .....</b>	<b>55</b>
<b>4.2. Description of Daily SWE Retrieval Methodology .....</b>	<b>59</b>
4.2.1 Satellite Data .....	59
4.2.2 Daily SWE Retrieval Methodology .....	60
<b>4.3. Validation of Developed Methodology .....</b>	<b>63</b>
4.3.1 Description of Ground Snow Data .....	63
4.3.2 Validation Methodology .....	65
4.3.3 Validation Results .....	67
<b>5. DISCUSSION OF THE RESULTS .....</b>	<b>79</b>
<b>5.1. Fine Tuning of SWE Retrieval Methodology .....</b>	<b>79</b>
<b>5.2. Validation Results of Fine Tuned Methodology .....</b>	<b>83</b>
<b>6. CONCLUSIONS AND RECOMMANDATIONS .....</b>	<b>90</b>
<b>REFERENCES .....</b>	<b>93</b>
<b>CURRICULUM VITAE .....</b>	<b>99</b>

## LIST OF FIGURES

### FIGURES

Figure 2.1 Calculated microwave spectra of the absorption, scattering, and extinction coefficients of dry snow containing ice crystals 0.5 mm in radius. (adopted from Ulaby et al.,1990) .....	9
Figure 2.2 Calculated microwave spectra of the penetration depth of snow (Ulaby et al.,1990) .....	10
Figure 2.3 Measured values of $\kappa_e$ with the curves calculated for $\rho_s=0.24\text{g/cm}^3$ , $r = 0.5$ mm at 4, 16 and 37 GHz (adopted from Ulaby et al.,1990).....	11
Figure 2.4 Variation of snow albedo with liquid water content at 4 GHz, 10 GHz, 37 GHz frequencies. (adopted from Ulaby et al.,1990).....	12
Figure 2.5 Variation of penetration depth at 4 GHz, 10 GHz, 37 GHz frequencies. (adopted from Ulaby et al.,1990) .....	13
Figure 2.6 Variation of emissivity with snow water equivalent at 37 GHz (adopted from Ulaby and Stiles,1980) .....	14
Figure 2.7 SWE versus $T_b$ at 36 GHz for horizontal and vertical polarization (adopted from Schanda et al., 1983) .....	16
Figure 2.8 Frequency versus brightness temperature for horizontal and vertical polarization with $50^\circ$ nadir angle for winter, refrozen spring and wet spring snow. (adopted from Schanda et al.,1983).....	18
Figure 2.9 The main components of the energy observed by passive microwave sensor over snow covered ground.....	23
Figure 3.1 Transmission of electromagnetic wave through a slab of scatterers .....	28
Figure 3.2 Components of brightness temperature which is observed by microwave sensor. All these components are considered inside HUT	

Model: (1) upward emitted atmospheric radiation; (2) downward emitted reflected atmospheric radiation; (3) downward emitted reflected snowpack emission contribution; (4) upward emitted soil emission contribution; (5) upward emitted snowpack emission contribution .....	31
Figure 3.3 Contribution of snow layer and ground emissions to $T_{B,Scene}$	32
Figure 3.4 Sensitivity analysis of ground temperature.....	36
Figure 3.5 Sensitivity analysis of ground moisture .....	37
Figure 3.6 Sensitivity analysis of ground roughness .....	37
Figure 3.7 Sensitivity analysis of air temperature.....	38
Figure 3.8 Sensitivity analysis of air pressure .....	38
Figure 3.9 Sensitivity analysis of water vapour .....	39
Figure 3.10 Sensitivity analysis of snow salinity.....	39
Figure 3.11 Sensitivity analysis of snow temperature .....	40
Figure 3.12 Sensitivity analysis of snow density .....	40
Figure 3.13 Sensitivity analysis of snow moisture .....	41
Figure 3.14 Sensitivity analysis of snow grain size .....	41
Figure 3.15 Sensitivity analysis of snow depth.....	42
Figure 3.16 Input and output schema of HUT Model.....	44
Figure 3.17 Measured extinction coefficients against grain size and fitted equation by Hallikainen et al. (1987).....	44
Figure 3.18 Measured extinction coefficients against grain size and fitted equation by Roy et al. (2004).....	45
Figure 3.19 Snow cover classification map over eastern part of Turkiye and case study basin .....	46
Figure 3.20 Measured extinction coefficients against grain size and fitted equation given in (3.18) .....	48
Figure 3.21 AWOS located inside Karasu Basin .....	50
Figure 3.22 Data assimilation schema for obtaining grain size .....	52
Figure 4.1 Grain Size versus $SD/\Delta T_b$ plot for January .....	56
Figure 4.2 Grain Size versus $SD/\Delta T_b$ plot for February .....	57

Figure 4.3 Grain Size versus $SD/\Delta T_b$ plot for March.....	57
Figure 4.4 AMSR-E 89 GHz Horizontal Channel Descending Pass Sample Image of 07.02.2009.....	60
Figure 4.5 Process flow chart of developed methodology .....	61
Figure 4.6 Daily SWE Map of Europe for 24 January 2010.....	62
Figure 4.7 Daily snow depth map of Europe for 24 January 2010.....	62
Figure 4.8 Distribution of stations over digital elevation model.....	64
Figure 4.9 Distribution of stations over landuse .....	64
Figure 4.10 Distribution of stations over AMSR-E pixel median elevation map .....	66
Figure 4.11 Distribution of stations over snow classification map .....	66
Figure 4.12 Average calculated SD versus average measured SD of 2008.....	70
Figure 4.13 Average calculated SD versus average measured SD of 2009.....	71
Figure 4.14 Average calculated SD versus average measured SD of 2010.....	71
Figure 4.15 Average calculated SD versus average measured SD of 2008, 2009 and 2010.....	72
Figure 4.16 Average measured SD versus RMSE, absolute RA and data count.....	72
Figure 4.17 Average calculated SWE versus average measured SWE of 2008.....	76
Figure 4.18 Average calculated SWE versus average measured SWE of 2009.....	76
Figure 4.19 Average calculated SWE versus average measured SWE of 2010.....	77
Figure 4.20 Average calculated SWE versus average measured SWE of 2008, 2009 and 2010.....	77

Figure 4.21 Average measured SWE versus RMSE, absolute RA and data count.....	78
Figure 5.1 Elevation of reference stations versus RMSE, absolute RA and data count for calculated SD.....	81
Figure 5.2 Elevation of reference stations versus RMSE, absolute RA and data count for calculated SWE.....	81
Figure 5.3 Process flow chart of fine tuned developed methodology ....	83
Figure 5.4 Average re-calculated SD versus average measured SD of 2008, 2009 and 2010 .....	85
Figure 5.5 Elevation of reference stations versus RMSE, absolute RA and data count for re-calculated SD. ....	86
Figure 5.6 Average re-calculated SWE versus average measured SWE of 2008, 2009 and 2010 .....	87
Figure 5.7 Elevation of reference stations versus RMSE, absolute RA and data count for re-calculated SWE. ....	88

## LIST OF TABLES

### TABLES

Table 2.1 Characteristics of satellite microwave imaging instruments .	22
Table 3.1 Range and prefixed values of parameters used for sensitivity analysis. ....	35
Table 3.2 Standard deviation of modeled brightness temperature for vertical polarization frequencies. ....	35
Table 3.3 Standard deviation of modeled brightness temperature for horizontal polarization frequencies. ....	36
Table 3.4 Calculated $\alpha$ coefficients.....	47
Table 3.5 Calculated a coefficients.....	47
Table 3.6 Calculated a, b, $\alpha$ coefficients and obtained R-square values of fitted equations for 18 GHZ and 35 GHz frequencies against Hallikainen's data. ....	49
Table 3.7 Prefixed HUT model parameters .....	51
Table 3.8 Calculated mean grain sizes for stations over period 2003-2007 .....	53
Table 3.9 Calculated mean of model error for 18.7 GHz channel for stations over period 2003-2007 .....	54
Table 3.10 Calculated mean of model error for 36.5 GHz channel for stations over period 2003-2007 .....	54
Table 4.1 Calculated a and b coefficients for January, February and March .....	58
Table 4.2 Calculated and measured snow densities at three AWOS... ..	59
Table 4.3 Calculated x, y coefficients and RMSE for equation (4.4)....	59
Table 4.4 Comparison of measured and calculated SD of 2008.....	68
Table 4.5 Comparison of measured and calculated SD of 2009.....	69



Table 4.6 Comparison of measured and calculated SD of 2010.....	69
Table 4.7 Comparison of measured and calculated SD of 2008, 2009 and 2010. ....	70
Table 4.8 Comparison of measured and calculated SWE of 2008. ....	74
Table 4.9 Comparison of measured and calculated SWE of 2009. ....	74
Table 4.10 Comparison of measured and calculated SWE of 2010 ....	75
Table 4.11 Comparison of measured and calculated SWE values of 2008, 2009 and 2010. ....	75
Table 5.1 Comparison of measured and calculated SD values of 2008, 2009 and 2010 regarding reference station elevations.....	80
Table 5.2 Comparison of measured and calculated SWE values of 2008, 2009 and 2010 regarding reference station elevations.....	80
Table 5.3 Comparison of measured and re-calculated SD of 2008, 2009 and 2010. ....	84
Table 5.4 Comparison of measured and re-calculated SD values of 2008, 2009 and 2010 regarding reference station elevations.....	85
Table 5.5 Comparison of measured and re-calculated SWE of 2008, 2009 and 2010. ....	87
Table 5.6 Comparison of measured and re-calculated SWE values of 2008, 2009 and 2010 regarding reference station elevations.....	88
Table 5.7 Test results summary of SD retrieval algorithms. ....	89
Table 5.8 Test results summary of SWE retrieval algorithms. ....	89

# CHAPTER 1

## INTRODUCTION

### 1.1 General

Monitoring snow parameters (snow depth, density, Snow Water Equivalent (SWE) and cover) at regional scale is essential for the management of water generating from snowmelt and climate change studies.

In the eastern part of Turkey seasonal runoff from snow melting is extremely important because most of the water originate from upper elevations of high mountains and contribute to large dams like Keban Dam, which is located on Euphrates River. 65 – 70 % of the total annual flow contributes to reservoir during early spring months.

In snow hydrology, it is crucial to have information over the whole basin that is going to be modeled by taking advantage of dense point measurements from weather stations in order to be able to represent the basin entirely. The major difficulties in reaching the remote areas, setting up measurement stations and running them properly, make the use of remote sensing data more important. After the profound technological improvements on the latest satellite sensor imageries; higher temporal, spatial, and spectral resolution provide the scientists with better coverage of the region of interest which is a mountainous watershed that its snow potential is concerned in this case. Using the data from satellite sensors for remote sensing of snow extent and other snow parameters gives the

scientists the chance of monitoring and evaluating the seasonal changes of snow cover more accurately than coarse point measurements.

Snow covered area determination methodologies using satellite data over eastern part of Turkey have been studied by several researchers. (Gökdemir, 2009; Sürer, 2009; Akyürek 1998). Satellite data and distributed snow model coupling have been applied by Sorman (2005) and Şensoy (2005) over Karasu basin which is located in the eastern part of Turkey. Until now, no researchers have been focused on Snow Depth (SD) or SWE modeling based on satellite data over Turkey.

In practice, MW radiometers and scatterometer are the only space-borne remote sensing instruments that can supply data for calculation of snow parameters for hydrological applications. The spatial resolution of satellite microwave data is coarser than that of visible and thermal observations. The weak sensitivity to atmospheric conditions and large swath width of passive microwave sensors allow collecting continues data globally on a daily basis. The retrieval of SD or SWE from microwave data is possible because the microwave observations are sensitive to interaction between electromagnetic waves and snowpack over underlying ground.

The frequencies used for SD or SWE determination are near 19 GHz and 37 GHz. Data obtained from 37 GHz are more sensitive to snow parameters because the radiation scattered by the snow at 37 GHz is more than that at 19 GHz. As SD increases the amount of emission decrease at 37 GHz is more than that at 19 GHz, but the amount of brightness temperature difference at these frequencies increases with SD. Many methodologies based on space-born passive microwave data have been developed in the literature since 1970s, which exploit this sensitivity (Chang et al., 1987; Foster et al., 1997; Kelly et al., 2003). These approaches typically use a linear or quadratic regression between SD and

the brightness temperature difference at the 19 GHz and 37 GHz bands. More recent studies (Kelly et al.,2003 and Foster et al.,2005) have investigated to use dynamic regression equations especially for different snow classes defined by Sturm (1995).

Electromagnetic models have been developed to retrieve SD or SWE from satellite microwave brightness temperatures (Tedesco and Kim, 2006; Pulliainen, 2006). The retrieval of snow parameters through these models are achieved by numerical techniques that aimed to minimize the difference between modeled and measured brightness temperatures. Electromagnetic models based on developed approaches can provide better results than regression methods (Pulliainen and Hallikainen, 2001; Pulliainen, 2006).

## **1.2 Objectives**

For this study, one of the well known EM models, Helsinki University of Technology (HUT) model, is used for the first time in Turkey. HUT is a semi-empirical snow emission model that is trying to represent the physical processes that are occurring inside snow and underlying ground with simplified electromagnetic algorithms. In the first part of the study, HUT model equations are modified for mountainous areas and performance of modified model was compared with the original and other modified cases using ground truth data of 2003-2007 years.

In the second part, a methodology for development of daily SD and SWE maps without using ground data is proposed based on modified HUT model. Performance metrics of obtained results for January to March period of 2008, 2009 and 2010 years were calculated.

The study is targeted at individuals and organizations that are interested in SD/SWE modeling in mountainous areas, where ground snow measurements are not dense enough to produce SD/SWE distribution maps. In this respect, the algorithms developed in this study can be considered as “hopeless man’s” data assimilation schema layout.

So the objectives of the study can be listed as follows:

- modification of existing HUT model parameters in order to model SD/SWE better in mountainous areas
- development of a methodology for retrieval of SD/SWE daily maps using passive microwave data with HUT model over eastern part of Turkey without integration of ground measurement values.
- validation of the developed methodology using ground truth snow measurements

## **1.2 Thesis Outline**

The subjects described in the following chapters are given below:

In Chapter 2, microwave radiation from natural surfaces and emission behavior of snow are introduced. Passive microwave systems and microwave emission model approaches are discussed.

In Chapter 3, existing HUT model’s physical principles are presented. Model sensitivity to each input parameters are depicted. Afterwards, model’s empirical extinction coefficient modification process is explained in details. Finally modified model performance is checked against original and other modified cases.

Chapter 4 constitutes the first part of the SD/SWE daily map development methodology based on HUT model. Grain size and density retrieval approaches that are integrated to developed data assimilation schema are described. Satellite data used in daily SD/SWE maps are discussed. At last, validation of the produced products is performed and the followed procedure during performance tests is explained in details.

Chapter 5 forms the second part of the developed methodology. Necessity of the fine tuning of the algorithm for pixels whose median elevation is less than 1750.0 m is discussed in details. A new approach for this case is proposed and validation of the fine tuned methodology is made.

Finally, Chapter 6 summarizes the main results of the study, discusses the implications of the work within the context of existing snow hydrology literature and makes recommendations for further research.

## CHAPTER 2

### USING PASSIVE MICROWAVE REMOTE SENSING TO MONITOR SWE

#### 2.1 Microwave Radiation from Natural Surfaces

If material temperature is greater than zero Kelvin, material absorbs and emits electromagnetic (EM) energy at the same time according to principles of thermodynamics. EM wave is vertically polarized if the electric field vector of the wave is parallel to the plane of incidence. The radiation is said to be horizontally polarized, when the electric field vector is perpendicular to the plane of incidence.

A blackbody is a medium which perfectly absorbs and emits energy. According to Planck's radiation law, a spectral brightness, B is radiated by a blackbody uniformly in all directions (Ulaby et al., 1990):

$$B = \frac{2hf^3}{c^2} \left( \frac{1}{e^{hf/k_B T} - 1} \right) \quad (2.1)$$

where h is Planck's constant =  $6.63 \times 10^{-34}$  joules; f is frequency in Hz; c is velocity of light =  $3 \times 10^8$  m/s;  $k_B$  = Boltzmann's constant =  $1.38 \times 10^{-23}$  joule/K; T is temperature in Kelvin.

In the microwave region for frequencies less than 100 GHz, where  $hf / k_B T \ll 1$ , the Rayleigh-Jean law can be used to approximate the blackbody radiation described by Planck's law. Therefore Equation (2.1) simplifies to:

$$B = \frac{2k_B T}{\lambda^2} \quad (2.2)$$

where  $\lambda$  is the wavelength in meters.

In the microwave region, the brightness  $B_{bb}$  of a black body at temperature  $T$  for a narrow bandwidth  $\Delta f$  is (Ulaby et al., 1990):

$$B_{bb} = B\Delta f = \frac{2k_B T}{\lambda^2} \Delta f \quad (2.3)$$

The emissivity  $e(\theta, \phi)$  along  $(\theta, \phi)$  direction is defined as the brightness of the material relative to that of a blackbody at the same temperature (Ulaby et al., 1990):

$$e(\theta, \phi) = \frac{B(\theta, \phi)}{B_{bb}} \quad (2.4)$$

where  $B(\theta, \phi)$  is the real material brightness along  $(\theta, \phi)$  direction.

The emissivity of a surface is dependent on the view angle, the polarization and the dielectric constant of the surface material. Non-blackbodies, also called grey-bodies, have emissivity in between zero and one.

For a non-blackbody media, the corresponding derived brightness is usually expressed as a microwave brightness temperature,  $T_b$ , which is equivalent to the emissivity of the media times its physical temperature:



$$Tb = e(\theta, \phi)T \quad (2.5)$$

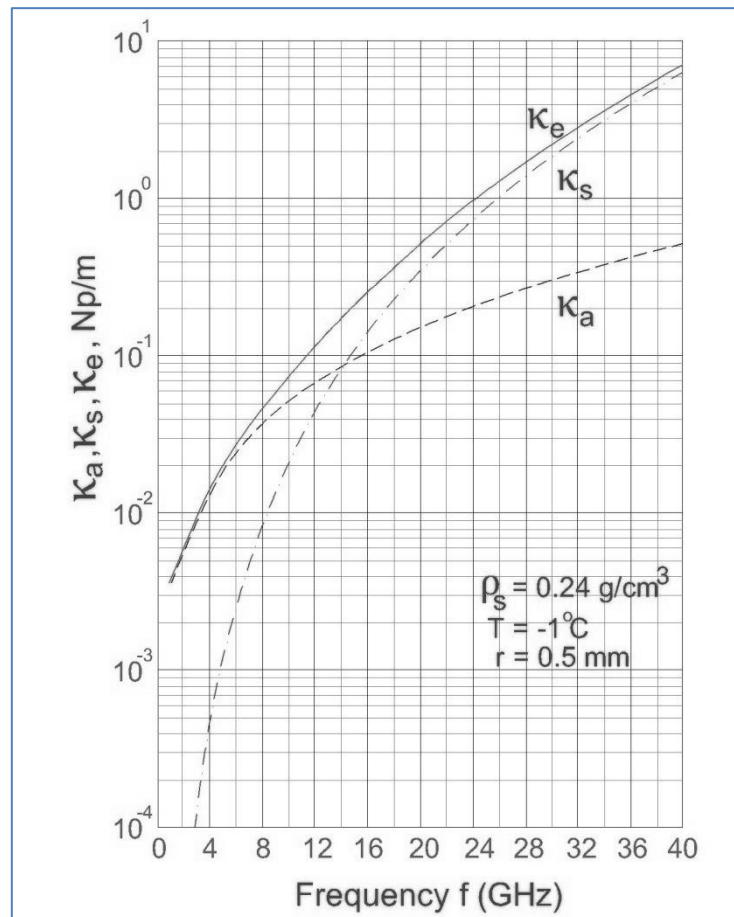
## 2.2 Emission Behavior of Snow

The propagation parameters of a medium containing scattering particles are the volume absorption and scattering coefficients  $\kappa_a$  and  $\kappa_s$  respectively, whose sum is defined as the extinction coefficient  $\kappa_e$ . Scattering in both dry and wet snow is attributed to the ice particles in the snow. Ignoring the mutual interaction between the ice particles in snow,  $\kappa_s$  is the sum of the scattering cross sections of all ice spheres contained in a unit volume (Ulaby et al., 1990).

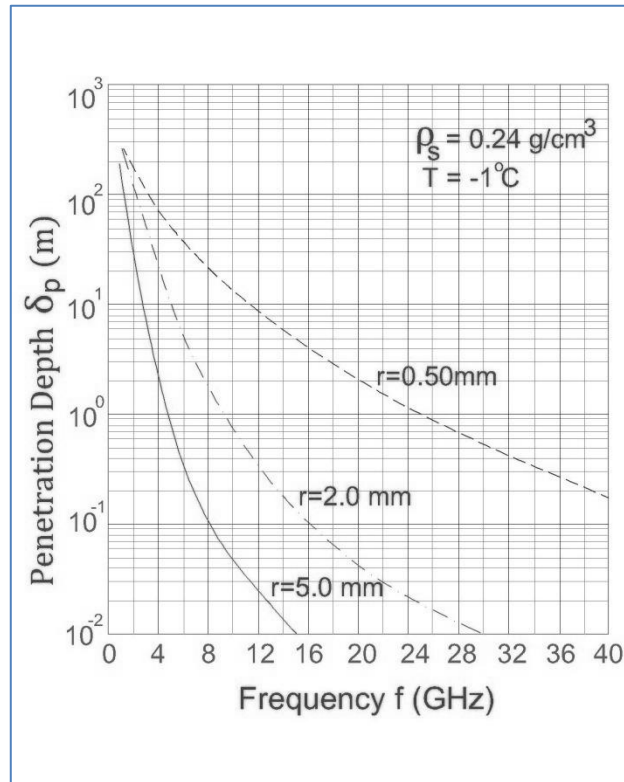
For dry snow the background is taken to be air, but for wet snow the background is taken to be the air-water mixture. In the general case, the absorption coefficient  $\kappa_a$  consists of two components, i.e. ,  $\kappa_a = \kappa_{ai} + \kappa_{ab}$  , where  $\kappa_{ai}$  denotes absorption by the ice spheres and  $\kappa_{ab}$  denotes absorption by the background.. For dry snow, the background is air, and  $\kappa_{ab} = 0$  and  $\kappa_a = \kappa_{ai}$ . i.e. , there is no absorption by the background material. However, for wet snow there is an absorption by background and  $\kappa_{ab} \neq 0$  (Ulaby et al., 1990).

Figure 2.1 shows spectral plots of  $\kappa_s$ ,  $\kappa_a$ ,  $\kappa_e$  for a dry snow medium containing spherical ice crystals which are 0.5 mm in radius. Computations were done using Mie expressions. As seen from Figure 2.1 below about 5 GHz where  $\kappa_s \ll \kappa_a$  and the albedo  $a = \kappa_s / (\kappa_s + \kappa_a)$  is very small. Scattering becomes the principal component of the total extinction loss of the medium at frequencies above 20 GHz (Ulaby et al., 1990). For dry snow, an increase in the frequency  $f$  results in increases in  $\kappa_e$ ,  $\kappa_a$ ,  $\kappa_s$  which means that for a given snow-layer thickness  $d$  (or water equivalent SWE),  $Tb$  should decrease with increasing frequency.

Plots of the penetration depth  $\delta_p=1/\kappa_e$  versus frequency  $f$  for grain sizes  $r=0.5$ ,  $r=2.0$  and  $r=5.0$  mm are shown in Figure 2.2. The penetration depth indicates the maximum depth of the medium that contributes to the backscattering coefficient and brightness temperature (Carsey, 1992). It can be observed that  $\delta_p$  may vary from a few centimeters to tens of meters depending on the particle size and the microwave frequency. Penetration depth decreases with increasing grain radius and increases with decreasing frequency.



**Figure 2.1** Calculated microwave spectra of the absorption, scattering, and extinction coefficients of dry snow containing ice crystals 0.5 mm in radius. (adopted from Ulaby et al.,1990)



**Figure 2.2 Calculated microwave spectra of the penetration depth of snow (Ulaby et al.,1990)**

When water in liquid form is present in snow, the snow medium becomes a mixture of ice particles, water droplets and air. The volumetric water content of snow,  $m_v$ , which is also called wetness, usually does not exceed a few percent, and the water droplets usually are much smaller than the ice particles. Therefore, it can be assumed that scattering in the medium is caused mainly by the ice particles, and that the background medium may be regarded as a mixture of water droplets and air. (Ulaby et al.,1990),

The fitted curves in Figure 2.3 are plots of  $\kappa_e$  versus  $m_v$  at 4, 16 and 37 GHz. The data points are based on transmission measurements made for snow samples of varying wetness. Observations of the snow samples

under a microscope indicate that a typical value for  $r$  is 0.5 mm; hence, this was the value used in calculating the curve in Figure 2.3 (Ulaby et al., 1990). Extinction coefficient increases with increasing  $m_v$ .

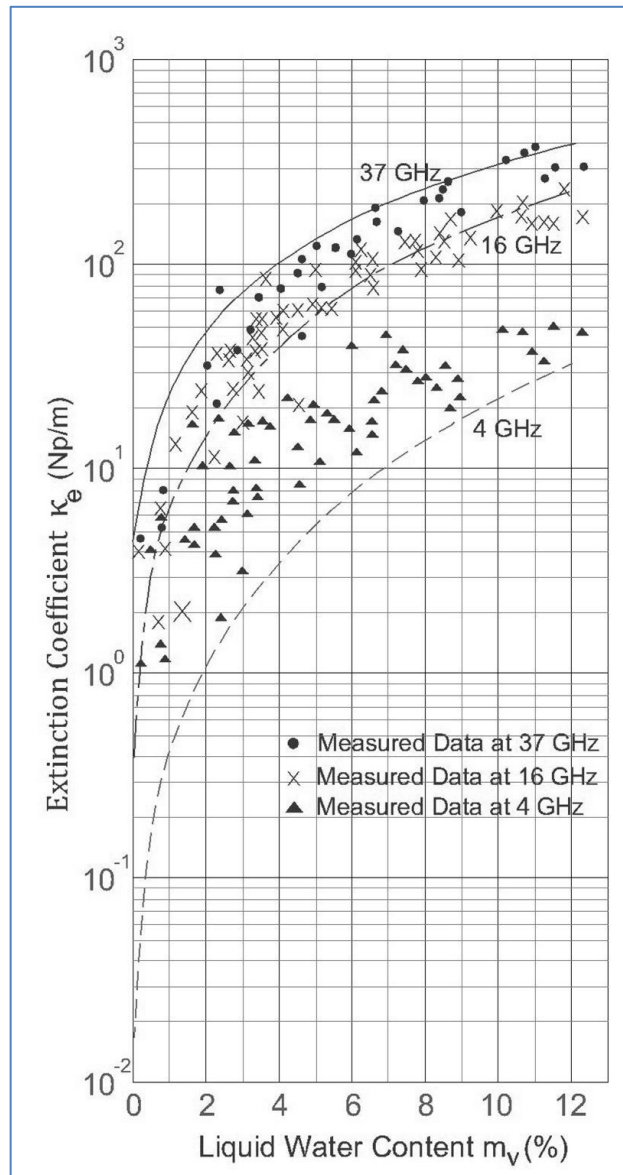


**Figure 2.3 Measured values of  $\kappa_e$  with the curves calculated for  $\rho_s=0.24\text{g/cm}^3$ ,  $r = 0.5$  mm at 4, 16 and 37 GHz (adopted from Ulaby et al.,1990)**

The background medium absorption coefficient,  $\kappa_{ab}$ , increases from zero for dry snow to a value larger than  $\kappa_s$  when  $m_v \geq 0.01$  during snow melting process. As a result the magnitude of scattering albedo “a” reduces to a very small value even if the amount of liquid water is very small inside snow. This phenomena is depicted in Figure 2.4 where grain radius  $r=0.5$  mm. For  $m_v \geq 0.02$ , the albedo is so small in magnitude that its dependence on “r” becomes negligible. Thus, when snow is wet, medium approaches the non-scattering condition characteristic of a blackbody radiator (Ulaby et al., 1990).

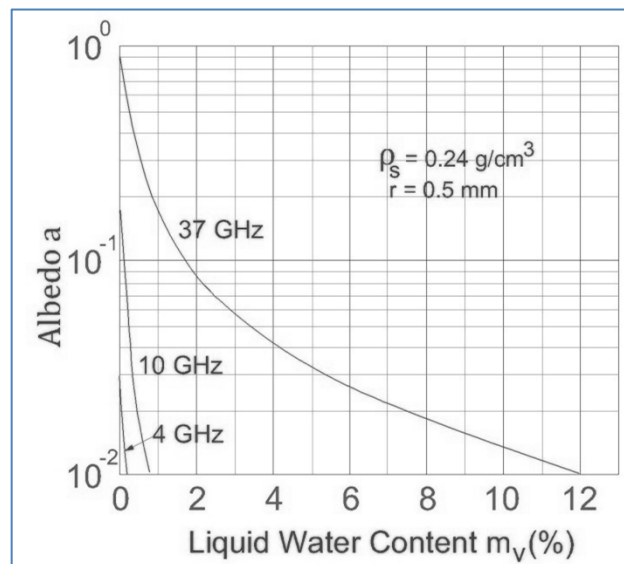


**Figure 2.4 Variation of snow albedo with liquid water content at 4 GHz, 10 GHz, 37 GHz frequencies. (adopted from Ulaby et al.,1990)**

Variation of the penetration depth  $\delta_p$  as a function of  $m_v$  is shown in Figure 2.5 for 4, 10 and 37 GHz.  $\delta_p$  decreases with increasing  $m_v$ . Penetration depth increases with decreasing frequency.

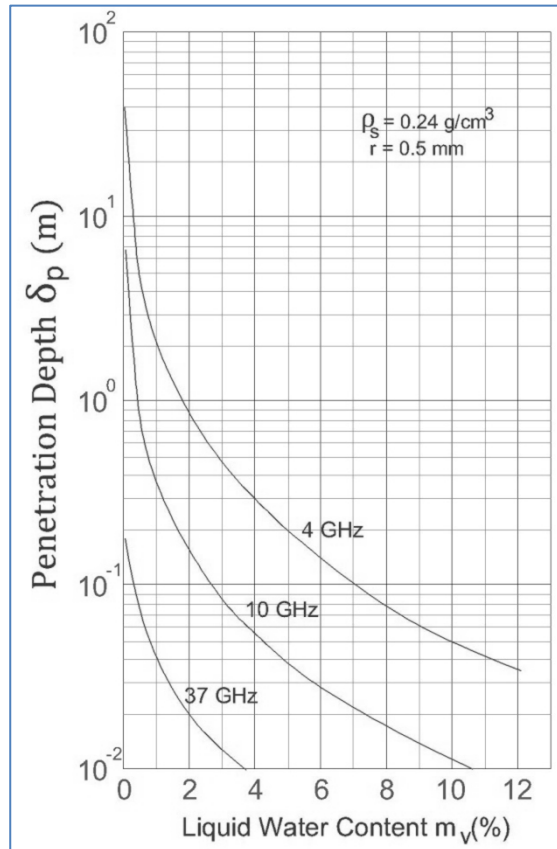


**Figure 2.5 Variation of penetration depth at 4 GHz, 10 GHz, 37 GHz frequencies. (adopted from Ulaby et al.,1990)**

Ulaby and Stiles (1980) has added horizontal layers of newly fallen snow in 30-40 cm increments until 170 cm depth and made radiometric measurements after each addition. Each layer which was composed of fresh snow that can be more or less considered as uniform snowpack in terms of the density and size distribution of the ice crystals, SWE versus emissivity “e” measurements of the dataset is depicted in Figure 2.6 for 37 GHz frequency. For a given nadir angle  $\theta$  and density  $\rho$ , emissivity decreases with increasing SWE.

Tb or emissivity would be a smooth curve similar to the one shown in Figure 2.6, if Tb was only function of SWE. But for natural snowpack Tb is dependent on other snow parameters and underlying ground parameters other than SWE. Snowpack observed in nature consists of several layers that have different densities and grain size distributions. The properties of these layers are the result of the history of the snowpack, which usually is related to the location and elevation of the snowpack above sea level. The crystals contained in snow that has undergone many cycles of melting are very different in both shape and size from crystals of newly fallen snow (Ulaby et al., 1990).

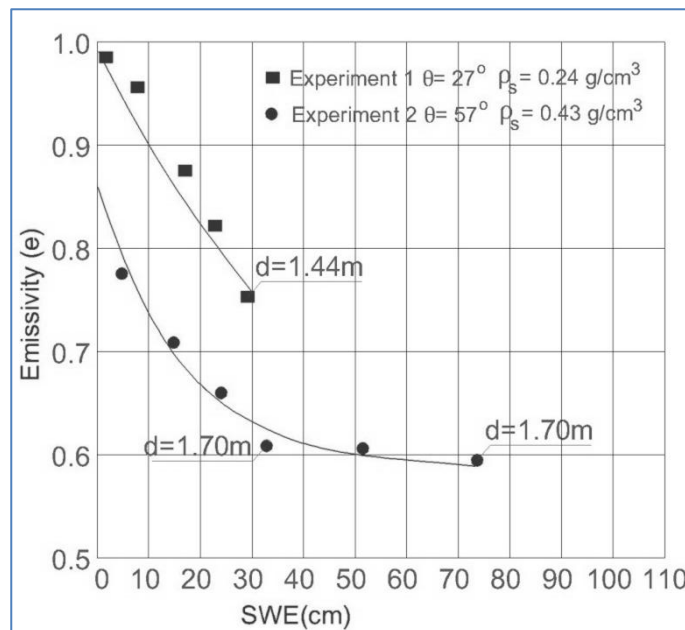


**Figure 2.6 Variation of emissivity with snow water equivalent at 37 GHz (adopted from Ulaby and Stiles,1980)**

Figure 2.7 shows  $T_b$  measurements at 37 GHz for snowpacks in Switzerland, 2450 m above sea level (Matzler et al., 1982), plotted as a function of SWE. The data shows the figure cover a wide range of conditions for dry winter snow extending from the beginning of the snow season in October to the end of the season March (Ulaby et al., 1990).

In Figure 2.7  $T_b$  decreases with increasing SWE for  $SWE \leq 20$  cm (corresponding to a depth of 60-80 cm). But for the artificially created snowpile,  $T_b$  (or emissivity) continues to decrease while SWE increases beyond 20 cm.  $T_b$  in Figure 2.7 changes downward trend to upward trend with increasing SWE about equal to 20 cm. This reversal raises two questions: (1) What causes the reversal in slope? and (2) will the fact that a single value of  $T_b$  can correspond to two very different values of SWE present being an interpretation problem? (Ulaby et al., 1990). For areas where snow accumulation exceeds 80 cm, multichannel observations are needed to resolve ambiguity in the estimated value of SWE (Matzler et al., 1982). Clearly there is nothing magical about the 20-cm figure, it simply happens to be characteristic of the cumulative weather history of the test site at which the data were obtained (Ulaby et al., 1990). According to Matzler et al. (1982), the behavior of  $T_b$  depicted in Figure 2.7, which includes data from four consecutive snow seasons, was characteristic of dry winter snow, even though very different snow histories were encountered during four seasons.



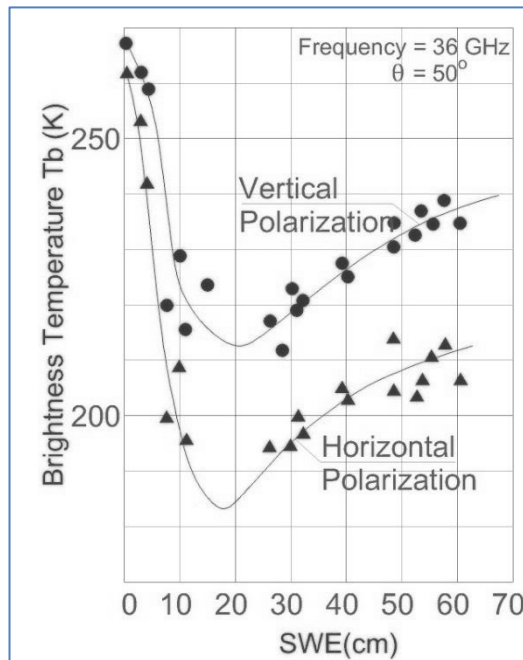


**Figure 2.7 SWE versus Tb at 36 GHz for horizontal and vertical polarization (adopted from Schanda et al., 1983)**

Schanda et al., (1983) divided snow into three classes, based on five years of extensive microwave observations of snow, the research group at the University of Bern:

- Winter Snow: Snow that has not undergone any melting metamorphism. At high altitudes, this condition usually is satisfied during the period between November and March (in the Northern Hemisphere).
- Wet Spring Snow: The snowpack surface consists of thick (at least several centimeters deep), firm layers of wet, quasi-spherical ice crystals (diameter in between 1-3 mm) formed during the day at temperatures above the freezing point and usually associated with either the passage of warm fronts or sunny, clear-sky conditions.

- Dry (Refrozen) Spring Snow: The surface of the snowpack consists of a layer of refrozen, firm snow that forms during clear, cold nights and is several centimeters thick.

T<sub>b</sub> measurements are plotted against frequency in Figure 2.8 for three snow types described above. All T<sub>b</sub> measurements have been normalized to SWE = 48 cm. T<sub>b</sub> should decrease with increasing frequency in both horizontal and vertical polarization for dry snow. This issue is depicted in Figure 2.8 for winter and spring dry snow conditions. There are mainly two significant differences in between two dry snow T<sub>b</sub> measurements. Firstly, polarization difference  $\Delta T_b = T_b(v) - T_b(h)$  is much larger for winter snow than for spring snow. Secondly, T<sub>b</sub> of spring snow decreases with increasing frequency (especially for  $f > 10$  GHz) more steeply than winter snow. These differences are attributed to differences in the shapes and sizes of the ice crystals characteristic of the two snow conditions (Schanda et al., 1983)..

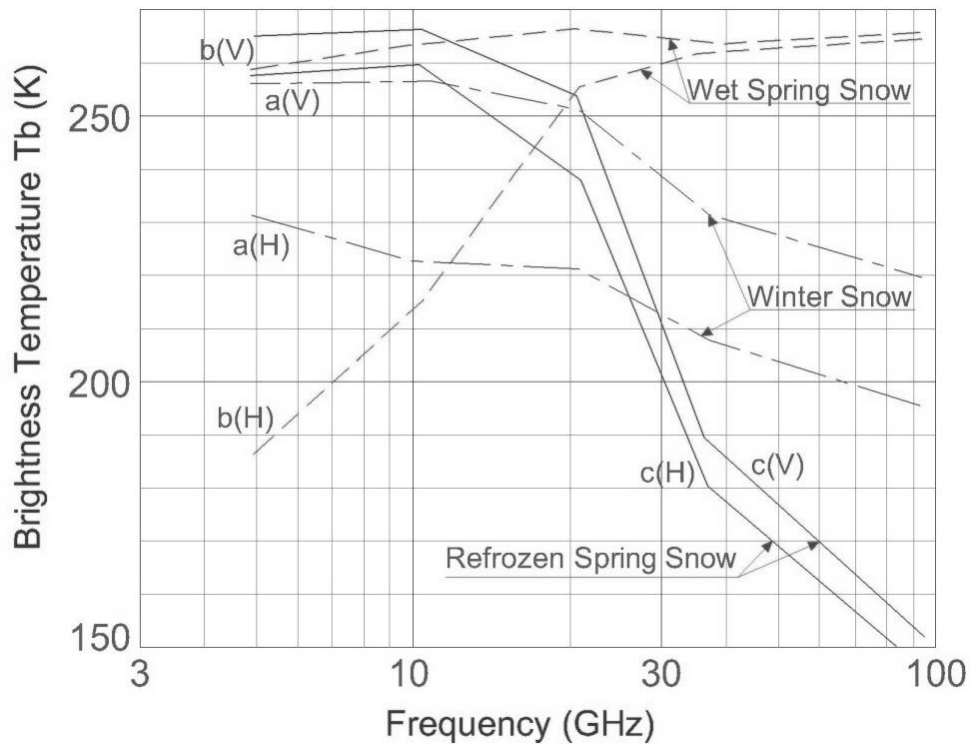


**Figure 2.8** Frequency versus brightness temperature for horizontal and vertical polarization with  $50^\circ$  nadir angle for winter, refrozen spring and wet spring snow. (adopted from Schanda et al.,1983)

### 2.3 Passive Microwave Systems

Passive microwave systems detect black-body radiation in the microwave (wavelengths typically 3 mm to 6 cm, or equivalently frequencies between 5 and 100GHz) region. It is a passive technique, as the name implies. It has the ability to penetrate through most clouds, since it is a microwave technique. It can thus be characterized as an all-weather, day-and-night, technique. As with thermal systems, the purpose is to measure the  $T_b$  of

the incident radiation, to infer either the physical temperature of the Earth's surface or its emissivity.

The much longer wavelengths of microwave radiation indicate that the photons are very much less energetic than those of visible light (typically a few tens of micro electron volts, compared with a few electron volts), therefore completely different detection techniques are used. A passive microwave radiometer is effectively a radio telescope viewing downward. An antenna collects the incident radiation and converts it into a fluctuating voltage difference that can be amplified and detected.

Diffraction limit sets the spatial resolution of a passive microwave radiometer. The angular Full width to half height (FWHH) is of the order of  $\lambda/D$ , where  $\lambda$  is the wavelength and  $D$  is the width (e.g., the diameter in the case of a dish) of the antenna. The long wavelengths imply coarse angular resolutions: for an antenna 1m in diameter operating at a wavelength of 2cm, the angular resolution is of the order of  $1^\circ$ , which would give a horizontal spatial resolution of about 14km from a typical spacecraft altitude of 700km. This issue is perhaps the main disadvantage of passive microwave systems.

Passive microwave radiometers do not need to achieve particularly high spectral resolution, except of instruments designed for atmospheric profiling. Bandwidths are typically around 1% of the operating frequency.

Most passive microwave radiometers provide coverage of a number of different frequencies, often in two polarizations. Data gathered at frequencies below about 5 GHz are unsuitable because of the very poor spatial resolution. Frequencies below about 15 GHz, the detected brightness temperature will be dominated by surface emission and atmospheric water vapor causes a correction of a few Kelvin (Rees, 2006).

Between about 15 and 35 GHz the surface signal still dominates, although the contribution due to water vapor is significantly larger, and observations in this frequency range are often used to provide a simple correction for this (Rees, 2006). The effects of molecular absorption in the atmosphere become dominant at frequencies higher than 35 GHz, and these frequencies are more useful for atmospheric profiling than for surface imaging.

As for the thermal infrared systems, the sensitivity of a passive microwave radiometer can most usefully be defined in terms of the detectable change in brightness temperature (Rees, 2006). This is determined by the “system noise temperature” (a function of the instrument design and its physical temperature), the integration time, and the bandwidth. Values of a few tenths to 1 K are typical.

Table 2.1 gives details of those satellites microwave instruments which have flown on meteorological satellites since the early 1970's, and that are not exclusively used for atmospheric sounding, i.e., those that have at least some capability for surface imaging. The Electronically Scanning Microwave Radiometer 5 (ESMR-5), ESMR-6 and Scanning Multispectral Microwave Radiometer (SMMR) instruments all flew on Nimbus satellites and all are now defunct. The Special Sensor Microwave / Imager (SSM/I), as a part of the payload of the current Defense Satellite Meteorological Program (DMSP) Block spacecrafts F8, F10, F11, F12, F13 and F15 is both currently functional and a significant advance over previous microwave imaging instruments. DMSP SSM/I became operational in June 1987 on the F-8 satellite. Subsequent SSM/I's have been flown on the F-10 (December 1990), F-11 (October 1991), F-12 (August 1994), F-13 (March 1995) and most recently, F-15 (December 1999) satellites. The next generation SSM/I instrument, the Special Sensor Microwave Imager/Sounder (SSM/I/S), is carried aboard the DMSP F17. which was

launched in November 2006. SSMI/S senses 24 channels covering a wide range of frequencies from 19 - 183 GHz. The Level 1C dataset of SSMI/S contains only 11 of these channels (listed in Table 2.1), which are most relevant to sensing of land.

The Advanced Microwave Scanning Radiometer (AMSR-E) on the Earth Observing (EOS) Aqua platform provides daily ascending and descending passive microwave measurements for climate and hydrology studies. AMSR-E is modified from AMSR which was on ADEOS-II platform. AMSR antenna size is scaled down from 2.0 to 1.6 m for AMSR-E because of limitation of fairing size. Spatial resolution of the modified antenna of AMSR-E remained unchanged by this downsizing, because of orbit altitude of Aqua is lower than that of ADEOD-2. A deployable antenna is installed at AMSR-E instrument. The 50GHz channels are removed at AMSR-E because another Aqua instrument Advanced Microwave Sounding Unit (AMSU) provides the information in the 50- to 60-GHz band.

**Table 2.1 Characteristics of satellite microwave imaging instruments**

Instrument	Satellite	Years	Spatial Resolution (km)	Freq. (GHz) and Polar.	Swath Width (km)	Maximum Latitude (degree)
EMSR	Nimbus 5	1972-1976	25	19.35 H	3000	90
SMMR	Nimbus7	1978-1988	136 x 89	6.6 H, V	780	84.2
			87 x 57	10.7 H, V		
			54 x 35	18.0 H, V		
			47 x 30	21.0 H, V		
			28 x 18	37.0 H, V		
SSM/I	DMSP	1987-	70 x 45	19.35 H, V	1400	87.5
			60 x 40	22.24 V		
			38 x 30	37.0 H, V		
			16 x 14	85.5 H, V		
AMSR-E	Aqua	2002-	74 x 43	6.93 H, V	1445	88.3
			51 x 30	10.65 H, V		
			27 x 16	18.7 H, V		
			31 x 18	23.8 H, V		
			14 x 8	36.5 H, V		
			6 x 4	89.0 H, V		
SSMIS	DMSP	2006-	74 x 45	19.35 H, V	1700	87.5
			74 x 45	22.235 H, V		
			45 x 28	37.0 H, V		
			16 x 13	91.665 H, V		
			16 x 13	150 H		
			16 x 13	183.311 +/- 1 H		
			16 x 13	183.311 +/- 3 H		
			16 x 13	183.311 +/- 7 H		

## 2.4 Microwave Emission Models

The main components of the energy observed by a passive microwave sensor over snow covered ground are depicted in Figure 2.9. In the figure “A”, “E” and “S” denote respectively absorption, emission and scattering. “a”, “g”, and “s” sub-notations indicate atmosphere, ground and dry snow.

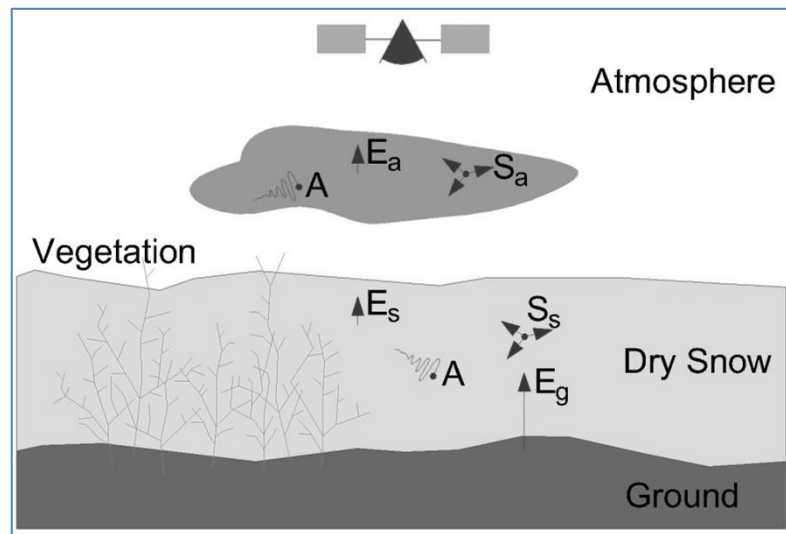


**Figure 2.9 The main components of the energy observed by passive microwave sensor over snow covered ground.**

The ground, the overlaying snowpack and the atmosphere are three main components in the energy budget and are shown in Figure 2.9:

- Ground emissivity and kinetic temperature combination can be accepted as ground surface emission. Emissivity of ground remains constant during winter season in high mountainous areas where ground freezes by late fall or latest early winter. Variations in passive microwave sensors emission measurements caused by ground emission should be due to temperature of ground which is mainly affected by air temperature and overlaying snow depth. The overlaying snow is like a blanket which ensures insulation. Therefore if depth of snow over ground increases the temperature change amount in the near surface air decreases.
- The snowpack over ground absorbs and scatters the radiation emitted by underlying ground. There exists also emission of snow



particles. For dry snow emission and absorption amounts are very low when compared with scattering amounts (Foster et al., 1991). Scattering phenomena inside snowpack reduces the amount of radiation generated by the snow layer (Armstrong et al., 1993).

- The radiation of snow and underlying ground is changed by absorption, scattering and self-emission of ice particles and water droplets in the atmosphere (Grody, 1991). Atmosphere effect increases with frequency. Vegetation amount over or inside snow layer also effects the snow emission. But the effects of atmosphere and vegetation can be neglected when compared with those of snow and snow parameters (Rott et al., 1991).

Several models and techniques have been developed to analyze and simulate factors effecting the radiation measured by a passive microwave sensor over snow covered areas. Depending on the approach, the models used to predict microwave emission and scattering can be divided in the following three groups: empirical, semi-empirical and theoretical (Tedesco and Kim, 2006).

Empirical models are based on the relationships obtained between remote sensing and ground truth data and snow parameters are obtained by regression equations or other kind of statistical analysis (Hallikainen and Jolma, 1992; Hallikainen et al., 2003; Oh et al., 1992). In order to develop an empirical model, the only need is datasets of ground and electromagnetic measurements which will be split in two parts: the first half is used to establish the equations and the other one to validate the model. Different statistical approaches such as regressions or artificial neural networks (ANN) relationships can be used to develop a relationship between two datasets.

Developed relationships have the limitation of being valid only locally, as they are not guaranteed to be valid for snow conditions different from

those used for obtaining the relationships used in the models. (Tedesco and Kim, 2006). Electromagnetic emission components depicted in Figure 2.9 can be different from place to place when ground, vegetation and snow characteristics are considered. But these models are very fast, needs no ground data to apply and easy to use.

For instance in Chang et. al (1987) the snow depth (SD) is estimated by:

$$SD=1.59(Tb_{18H} - Tb_{37H} ) \quad (2.6)$$

where  $Tb_{18H}$  and  $Tb_{37H}$  are respectively the 18 GHz and 37 GHz horizontally polarized brightness temperatures, and 1.59 is a constant obtained by a linear regression of the difference between 18 GHz and 37 GHz responses. If the 37 GHz brightness temperature is greater than the 18 GHz one, no snow is assumed present. While developing relationship given in (2.6) it is assumed that snow grain radius is 0.30 mm and density is  $0.30 \text{ g/cm}^3$ . Empirical models generally rely on brightness temperature difference of channels above and below 20 GHz.

The semi-empirical models are based on theoretical physical laws but some parts of them rely on some experimental measurements. The HUT snow emission model (Pulliainen et al., 1999) is a semi-empirical approach that has been successfully used to simulate  $Tb$  of single layer snowpacks. The basic assumption in the HUT snow emission model is that the scattering is mostly concentrated in the forward direction. Details of HUT model is given in Chapter 3. Another example of semi-empirical model is the Microwave Emission Model of Layered Snowpacks (MEMSL) that has been developed by Wiesman and Matzler (1999) for dry winter snow and extended to wet snow by Matzler and Wiesmann (1999).

Theoretical models do not use any experimental data and are only based on the solution of the Maxwell's equations. The dense-medium radiative theory (DMRT) (e.g., Tsang et al., 1985) and the strong fluctuation theory (SFT) (e.g., Stogryn, 1986) are theoretical models that have been widely used to simulate snow emission. These models need an accurate characterization of the media interacting with the electromagnetic waves and are more useful to understand the phenomena which happen rather than estimate the physical properties of the target (snow) by inverting the experimental data. (Brogioni, 2008). Indeed, the formulae describing the scattering or the emission are usually non-linear and very complex. Moreover the electromagnetic problem is multiparametric and ill-posed (different combination of input parameters give the same electromagnetic prediction), making almost impossible to invert the equations (theoretical methods) (Brogioni, 2008).

## CHAPTER 3

### HUT SNOW EMISSION MODEL

#### 3.1 Description of HUT Model

This section describes the derivation of the Helsinki University of Technology (HUT) microwave snow emission model. First, scalar radiative transfer approach is used to calculate the emission and total attenuation properties of snow which is assumed to be homogenous. Second, the effects of underlying ground, atmosphere and layer boundaries are considered and the scene brightness temperature that can be measured by passive microwave sensors is derived. (Pulliainen et al.,1999). The approach used in the HUT snow emission model to estimate the brightness temperature of snow-covered ground is based on the following assumptions: 1) the snowpack is a single homogeneous layer and 2) the scattered microwave radiation is mostly concentrated in the forward direction (Roy et al., 2004).

##### 3.1.1 Emission from a Homogenous Snowpack

The radiative transfer equation for radiation propagating in a snowpack at depth  $d$  in angle  $\theta$  from vertical can be written as:

$$\begin{aligned} \frac{\partial T_B(d, \theta)}{\partial d'} &= \kappa_a \sec \theta T_S + \kappa_s \sec \theta \\ &\quad - \frac{1}{4\pi} \iint 4\pi \psi(\bar{r}_{\theta}, \theta', \varphi') T_B(d', \theta', \varphi') \sin \theta' d\theta' d\varphi' \\ &\quad - \kappa_e \sec \theta T_B(d', \theta) \end{aligned} \quad (3.1)$$

where

$T_B$  : brightness temperature

$T_s$  : physical snow temperature

$\kappa_a$  : absorption coefficient

$\kappa_s$  : scattering coefficient

$\kappa_e$  : extinction coefficient ( $\kappa_e = \kappa_a + \kappa_s$ )

$\Psi$  : scattering phase function

$\bar{r}_\theta$  : unit vector to the angle of observation

The basic assumption of the HUT model is that the scattering is mostly concentrated in the forward direction. Hallikainen et al.(1987) used the same approach previously and current model theory and calculations mostly uses this investigation. The geometry of problem is depicted in Figure 3.1 where the total intensity incident on the slab is denoted by  $I(0)=I_0$ . In the case of dominant forward scattering, the (forward) scattered incoherent intensity ( $I_{inc}$ ) for a thin snow slab with a thickness of  $d$  and for nominal incidence ( $I_{inc}$ ) is (Ishimaru, 1978):

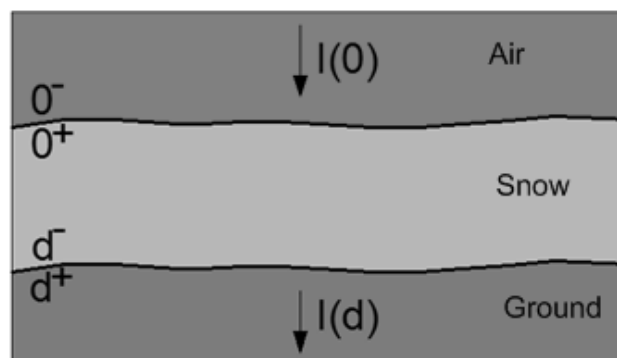


**Figure 3.1 Transmission of electromagnetic wave through a slab of scatterers**

$$I_{inc} = I(0^+)q[e^{\kappa_a d} - e^{-\kappa_e d}] \quad (3.2)$$

where  $q$  is a constant that describes the ratio of intensity which is scattered toward the receiver antenna beam.

Assuming that (3.2) is valid then (3.1) simplifies to

$$\frac{\partial T_B(d', \theta)}{\partial d'} = \kappa_a \sec \theta T_S + \sec \theta (q\kappa_S - \kappa_e) T_B(d', \theta) \quad (3.3)$$

For a homogeneous snow layer with a total thickness of  $d$ , (3.3) can be written as (3.4) which calculates the emitted brightness temperature just below the snow–air boundary:

$$\begin{aligned} T_B(d^-, \theta) &= T_B(0^+, \theta) e^{-(\kappa_e - q\kappa_S)d \sec \theta} \\ &+ \frac{\kappa_a T_S}{\kappa_e - q\kappa_S} (1 - e^{-(\kappa_e - q\kappa_S)d \sec \theta}) \\ &\equiv T_{B,g} + T_{B,s\uparrow} \end{aligned} \quad (3.4)$$

in which the first term ( $T_{B,g}$ ) corresponds to the brightness temperature contribution originating below the snow layer and attenuated by the snow layer. The second term ( $T_{B,s\uparrow}$ ) is the actual thermal emission contribution of the homogeneous snow layer.

The extinction properties of dry snow,  $\kappa_e$  in (3.1)–(3.4), as a function of snow grain size are modeled by formulas given in (Hallikainen et al., 1987).  $\kappa_a$  is calculated from the complex dielectric constant of dry snow. The real part of the snow dielectric constant is determined using the formulas given in Matzler, (1987). The imaginary part is treated with a formula based on the Polder–van Santen mixing model (Hallikainen et al.,

1986). For calculating the imaginary part of snow permittivity, the consideration of ice permittivity properties is also required. These (the imaginary part) are considered using an empirical formula (Matzler,1987).

The developed model includes one purely empirical parameter, the constant  $q$  introduced in (3.2)–(3.4). The value of  $q$  was evaluated to be 0.96 (the same value is employed at all frequencies). Controlled-conditions snowpack brightness temperature and propagation measurements conducted in Finland and Switzerland in the 1980's (Hallikainen et al.,1987), (Matzler,1987) were used for estimating the value of parameter  $q$  by fitting the model into multifrequency experimental observations.

### 3.1.2 Spaceborne Observed Scene Brightness Temperature

The HUT snow emission model estimates the space-borne observed microwave brightness temperature as a function of snow pack characteristics considering the effects of underlying ground, forest canopy and atmosphere. The major contributions to space-borne observed scene brightness temperature is given in Figure 3.2 while forest canopy can be neglected. The modeled brightness temperature can be written as:

$$T_{B,Model}(\theta) = t(\theta)T_{B,Scene}(\theta) + T_{B,Atm\uparrow}(\theta) + t(\theta)(1 - e_{scene}(\theta)) \times [T_{B,Atm\downarrow}(\theta) + t(\theta) \cdot 2.7K] \quad (3.5)$$

where  $\theta$  is the nadir angle;  $t$  is the atmospheric transmissivity modeled by a statistical model (Pulliainen et al.,1993);  $T_{B,Atm,\downarrow}$  is the up(down)welling atmospheric brightness temperature calculated from atmospheric transmissivity by a statistical model (Aschbacher, 1989);  $T_{B,Scene}$  is the terrain brightness temperature including the effect of snow ground surface and  $e_{scene}$  is the corresponding scene emissivity.  $T_{B,Scene}$  is the sum of

emission from snow and emission from underlying ground and can be given as:

$$T_{B,Scene} = T_{B,Snow} + T_{B,Grnd} \quad (3.6)$$

where  $T_{B,Snow}$  is the brightness temperature of snowpack;  $T_{B,Grnd}$  is the brightness temperature of underlying ground.

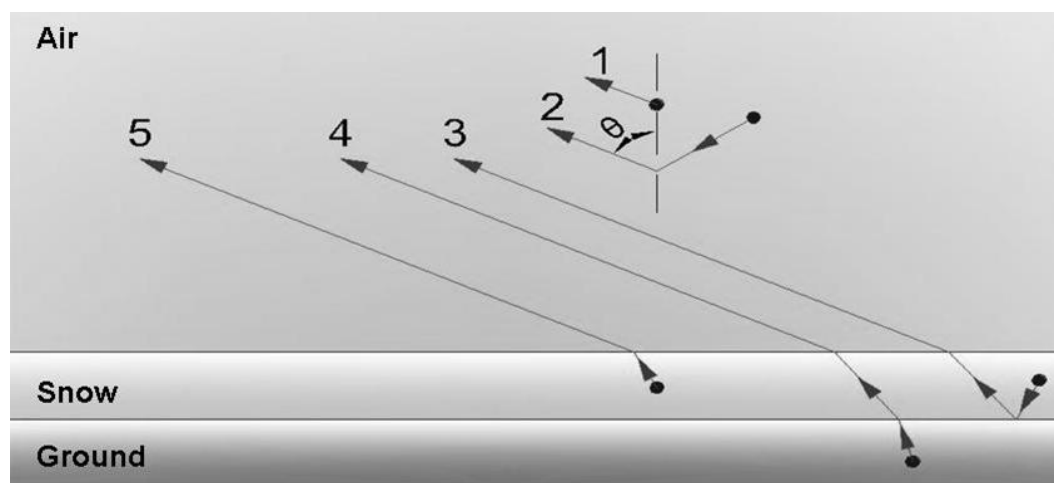


**Figure 3.2 Components of brightness temperature which is observed by microwave sensor. All these components are considered inside HUT Model: (1) upward emitted atmospheric radiation; (2) downward emitted reflected atmospheric radiation; (3) downward emitted reflected snowpack emission contribution; (4) upward emitted soil emission contribution; (5) upward emitted snowpack emission contribution**

When multiple reflections at snow-air and snow-ground boundaries are considered, incoherent approach (Ulaby et al.,1990) is used to calculate  $T_{B,Scene}$ . Snow layer upward and downward emission and multiple reflection schemas are given in Figure 3.3.



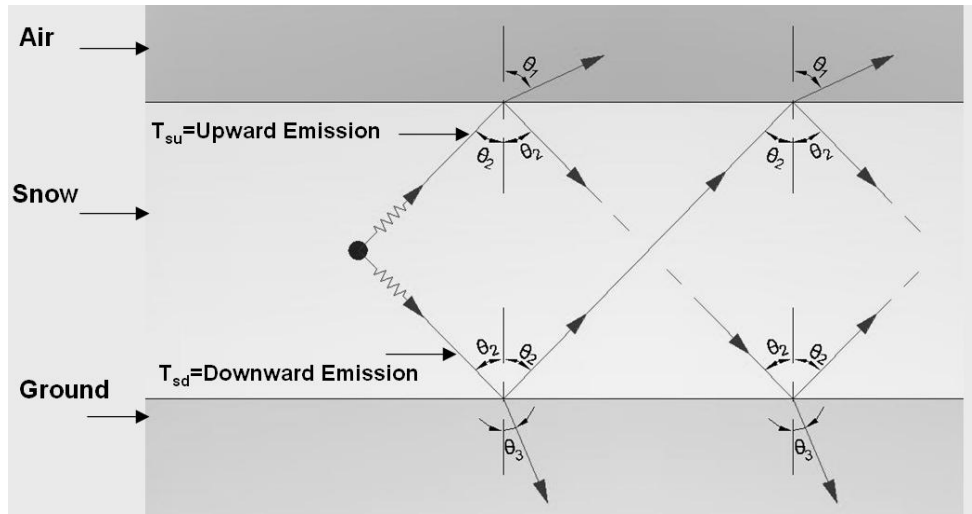


**Figure 3.3 Contribution of snow layer and ground emissions to  $T_{B,Scene}$**

$T_{B,Snow}$  can be written as

$$T_{B,Snow} = T_{su} + T_{sd} \quad (3.7)$$

where  $T_{su}$  is the upward emission;  $T_{sd}$  is the downward emission in snow layer. Upward emission in snow layer can be formulated as:

$$T_{su} = \frac{(1-\Gamma_1)T_{ss}}{1 - \frac{\Gamma_1\Gamma_2}{L^2}} \quad (3.8)$$

where  $\Gamma_1$  is reflectivity at air snow boundary;  $\Gamma_2$  is the reflectivity at ground snow boundary; the snow cover loss factor  $L$  is:

$$L = e^{(\kappa_e - q\kappa_s)d \sec \theta_2} \quad (3.9)$$

where  $\kappa_e$  is extinction coefficient,  $\kappa_s$  is scattering coefficient,  $d$  is snow depth.

$T_{ss}$  in equation (3.8) is:

$$T_{ss} = (1-a)T_{SnowPhys} \left[ 1 - \frac{1}{L} \right] \quad (3.10)$$

where  $T_{SnowPhys}$  is physical temperature of snow layer;  $a$  is single scattering albedo and given in equation (3.11).

$$a = \frac{\kappa_s}{\kappa_e} \quad (3.11)$$

Downward emission in snow layer can be formulated as:

$$T_{sd} = \frac{\Gamma_2(1-\Gamma_1)T_{ss}}{L(1-\frac{\Gamma_1\Gamma_2}{L^2})} \quad (3.12)$$

$T_{B,Grnd}$  can be calculated by equation (3.13).

$$T_{B,Grnd} = \frac{(1-\Gamma_1)(1-\Gamma_2)T_{GrndPhys}}{L(1-\frac{\Gamma_1\Gamma_2}{L^2})} \quad (3.13)$$

where  $T_{GrndPhys}$  is the physical temperature of underlying soil.

By using equations (3.8) to (3.13) scene brightness temperature can be written as:

$$T_{B,Scene}(\theta_1, p) = \frac{1-\Gamma_1}{1-\frac{\Gamma_1\Gamma_2}{L^2}} \times \left[ \left(1 + \frac{\Gamma_2}{L}\right) \left(1 - \frac{1}{L}\right) (1-a)T_{SnowPhys} + \frac{1-\Gamma_2}{L} T_{GrndPhys} \right] \quad (3.14)$$

where  $p$  donates for polarization.

### **3.2 Sensitivity Analysis of HUT Model**

Accuracy of the parametric values given inside model during calibration effects the correlation in between the measured and calculated brightness temperatures (Butt and Kelly, 2008). A sensitivity analysis of the model to input parameters such as ground surface, atmosphere and snow surface conditions was performed in order to determine each parameter impact over modeled brightness temperature. This analysis was done for frequencies for both horizontal and vertical polarizations that are available in AMSR-E spectral range. Details of AMSR-E instrument are given in Chapter 2.3. The range of variations of the considered parameters depends on the possible values as shown in Table 3.1. Each parameter under consideration was changed in between given range while the other parameters were fixed to a preset value which is also given in Table 3.1. The standard deviations of modeled brightness temperature for each parameter in given range for selected frequencies are tabulated in Table 3.2 for horizontal polarization and in Table 3.3 for vertical polarization. The sensitivity analysis plot of each parameter is given in Figure 3.4 to Figure 3.15.

**Table 3.1 Range and prefixed values of parameters used for sensitivity analysis.**

<b>Parameter</b>	<b>Range</b>	<b>Increment</b>	<b>Prefixed Value</b>
Ground Temperature(°C)	-10.0 to +4.0	1.0	-1.0
Ground Moisture Content (%)	0.00 to 0.20	0.01	0.01
Ground Roughness(m)	0.00 to 0.003	0.0002	0.002
Air Temperature(°C)	-15.0 to +4.0	1.0	-10.0
Pressure(mbar)	950.0 to 1100.0	5.0	1000.0
Water Vapour(g/cm <sup>3</sup> )	5.0 to 10.0	0.5	7.5
Snow Salinity(%)	0.00 to 0.20	0.1	0.00
Snow Temperature(°C)	-10.0 to 0.0	1.0	-3.0
Snow Density(g/cm <sup>3</sup> )	0.05 to 3.50	0.01	0.25
Snow Moisture(%)	0.00 to 0.20	0.10	0.00
Snow Grain Size(mm)	0.30 to 2.00	0.10	1.00
Snow Depth(m)	0.10 to 1.50	0.10	0.50

**Table 3.2 Standard deviation of modeled brightness temperature for vertical polarization frequencies.**

<b>Parameter</b>	<b>6.925</b>	<b>10.65</b>	<b>18.7</b>	<b>23.8</b>	<b>36.5</b>	<b>89</b>
Ground Temperature	3.77	3.74	3.32	2.84	2.31	0.13
Ground Moisture Content	0.65	0.57	0.42	0.32	0.21	0.01
Ground Roughness	0.89	0.79	0.66	0.53	0.36	0.01
Air Temperature	0.09	0.12	0.39	0.81	0.35	0.66
Pressure	0.02	0.02	0.01	0.01	0.32	2.31
Water Vapour	0.00	0.00	0.15	0.51	0.49	5.57
Snow Salinity	0.00	0.00	0.00	0.01	0.02	0.07
Snow Temperature	0.03	0.07	0.20	0.31	0.78	2.76
Snow Density	2.70	2.78	3.31	3.68	6.35	17.34
Snow Moisture	0.93	1.55	3.69	4.97	9.64	16.75
Snow Grain Size	3.66	7.50	17.28	22.27	38.38	42.33
Snow Depth	2.97	6.04	13.49	16.90	26.56	16.10

**Table 3.3 Standard deviation of modeled brightness temperature for horizontal polarization frequencies.**

Parameter	6.925	10.65	18.7	23.8	36.5	89
Ground Temperature	3.55	3.53	3.15	2.70	2.20	0.13
Ground Moisture Content	0.74	0.65	0.47	0.37	0.24	0.01
Ground Roughness	1.15	1.19	1.09	0.93	0.73	0.04
Air Temperature	0.08	0.10	0.37	0.79	0.30	0.75
Pressure	0.00	0.00	0.05	0.00	0.40	2.40
Water Vapour	0.01	0.02	0.28	0.77	0.58	5.75
Snow Salinity	0.00	0.00	0.00	0.01	0.02	0.07
Snow Temperature	0.03	0.07	0.20	0.30	0.75	2.64
Snow Density	1.78	1.71	1.20	1.08	3.28	15.69
Snow Moisture	0.73	1.36	3.47	4.72	9.21	16.03
Snow Grain Size	3.50	7.18	16.53	21.30	36.73	40.54
Snow Depth	2.83	5.77	12.87	16.14	25.36	15.39

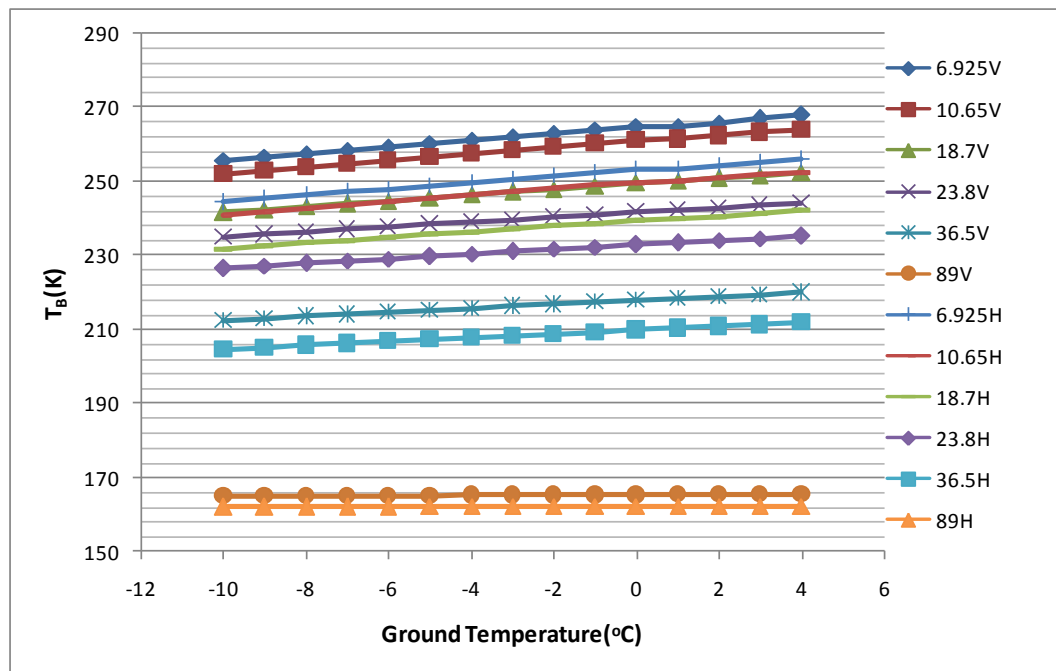


**Figure 3.4 Sensitivity analysis of ground temperature**

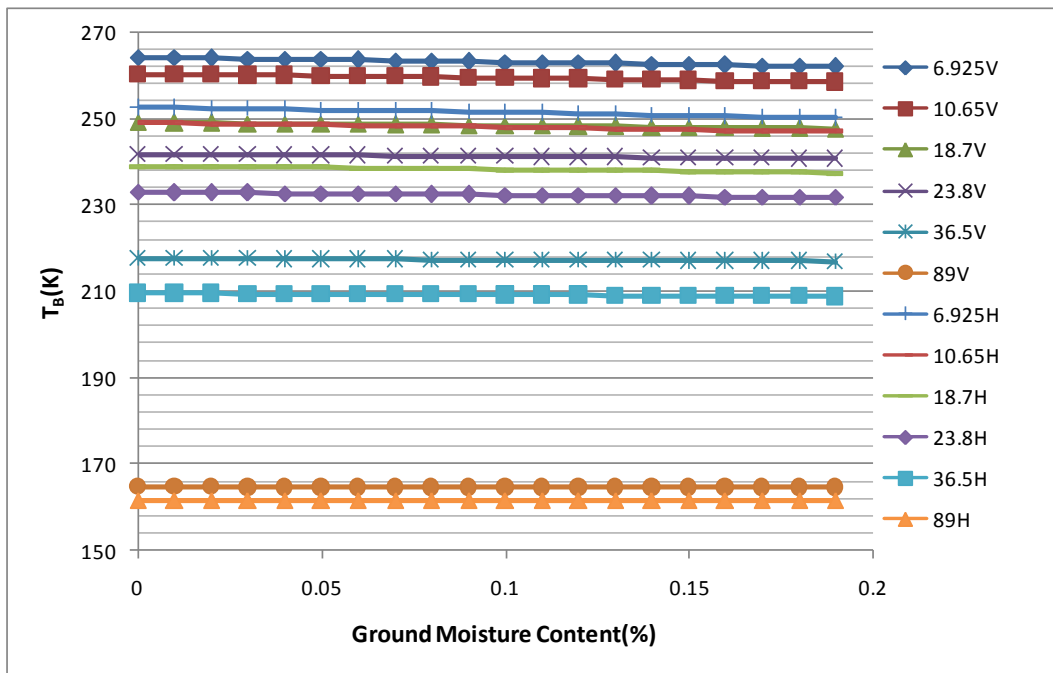


Figure 3.5 Sensitivity analysis of ground moisture

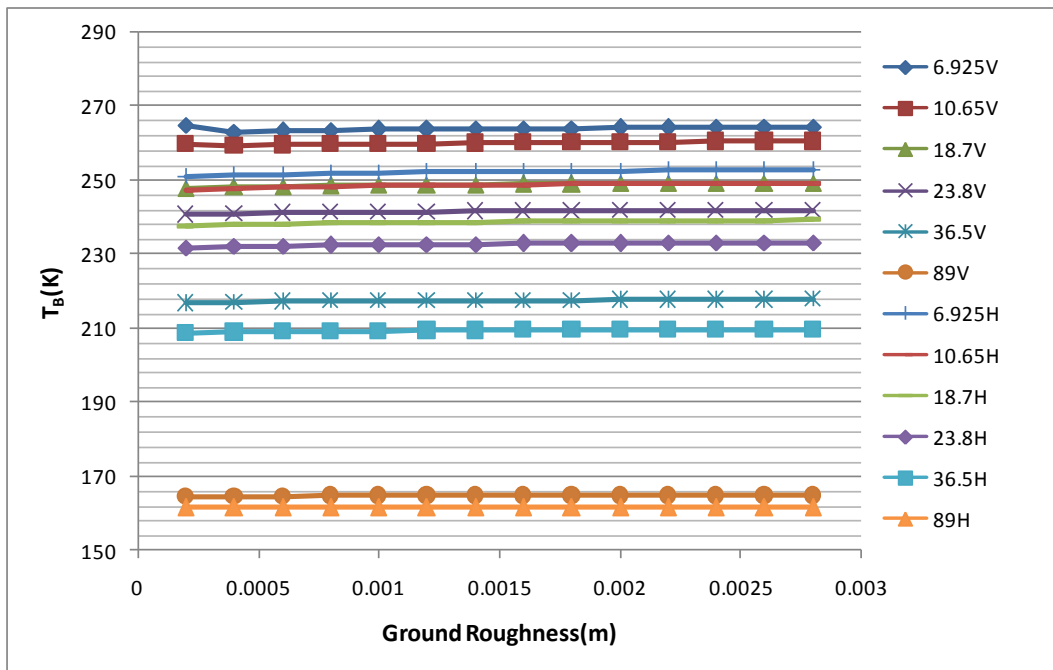


Figure 3.6 Sensitivity analysis of ground roughness

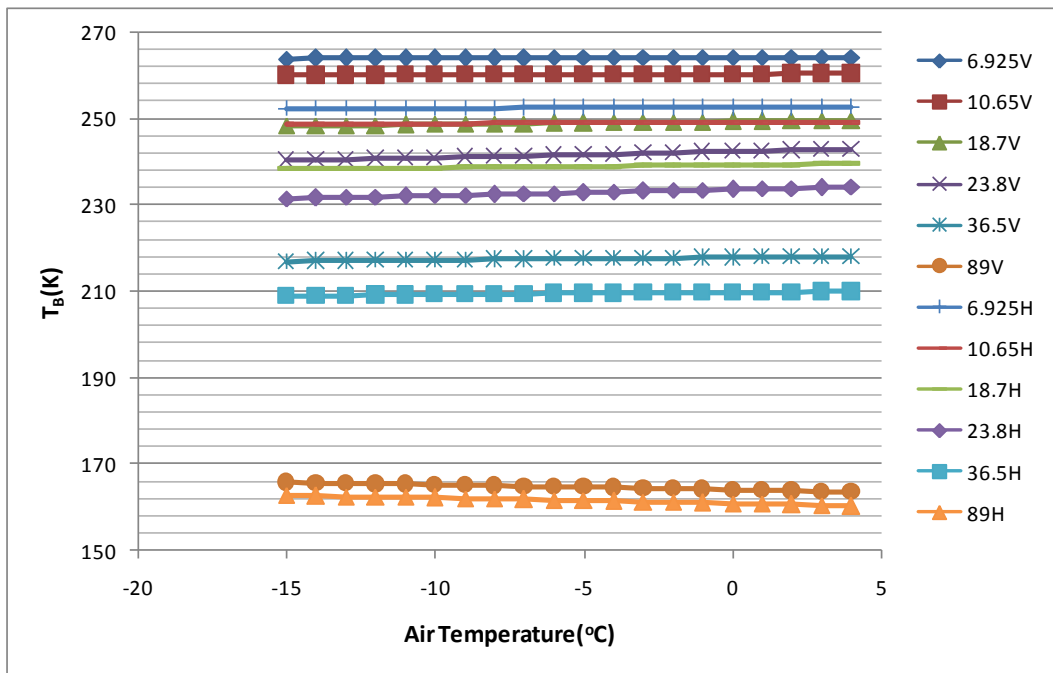


Figure 3.7 Sensitivity analysis of air temperature

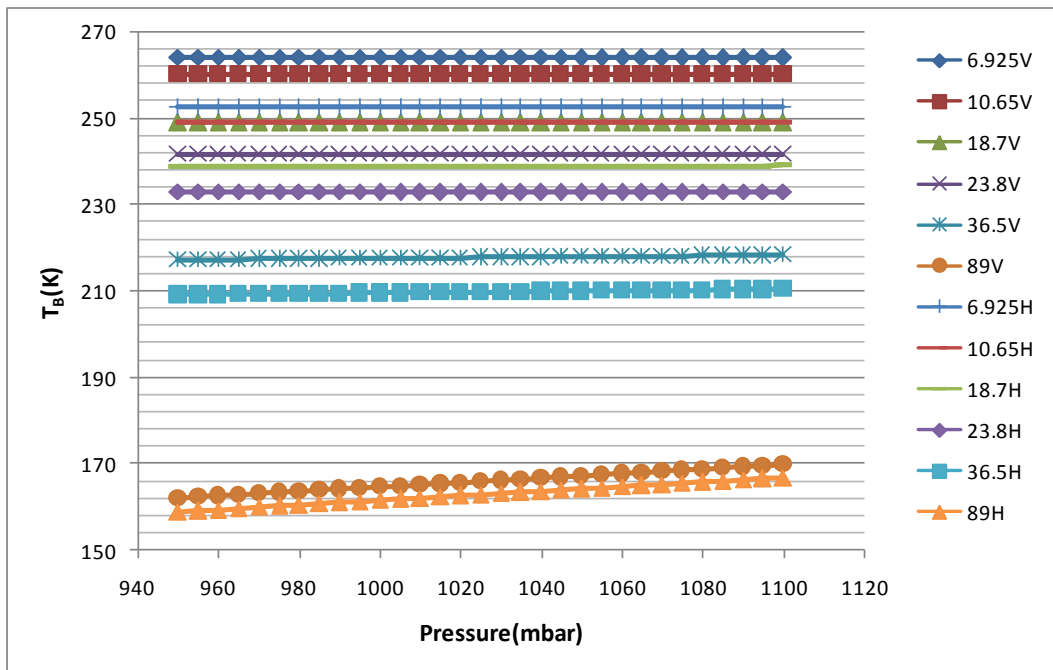


Figure 3.8 Sensitivity analysis of air pressure

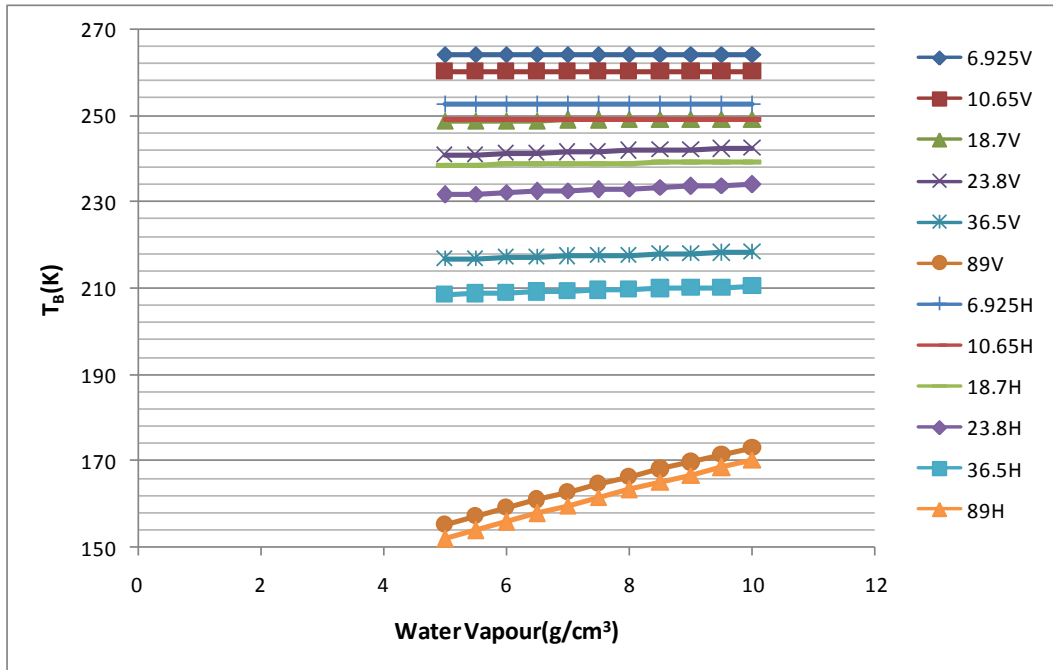


Figure 3.9 Sensitivity analysis of water vapour

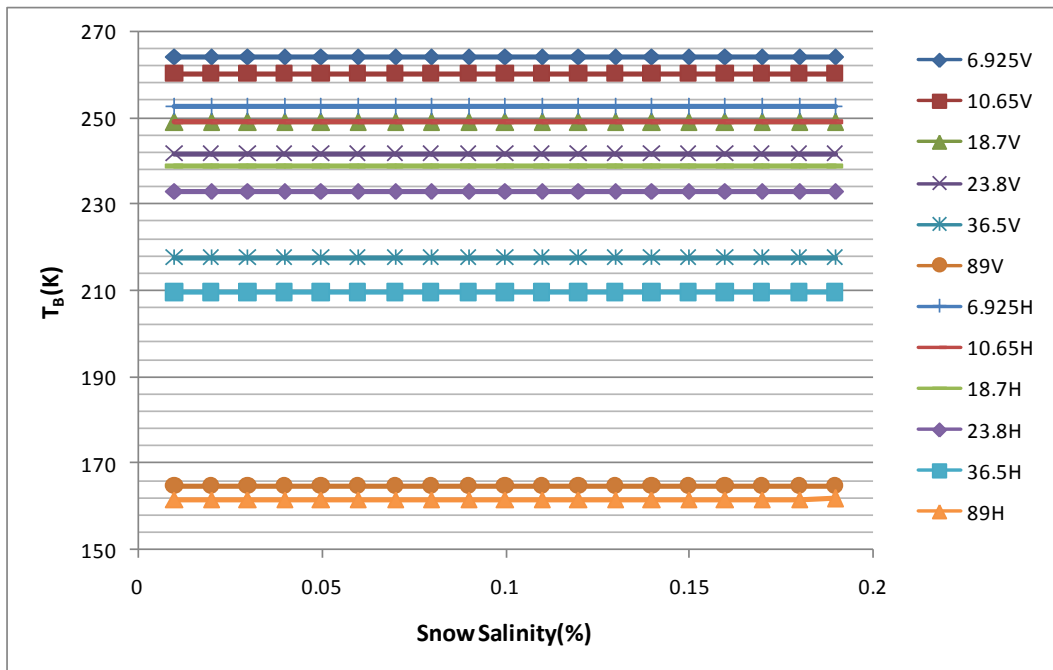


Figure 3.10 Sensitivity analysis of snow salinity



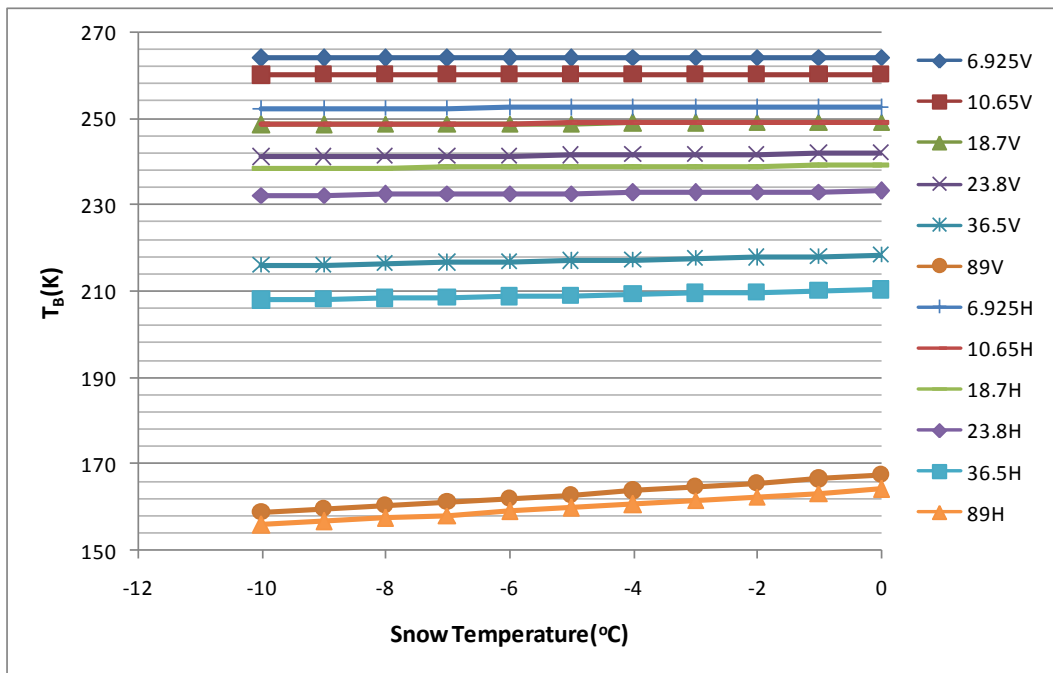


Figure 3.11 Sensitivity analysis of snow temperature

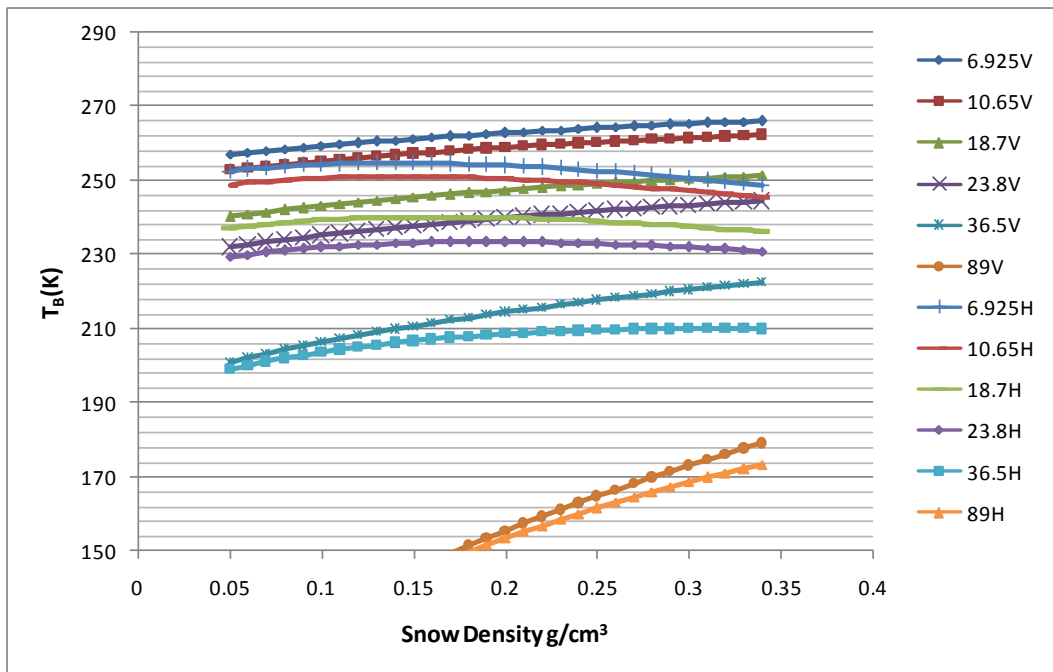


Figure 3.12 Sensitivity analysis of snow density

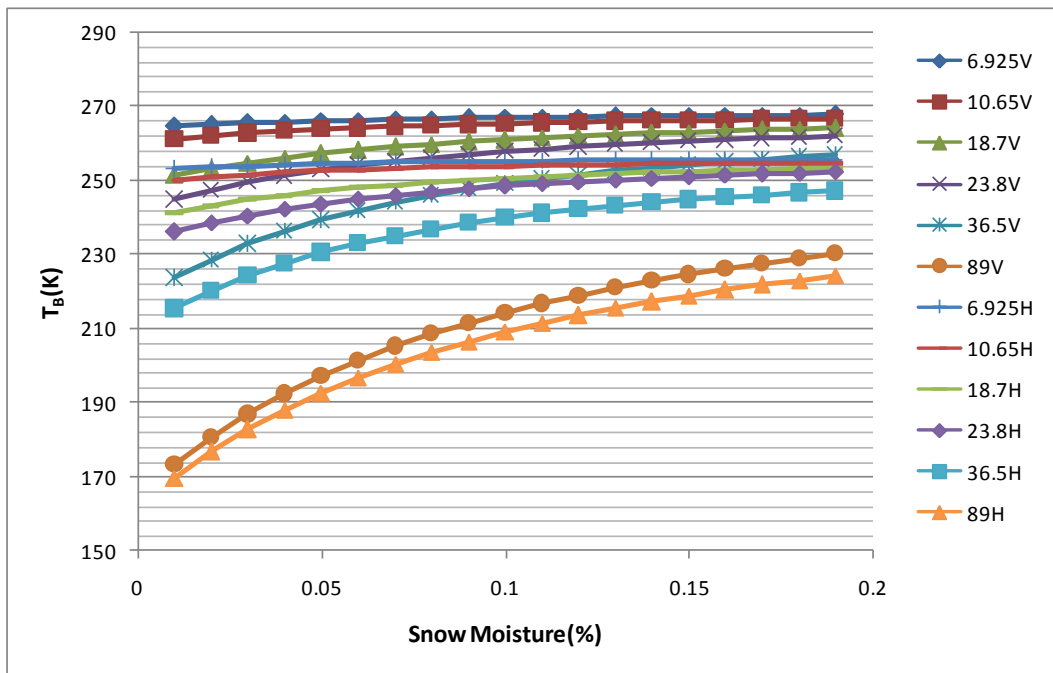


Figure 3.13 Sensitivity analysis of snow moisture

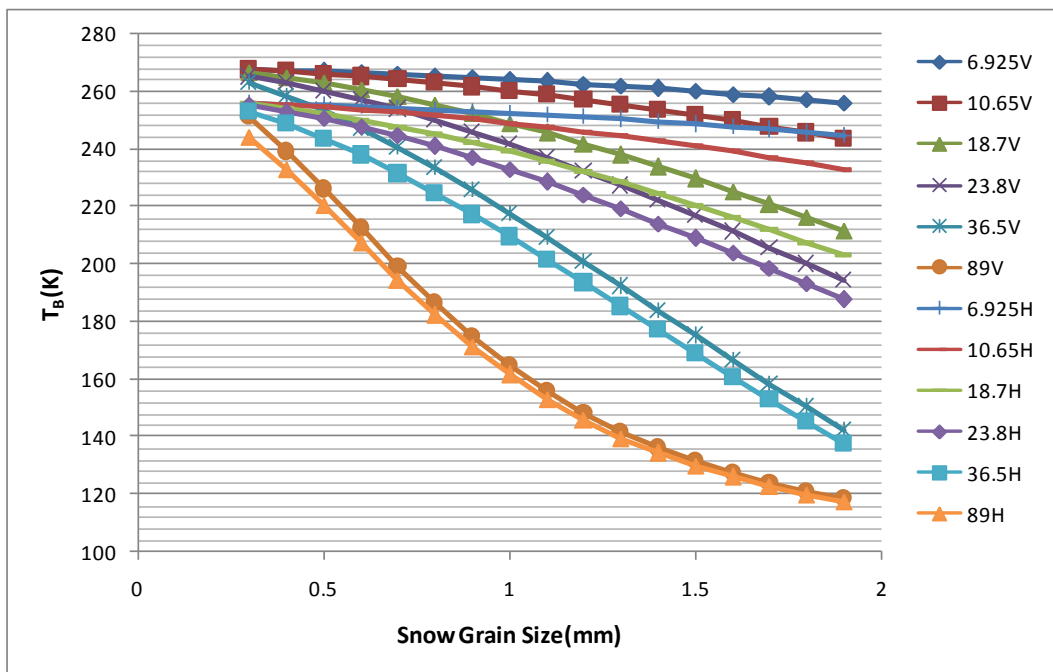
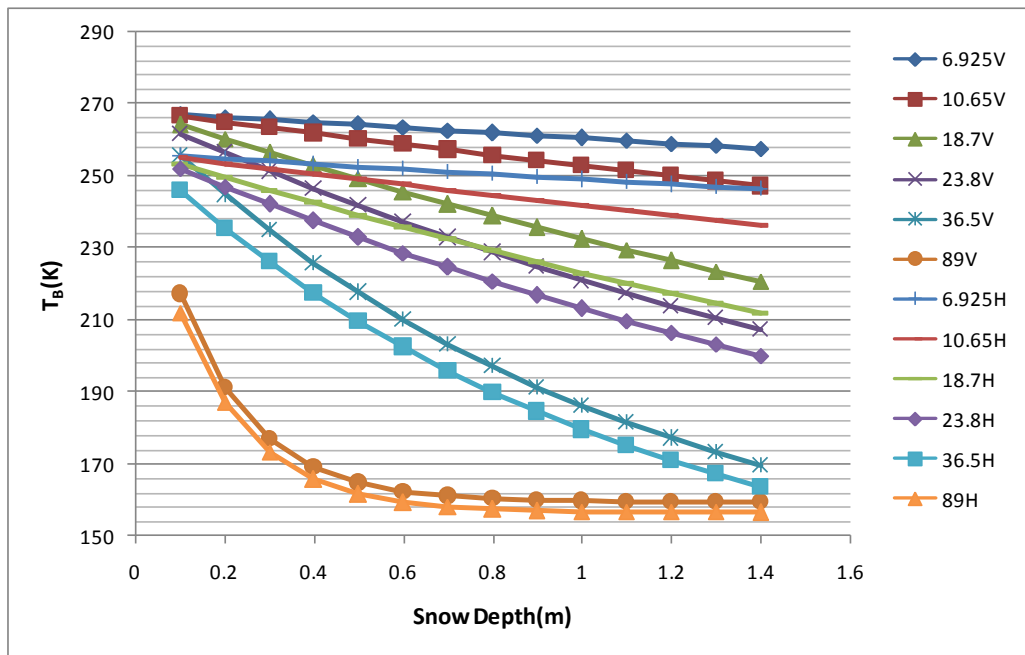


Figure 3.14 Sensitivity analysis of snow grain size



**Figure 3.15 Sensitivity analysis of snow depth**

The sensitivity analysis of the ground parameters show that ground moisture content and ground roughness are insensitive parameters, whilst ground temperature has a significant effect and is a sensitive parameter. Sensitivity of model to ground temperature decreases with increasing frequency for both polarizations because the penetration capability of microwave increases with decreasing frequency. Hence modeled brightness temperature at 6.925 GHz frequency is more sensitive to ground parameters than other frequencies.

Model is not sensitive to atmospheric parameters such as air temperature, air pressure and water vapor for all frequencies except 89 GHz. Atmospheric conditions especially pressure and water vapor amount effect model output significantly at 89 GHz frequency.

The sensitivity analysis of snow surface shows that the snow salinity and snow temperature are considered as insensitive parameters for all frequencies, whereas snow density, snow layer thickness, snow moisture and snow grain size are regarded as sensitive parameters. Sensitivity of model to snow parameters increases with increasing frequencies. The results of the analysis agree well with the work of other research groups such as Tedesco and Kim (2006) and Butt and Kelly (2008).

As a result, based on the sensitivity analysis, among all input parameters of the HUT model, the values of snow depth, snow grain size, snow density and snow moisture contents were the most sensitive parameters to modeled brightness temperature for all frequencies and for both polarizations.

### 3.3 Improvement of HUT Model

Input and output schema of HUT model is given in Figure 3.16. Extinction coefficient  $\kappa_e$  used in the model is based on an experiment done by Hallikainen et al. (1987). He measured properties of 23 snow samples and used 18 of them for determining empirical relationship between extinction coefficient of snow against grain size and frequency. The obtained empirical relationship is given in equation (3.15)

$$K_e = 0.0018f^{2.8}d_o^{2.0} \quad (3.15)$$

where  $d_o$  is grain size in mm and  $f$  is frequency in GHz.

Measured 18 GHz and 35 GHz extinction coefficients for 18 sample of snow coarse and fitted equation by Hallikainen is given Figure 3.17. R-square of fitted equation for 18 GHz is 0.38 and for 35 GHz is 0.85.

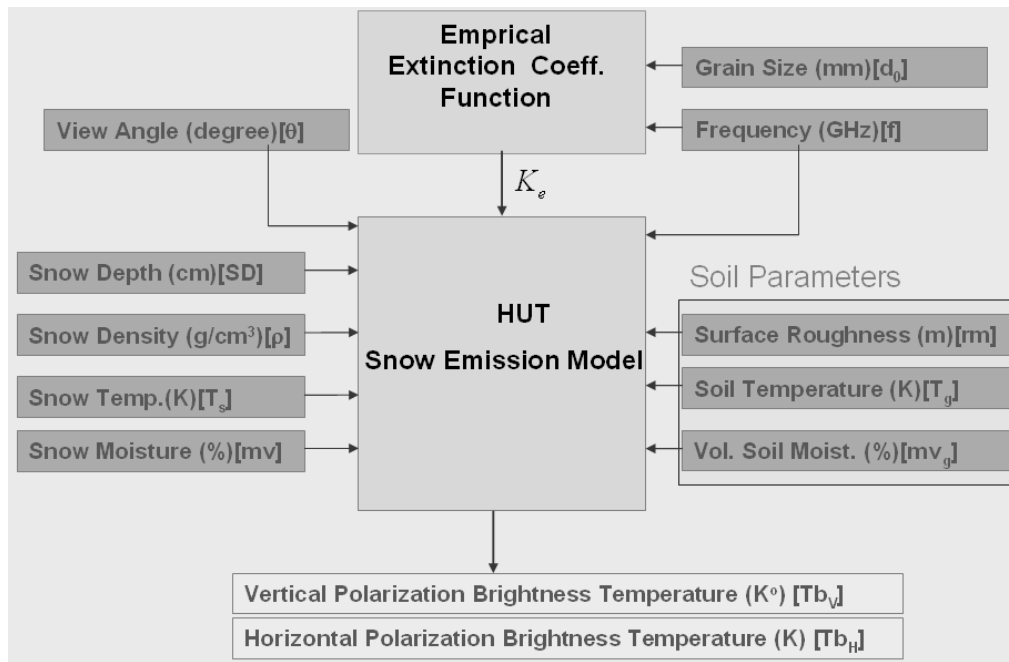


Figure 3.16 Input and output schema of HUT Model

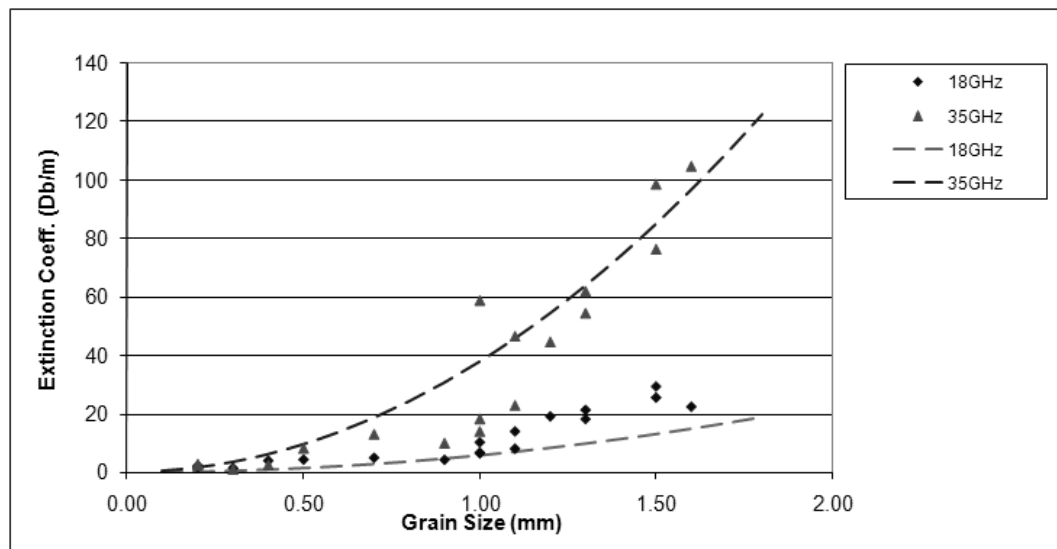
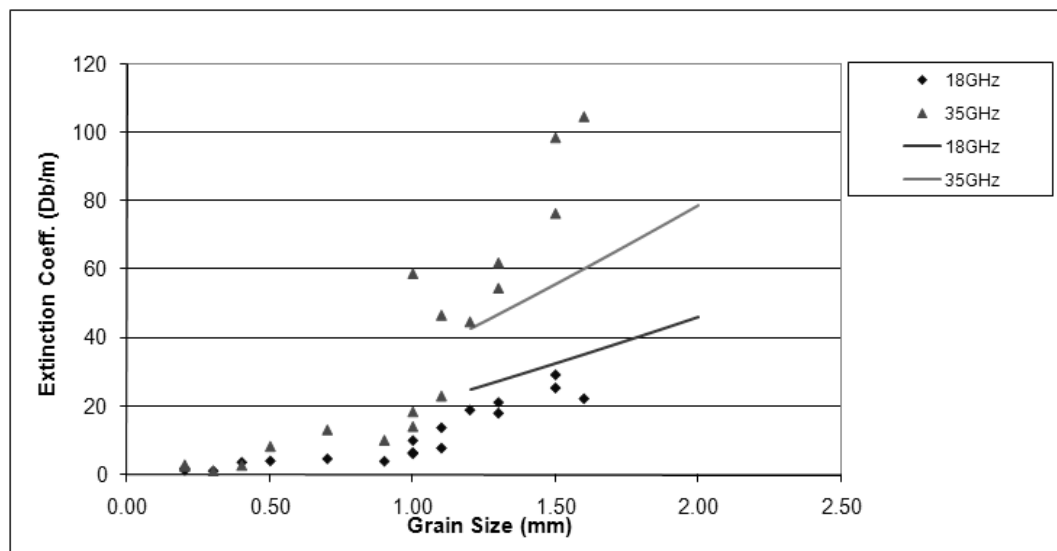


Figure 3.17 Measured extinction coefficients against grain size and fitted equation by Hallikainen et al. (1987)

Roy et al (2004) suggested an equation given in (3.16) for extinction coefficient that is valid for grain sizes in between 1.3 mm and 4.0 mm diameter

$$K_e = 2f^{0.8}d_o^{1.2} \quad (3.16)$$

Measured 18 GHz and 35 GHz extinction coefficients for 18 sample of snow coarse and fitted equation by Roy is given Figure 3.18. There exists no relationship between data and developed function.



**Figure 3.18 Measured extinction coefficients against grain size and fitted equation by Roy et al. (2004)**

Tedesco and Kim (2006) have investigated extinction coefficient versus frequency and grain size relationship for 6 types of snow which are defined by Sturm et. al. (1995) who classified snow into six classes based on

physical properties of snow and climate characteristics. He tested it over Northern Hemisphere. Snow classification map over eastern part of Türkiye and case study basin is given in Figure 3.19. Maritime, prairie and Ephemeral snow classes are observed in the eastern part of Türkiye.

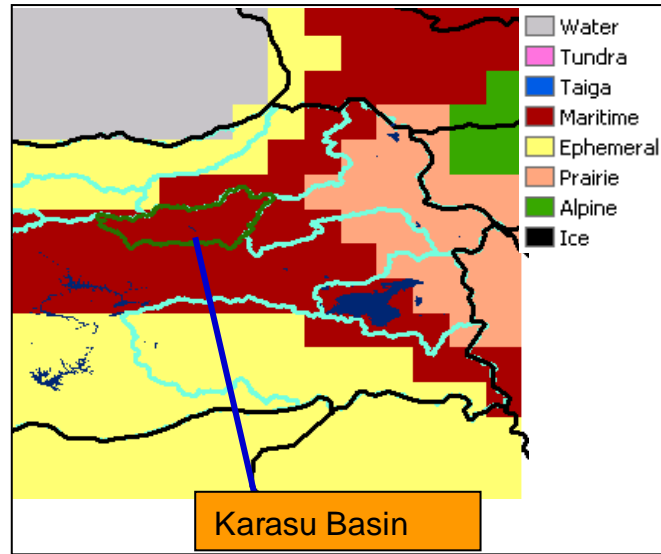


**Figure 3.19 Snow cover classification map over eastern part of Türkiye and case study basin**

Tedesco and Kim (2006) has simulated extinction coefficients for six different snow classes and assumed that extinction coefficient has a relationship with grain size and frequency as given in equation (3.17) He has calculated “ $\alpha$ ” and “ $a$ ” for each tested model namely HUT, DMRT, SFT and MEMLS. Calculated “ $\alpha$ ” and “ $a$ ” are given in Table 3.4 and Table 3.5 respectively.

$$K_e = \alpha f^a d_o^2 \quad (3.17)$$

R-square of each relationship obtained by Tedesco (2006) is calculated against Hallikainen's data. DMRT model based maritime snow class extinction coefficient equation with  $\alpha=0.093$  and  $a=1.75$  gave highest correlation. R-square of fitted equation for 18 GHz is 0.50 and for 35 GHz is 0.65. Snow depth in maritime snow type is generally above 100 cm and density is greater than  $0.30 \text{ g/cm}^3$  and grain size is greater than 0.70 mm.

**Table 3.4 Calculated  $\alpha$  coefficients**

Snow Class	DMRT	HUT	SFT	MEMLS
PR	0.094	0.0018	0.1250	0.4599
TU	0.095	0.0018	0.2312	0.4156
TA	0.094	0.0018	0.0992	0.4348
AL	0.097	0.0018	0.1714	0.5826
MA	0.093	0.0018	0.1760	0.5229
EP	0.092	0.0018	0.3209	0.8333

**Table 3.5 Calculated  $a$  coefficients**

Snow Class	DMRT	HUT	SFT	MEMLS
PR	1.82	2.80	2.44	1.96
TU	0.95	2.80	2.34	1.96
TA	2.96	2.80	2.30	2.01
AL	2.07	2.80	2.25	1.90
MA	1.75	2.80	2.48	1.90
EP	1.79	2.80	2.22	1.82

A new relationship has been proposed in this study for modeling extinction coefficient based on Hallikainen's data and given in equation (3.18):

$$K_e = 0.08f^{1.75}d_o^{1.8} \quad (3.18)$$



Measured 18 GHz and 35 GHz extinction coefficients for 18 sample of snow coarse and fitted equation given in (3.18) is given in Figure 3.20.

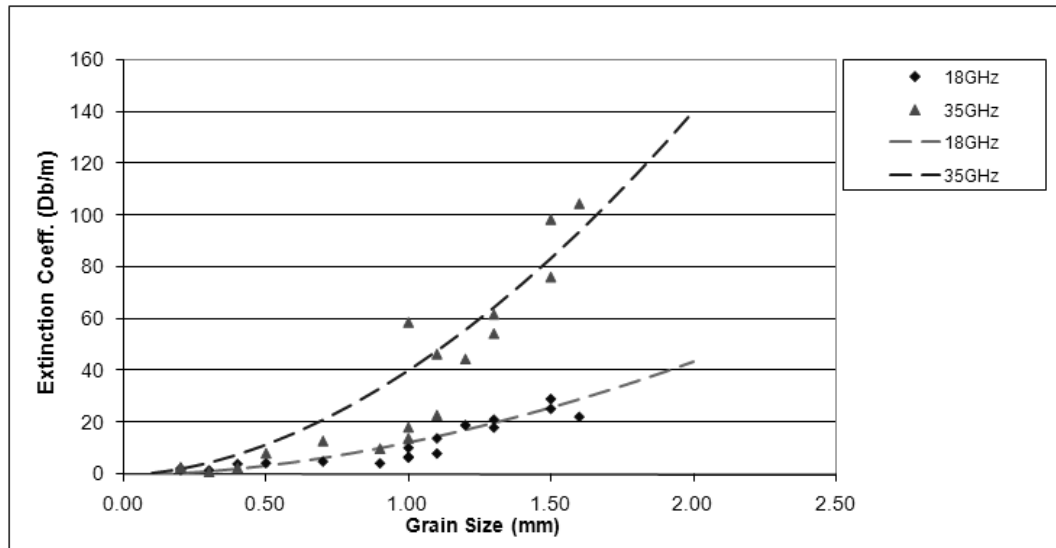


**Figure 3.20 Measured extinction coefficients against grain size and fitted equation given in (3.18)**

R-square of fitted equation given in (3.18) for 18 GHz is 0.83 and for 35 GHz is 0.83.

All of the methods described above tried to express extinction coefficient in the form of (3.19).

$$\kappa_e = \alpha f^a d_o^b \tag{3.19}$$

The  $\alpha$ ,  $a$ ,  $b$  coefficients and obtained R-square values of the fitted equations for 18 GHz and 35 GHz frequencies against Hallikainen's data for each discussed extinction coefficient relationship is summarized in Table 3.6. DMRT model based developed maritime snow class extinction coefficient, which has highest R-square value against experimental data among other studies done by Tedesco and Kim (2006) was only analyzed.

**Table 3.6 Calculated  $a$ ,  $b$ ,  $\alpha$  coefficients and obtained R-square values of fitted equations for 18 GHz and 35 GHz frequencies against Hallikainen's data.**

	$\alpha$	$a$	$b$	$R^2_{18}$	$R^2_{35}$
Equation (3.18)	0.0800	1.75	1.80	0.82	0.82
Roy	2.0000	0.80	1.20	N/A	N/A
Tedesco [DMRT-Maritime]	0.0930	1.75	2.00	0.50	0.65
Hallikainen	0.0018	2.80	2.00	0.38	0.85

Highest R-square values against Hallikainen's data are obtained by proposed equation (3.18) for both 18 GHz and 35 GHz. Extinction coefficient function proposed by Hallikainen can only represent 35 GHz frequency.

### **3.4 Performance of Modified HUT Model**

#### **3.4.1 Ground Snow Data Description**

The snow measurements considered in this study were conducted inside Karasu Basin which is located in the eastern part of Turkey (see Figure 3.19). Snow observations were done by means of Automated Weather Observing Stations (AWOS) which measure snow depth, snow density and snow temperature every 10 minutes.

Hacimahmut, Güzelyayla, Ovacik and Cat stations snow data were used, while evaluating performance of modified HUT model. Elevations of these stations are 1965 m, 2065 m, 2130 m and 2340 m respectively. Layout of AWOS inside basin is given in Figure 3.21. Period of January 1st to March 15th of years 2003-2007 is analyzed. In selected period snow is mostly in dry state.



**Figure 3.21 AWOS located inside Karasu Basin**

### **3.4.2 Satellite Data Description**

During this study, AMSR-E passive microwave Level-2A product data were acquired using National Snow and Ice Data Center (NSIDC) web site.

The AMSR-E Level-2A data includes brightness temperatures measured at 6.9 GHz, 10.7 GHz, 18.7 GHz, 23.8 GHz, 36.5 GHz, and 89.0 GHz. Data are resampled to be spatially consistent, and therefore are available at a variety of resolutions that correspond to the footprint sizes of the

observations such as 56 km, 38 km, 24 km, 21 km, 12 km, and 5.4 km, respectively. Each given swath is stored with associated geolocation fields. Data are stored in Hierarchical Data Format - Earth Observing System (HDF-EOS) format and are available from 19 June 2002 to the present via FTP site of NSIDC. The precision level on these data is approximately 1°K.

### 3.4.3 Comparison Results of Original and Improved Models

The input parameters of the HUT model include the snow pack characteristics (snow depth (SD), density ( $\rho$ ), effective grain size ( $d_0$ ), and temperature( $T_s$ )), soil properties (temperature( $T_g$ ), effective soil surface roughness (RMS) variation( $r_m$ ), moisture content ( $mv_g$ )) and atmospheric conditions (near-surface air temperature ( $T_{atm}$ ), water vapour and pressure). Table 3.7 summarizes typical values of fixed model parameters, as the HUT model was applied to the inversion of space- borne data.

**Table 3.7 Prefixed HUT model parameters**

Parameter	Prefixed Value
Ground Temperature( $^{\circ}$ C)	-1.0
Ground Moisture Content (%)	0.01
Ground Roughness(m)	0.002
Air Temperature( $^{\circ}$ C)	-10.0
Pressure(mbar)	1000.0
Water Vapour( $g/cm^3$ )	7.5
Snow Temperature( $^{\circ}$ C)	-3.0
Snow Moisture(%)	0.00

For any AMSR-E pixel that includes any AWOS, it is assumed that station measured snow depth and density are homogenous inside that pixel.

Therefore only unknown parameter for that pixel is mean grain size of snowpack.

For each station, HUT model was run for every day in given period by changing grain sizes in order to minimize sum of measured and modeled brightness temperature differences at 18.7 GHz and 36.5 GHz vertical channels which are widely used in SWE calculations. HUT model inversion methodology for calculating grain size is given in Figure 3.22. This process was repeated by using four different extinction coefficient relationships that are given in Table 3.6. As a result daily mean grain size for each station for each extinction coefficient relationship was obtained based on station and satellite data. Calculated mean grain sizes for selected period of Hacimahmut, Guzelyayla, Ovacik and Cat stations are given in Table 3.8.

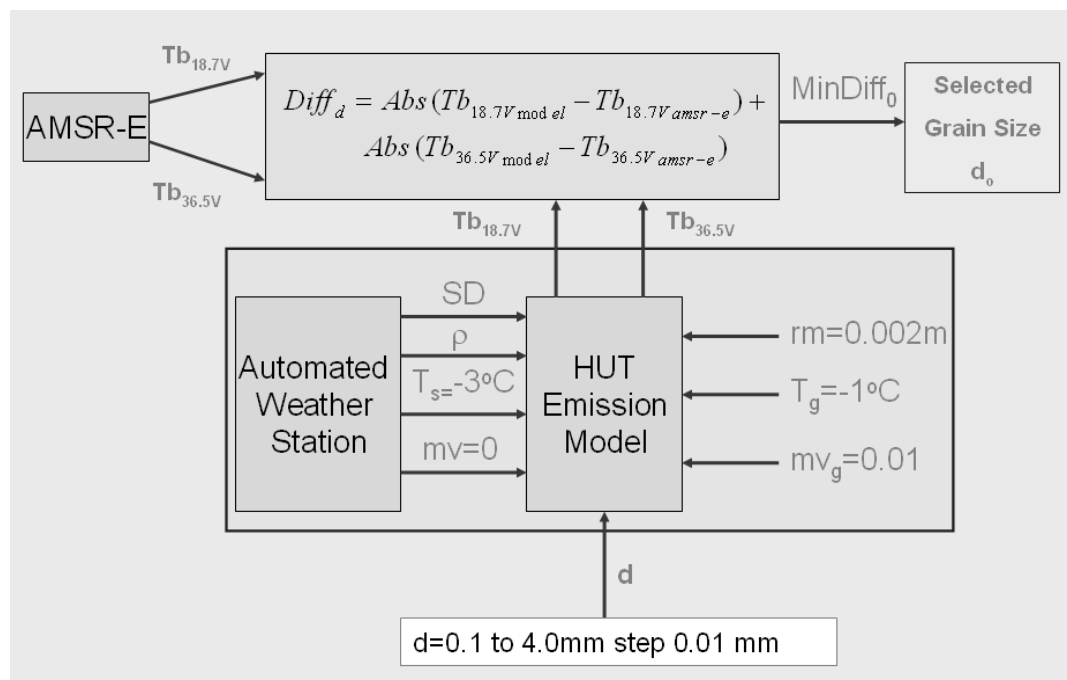


Figure 3.22 Data assimilation schema for obtaining grain size

**Table 3.8 Calculated mean grain sizes for stations over period 2003-2007**

	<b>Hallikainen</b>	<b>Eq-3.18</b>	<b>Roy</b>	<b>Tedesco</b>
2003	0.913	0.890	1.003	0.835
2004	0.838	0.808	0.875	0.763
2005	0.923	0.908	1.030	0.845
2006	0.867	0.843	0.917	0.793
2007	1.003	0.990	1.197	0.917
<b>Average</b>	<b>0.909</b>	<b>0.888</b>	<b>1.004</b>	<b>0.831</b>

It is apparent that Roy's relationship results with greater grain sizes than other relationships used. Tedesco's proposed extinction equation results smallest grain sizes for all stations considered.

For each considered year, mean of model error for channels 18.7 GHz and 36.5 GHz vertical polarization are given in Table 3.9 and Table 3.10 respectively. It is apparent that 36.5 GHz vertically polarized channel is simulated successfully by using all developed extinction coefficient relationships regarding mean error calculated. But at 18.7 GHz vertically polarized channel mean error of HUT with Roy's extinction coefficient is dramatically different than other three approaches. HUT model with extinction coefficient based on Eq. (3.18) and Tedesco's DMRT based maritime climate relationship have lowest mean errors for all stations. It is decided to use HUT model with extinction coefficient relationship given in Eq. (3.18) over mountainous areas located in Eastern part of Turkey where snow classification is mostly maritime based on Sturm's classification.

**Table 3.9 Calculated mean of model error for 18.7 GHz channel for stations over period 2003-2007**

	Hallikainen	Eq-3.18	Roy	Tedesco
2003	4.59	3.35	16.82	3.37
2004	6.41	1.54	14.20	1.57
2005	4.95	4.34	19.47	4.35
2006	7.80	1.34	13.31	1.31
2007	6.68	1.83	11.88	1.80
<b>Average</b>	<b>6.09</b>	<b>2.48</b>	<b>15.13</b>	<b>2.48</b>

**Table 3.10 Calculated mean of model error for 36.5 GHz channel for stations over period 2003-2007**

	Hallikainen	Eq-3.18	Roy	Tedesco
2003	0.28	0.44	0.17	0.39
2004	0.35	0.69	0.44	0.70
2005	0.35	0.37	0.35	0.38
2006	0.26	0.28	0.20	0.33
2007	0.18	0.47	0.14	0.49
<b>Average</b>	<b>0.28</b>	<b>0.45</b>	<b>0.26</b>	<b>0.46</b>

## CHAPTER 4

### DEVELOPMENT OF SNOW WATER EQUIVALENT RETRIEVAL METHODOLOGY

#### 4.1 Density and Grain Size Retrieval Approach

In order to calculate SWE in each domain pixel one should calculate snow density and snow depth for the particular pixel in interest. Calculation of these two parameters can be done by inversion of HUT emission model. Inputs of the HUT model is depicted in Figure 3.16 and prefixed values are listed in Table 3.7. The only unknown model input parameters are snow depth, snow density and effective grain size of snow layer.

Kelly et al. (2003) suggested a globally valid empirical model for determining snow depth (SD) related with brightness temperature difference of vertically polarized channels of 19 GHz and 37 GHz. This relationship is given in equation (4.1) as:

$$SD = \alpha(Tb_{19V} - Tb_{37V}) \Rightarrow SD = \alpha \Delta Tb \quad (4.1)$$

Kelly found coefficient  $\alpha$  in between 1.59 and 1.61 cm/K. A relationship between grain size ( $d_0$ ), snow depth and brightness temperature difference ( $\Delta Tb$ ) of vertically polarized channels 18.7 GHz and 36.5 GHz can be given as in equation (4.2):

$$SD = (ae^{-b(d_0)}) \Delta Tb \Rightarrow \frac{SD}{\Delta Tb} = ae^{-b(d_0)} \quad (4.2)$$



$\alpha$  in equation (4.1) can be written as  $(ae^{b(d_0)})$  regarding equation (4.2). The “a” and “b” coefficients for January, February and March were searched using calculated grain sizes by HUT model with extinction coefficient relationship given in equation (3.18) for 2003-2007 period data described in Section 3.4. Results for January, February and March are plotted in Figure 4.1 to Figure 4.3 respectively. Overall results for each month are tabulated in Table 4.1. All three months correlation coefficients are higher than 0.80. It is interesting that “a” coefficient decreases from January to March where “b” coefficient increases. Calculated mean grain sizes for selected period ranges in between 0.74 to 1.15 mm. If  $\alpha$  coefficient given in equation (4.1) is calculated using “a” and “b” coefficients given in Table 4.1,  $\alpha$  value changes in between 1.05 to 2.68 which includes the values proposed by Kelly et al (2003).

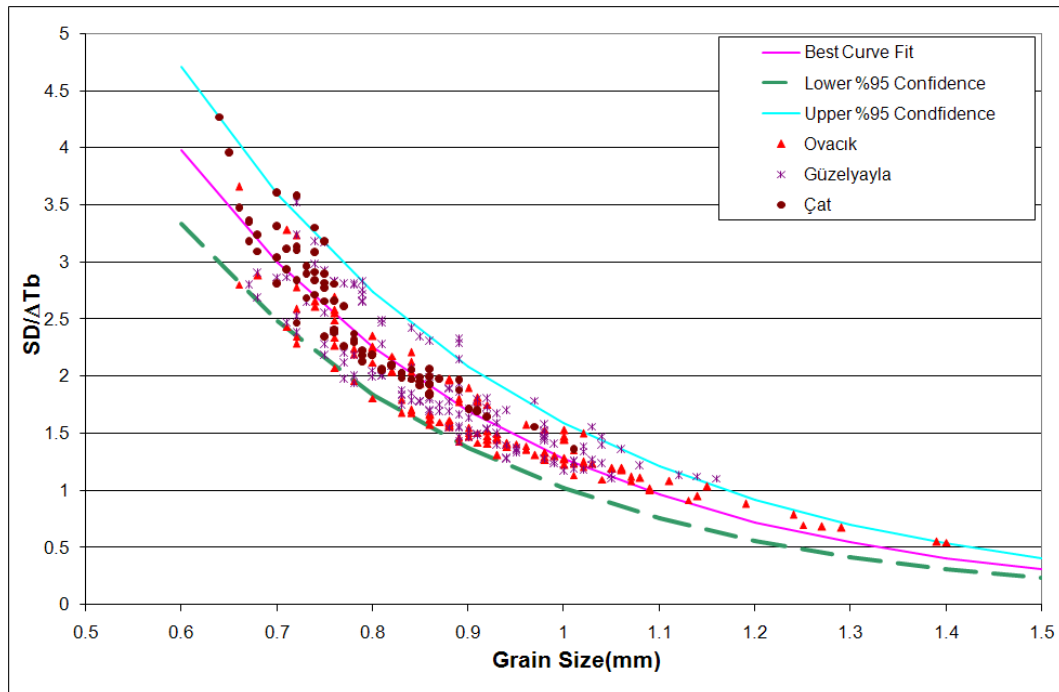


**Figure 4.1 Grain Size versus  $SD/\Delta T_b$  plot for January**

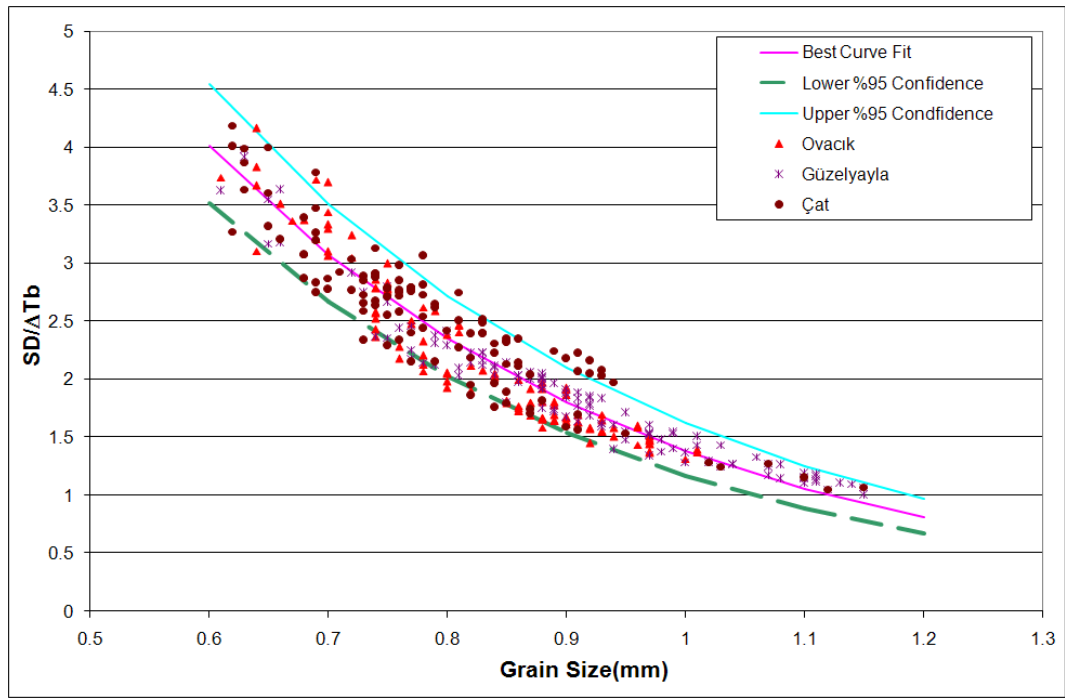


Figure 4.2 Grain Size versus  $SD/\Delta T_b$  plot for February

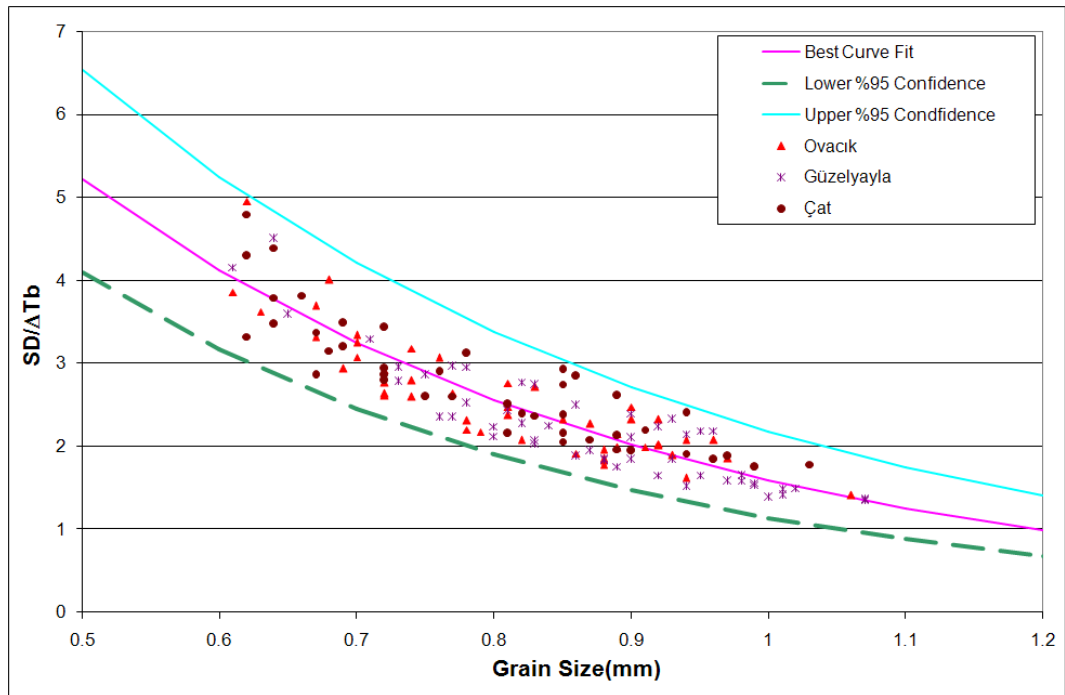


Figure 4.3 Grain Size versus  $SD/\Delta T_b$  plot for March

**Table 4.1 Calculated a and b coefficients for January, February and March**

	<b>a</b>	<b>b</b>	<b>RMSE</b>	<b>R<sup>2</sup></b>	<b>Sample Number</b>
<b>January</b>	21.94	-2.844	0.2344	0.8734	351
<b>February</b>	19.87	-2.666	0.2095	0.9120	341
<b>March</b>	17.14	-2.378	0.3098	0.8289	141

If both side of equation (4.2) is multiplied with snow density and logarithms are calculated equation (4.3) is obtained.

$$\frac{SD}{\Delta Tb} = ae^{bd_0} \Rightarrow \frac{\rho SD}{\Delta Tb} = \rho ae^{bd_0} \Rightarrow \frac{SWE}{\Delta Tb} = \rho ae^{bd_0}$$

$$\ln\left(\frac{SWE}{\Delta Tb}\right) = \ln(\rho) + \ln(a) + bd_0 \quad (4.3)$$

The calculated mean densities using Equation (4.3) for January, February and March of 2003-2007 period using “a” and “b” coefficients were compared by measured densities and the results are given in Table 4.2. Mean error of the calculated densities is 0.01 g/cm<sup>3</sup>. This error amount is approximately 3.7 % of the mean measured density. This validation approach shows that selected “a” and “b” values can be used to calculate grain size of a pixel under consideration where snow depth and vertically polarized brightness temperature difference of 18.7 GHz and 36.5 GHz channels are known.

A relationship between calculated grain sizes and measured densities in the form of equation (4.4) is searched. The power term of grain size is kept as 5 for each investigated month where grain size is measured in mm and density is in g/cm<sup>3</sup>. Calculated x and y coefficients and respective RMSE values are presented in Table 4.3.

**Table 4.2 Calculated and measured snow densities at three AWOS**

	JANUARY		FEBRUARY		MARCH	
	CALC.	MEAS.	CALC.	MEAS.	CALC.	MEAS.
GUZELYAYLA	0.25	0.25	0.27	0.27	0.30	0.30
OVACIK	0.22	0.21	0.25	0.24	0.28	0.28
CAT	0.28	0.30	0.28	0.30	0.30	0.32

$$\rho = xd_0^5 + y \quad (4.4)$$

**Table 4.3 Calculated x, y coefficients and RMSE for equation (4.4)**

Month	x	y	RMSE
JANUARY	-0.0473	0.2797	0.04056
FEBRUAR	-0.0374	0.2871	0.04278
MARCH	-0.0171	0.3015	0.05037

## **4.2 Description of Daily SWE Retrieval Methodology**

### **4.2.1 Satellite Data**

Daily SWE maps were produced by an assimilation technique using modified HUT snow emission model. AMSR-E ease gridded descending brightness temperature data downloaded from NSIDC ftp site was used. NSIDC produces AMSR-E gridded brightness temperature data by interpolating AMSR-E data (6.9 GHz, 10.7 GHz, 18.7 GHz, 23.8 GHz, 36.5 GHz, and 89.0 GHz) to the output grids from swath space using an inverse-distance squared method. AMSR-E/Aqua L2A Global Swath Spatially-Resampled Brightness Temperatures (AE\_L2A) input source

data are used to create the gridded brightness temperature data. These data are provided in three EASE-Grid projections (north and south Lambert azimuthal and global cylindrical) at 25 km resolution. Spatial coverage is global, data are daily, coverage begins 19 June 2002, and processing is ongoing. A sample satellite image of AMSR-E of 36.5 GHz vertical polarization channel is given in Figure 4.4.

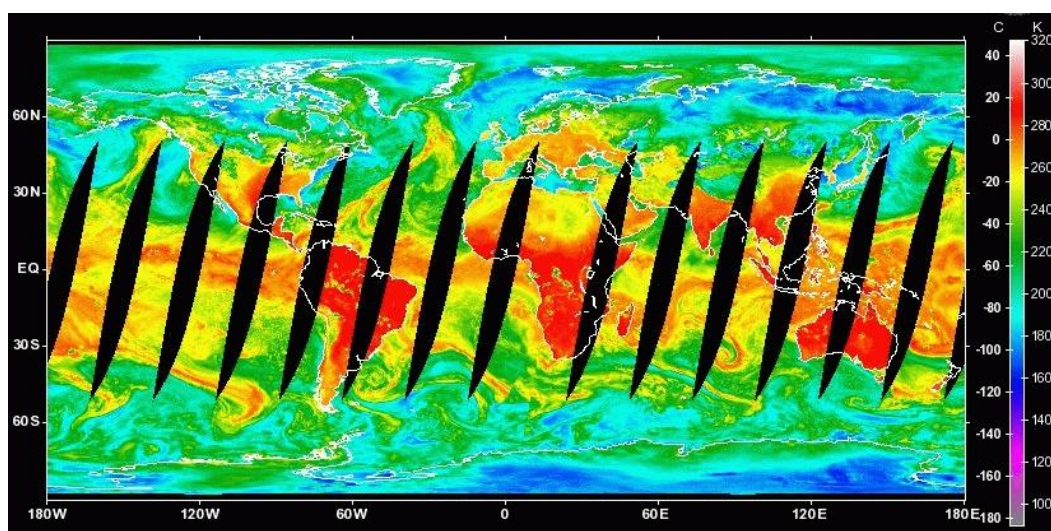


**Figure 4.4 AMSR-E 89 GHz Horizontal Channel Descending Pass Sample Image of 07.02.2009**

#### **4.2.2 Daily SWE Retrieval Methodology**

For every pixel for selected domain, HUT model was run by assuming snow depth from 0.05 m to 1.00 m by 0.05 depth intervals in order to minimize sum of measured and modeled brightness temperature differences at 18.7 GHz and 36.5 GHz vertical channels. During this stage snow grain size was dynamically calculated using Equation (4.2) with

selected empirical coefficients and density was calculated by inserting obtained grain size to Equation (4.4). As a result the depth value which leads to smallest brightness temperature error was selected as that pixels depth value. Density of that particular pixel was also calculated by Equation (4.4). SWE of the pixel is assigned as multiplication of calculated snow depth and density. Developed SWE retrieval methodology is depicted in Figure 4.5. A sample image of a daily SWE map is shown in Figure 4.6 and snow depth map is shown in Figure 4.7.

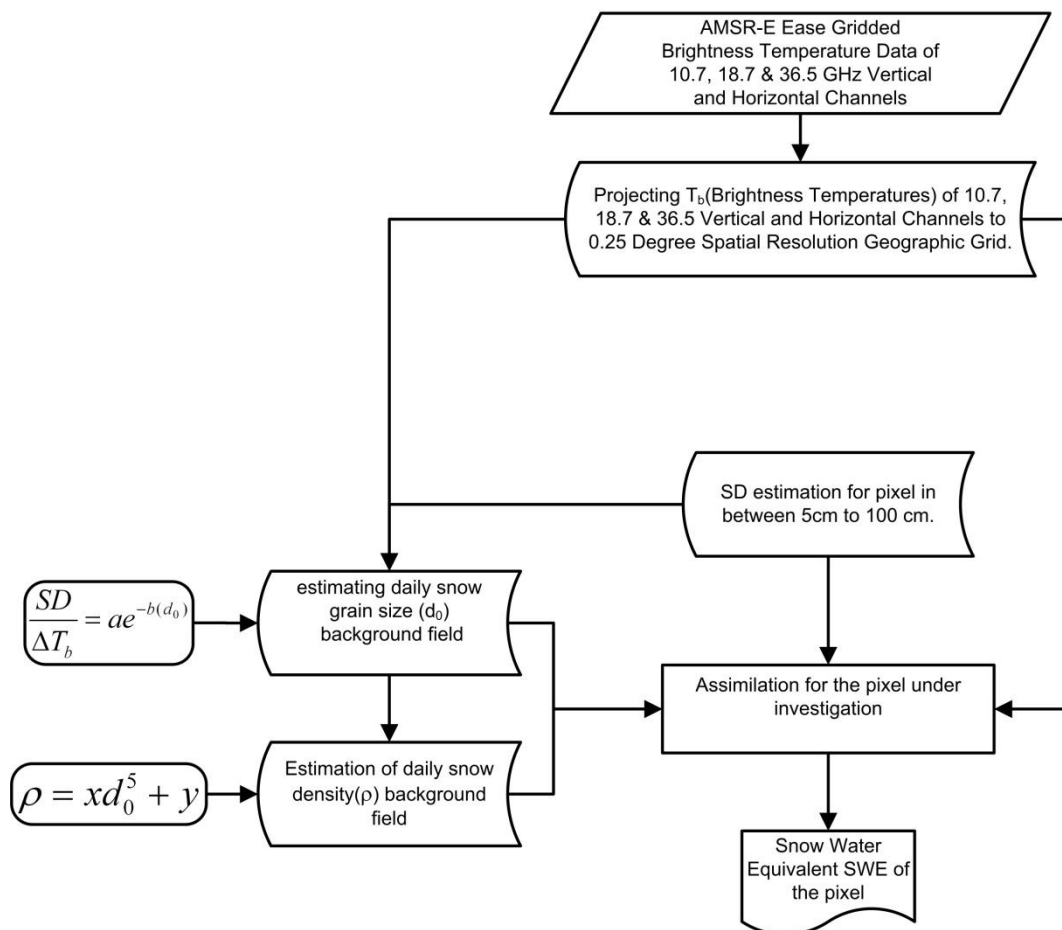


**Figure 4.5 Process flow chart of developed methodology**

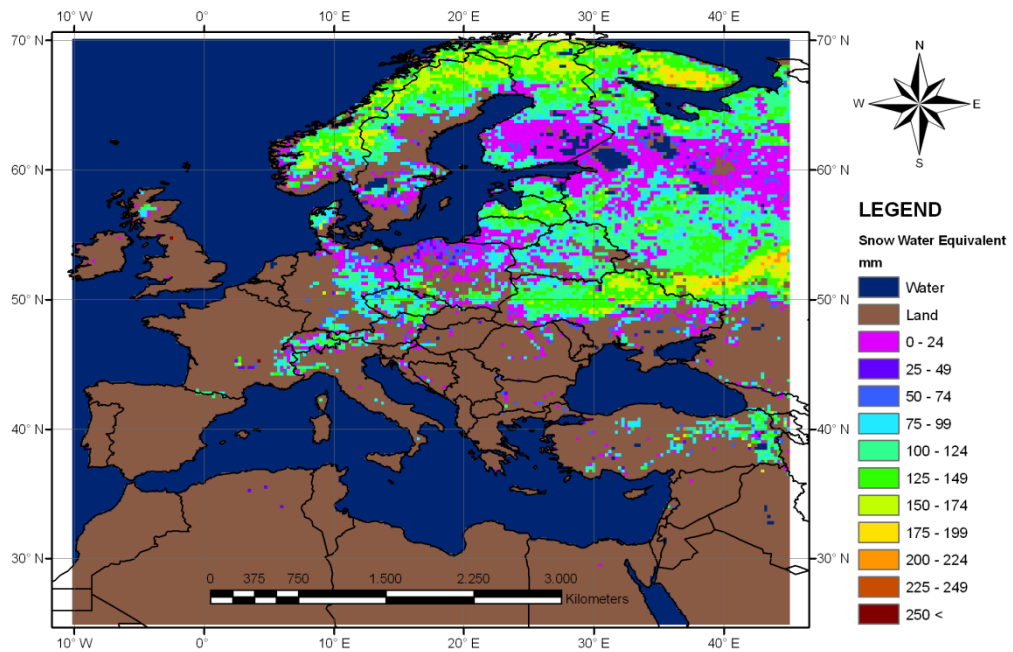


**Figure 4.6 Daily SWE Map of Europe for 24 January 2010**

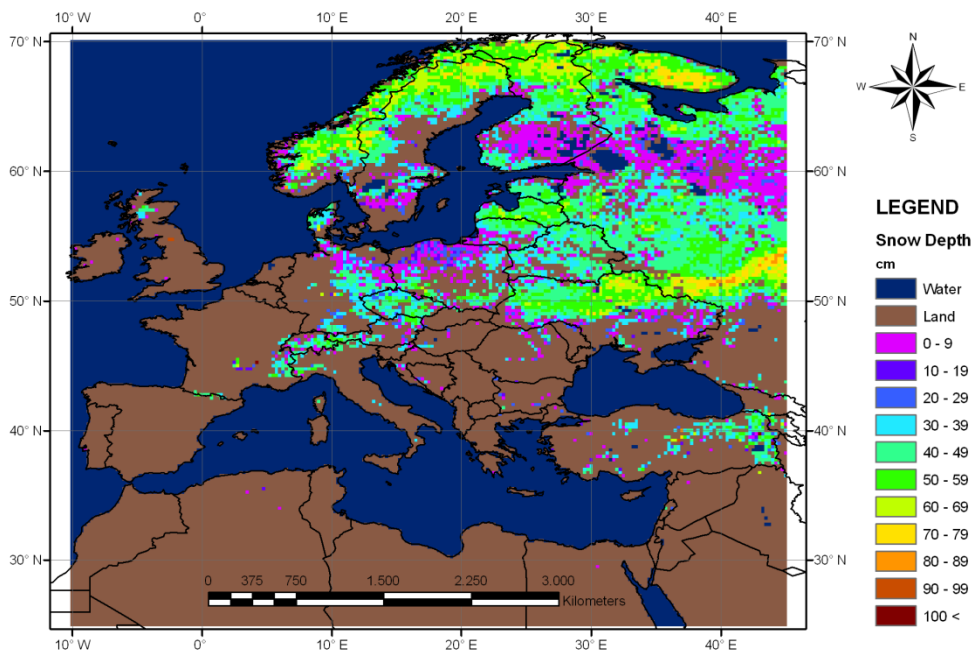


**Figure 4.7 Daily snow depth map of Europe for 24 January 2010**

### **4.3 Validation of Developed Methodology**

#### **4.3.1 Description of Ground Snow Data**

Validation studies were done based on ground truth measured snow depth and snow water equivalent values over eastern part of Turkey. Distribution of 100 snow measurement stations used in validation studies are given in Figure 4.8 over digital elevation model. The 27 of the stations are big climate stations, 16 of them are AWOS, 13 of them are synoptic and the resting 44 are snow course stations. All of the stations measure snow depth but only snow course and some of AWOS measure snow density. None of the stations measure snow grain size and snow moisture.

Landuse map of study area overlaid with validation stations is depicted in Figure 4.9. Landuse map developed by Tateishi et al. (2003) was downloaded from <http://www.gvm.jrc.it/glc2000> web address. There were 31 classes in the original data, but these classes were reduced to four which are forest, pasture, land and water. The main aim of displaying landuse map of the considered area is to visualize vegetation effect during snow covered terrain emission calculations. Brightness temperature calculations are affected by existence of any kind of forest whether evergreen or deciduous. In this study no vegetation effect has been considered during modeling of radiation originated from snow covered terrain, because there exists no forested area in the selected domain which is shown in Figure 4.9.



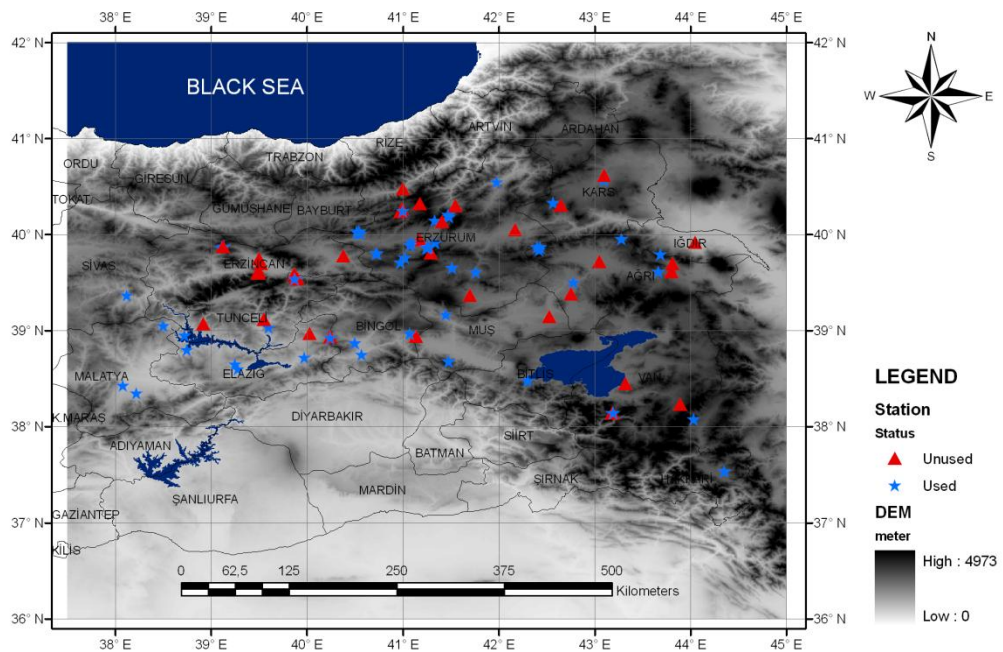


**Figure 4.8 Distribution of stations over digital elevation model**

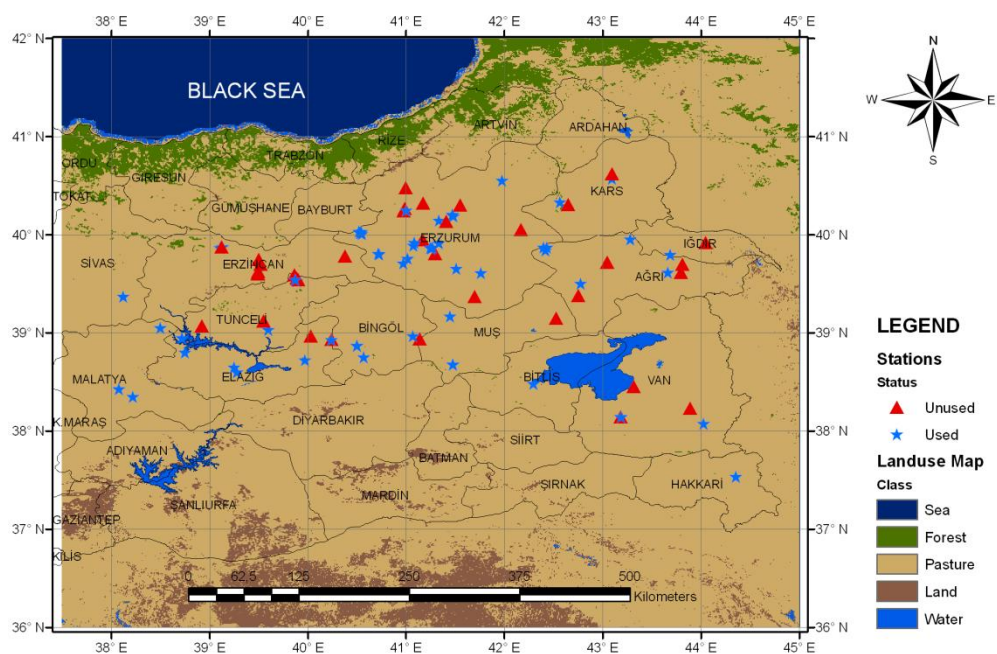


**Figure 4.9 Distribution of stations over landuse**

### 4.3.2 Validation Methodology

All in-situ measurements conducted in between January 1<sup>st</sup> to March 1<sup>th</sup> of 2008-2010 periods were compared individually with the corresponding 25x25 km<sup>2</sup> AMSR-E footprint. For each measurement location the elevation of the snow station was compared against the AMSR-E pixel median elevation where the measurement falls inside it. AMSR-E pixels median elevation map is plotted in Figure 4.10. If the elevation difference between measurement location and pixel elevation median value is greater than 400 meters that weather station or ground measurement was excluded from validation studies. Stations which were excluded during validation studies were colored as red and stations which were used in validation studies were colored as blue in Figure 4.10. Elevation range of 60 selected stations is from 808 meters to 2666 meters. The 14 of the selected stations are big climate stations, 11 of them are AWOS, 7 of them are synoptic and the resting 28 are snow course stations. Selected stations were plotted over Sturm's (1995) snow classification map in Figure 4.11. It is apparent that most of the stations are inside Maritime and Ephemeral snow class.

Developed SWE calculation methodology is valid only for dry snow. Hall et al. (2002) describe a simple algorithm to detect snow status. First they determine snow depth (SD):

$$SD=15.6(Tb_{18.7h}-Tb_{36.5h}) \quad (4.5)$$

where Tb is brightness temperature and subindices denote the channels. If the conditions in equation (4.6) are met, the data is classified as dry snow.

$$SD>80 \text{ and } Tb_{36.5v} <250K \text{ and } Tb_{36.5h} <240K \quad (4.6)$$

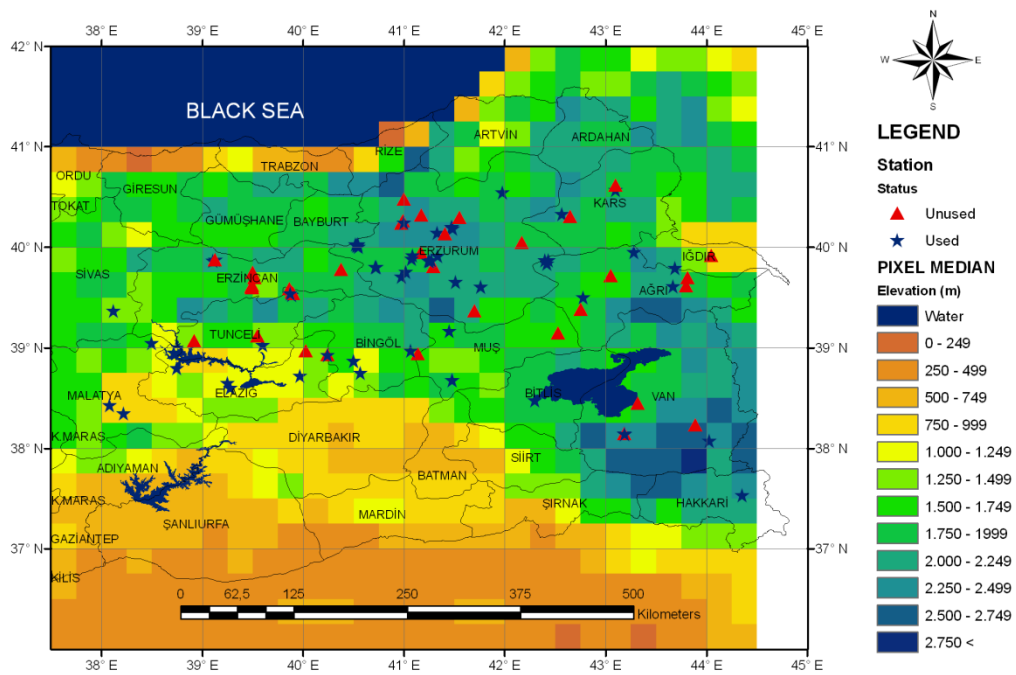


**Figure 4.10** Distribution of stations over AMSR-E pixel median elevation map

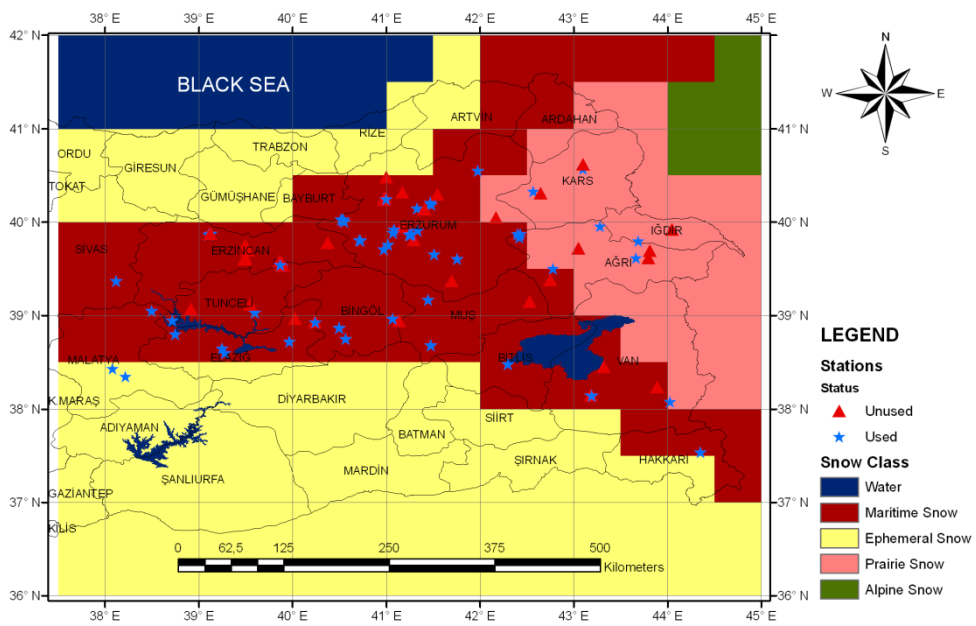


**Figure 4.11** Distribution of stations over snow classification map

### 4.3.3 Validation Results

Among all of the selected validation stations only some of AWOS and snow course stations measure snow water equivalent values. SWE values for stations where snow depth is only measured were calculated by multiplying snow depth of station with average monthly density values obtained among stations which measured density in same period. Therefore assumed average density values based on measured values for January and February is  $0.25 \text{ g/cm}^3$  and  $0.27 \text{ g/cm}^3$  respectively.

Comparison of in-situ measured SD with calculated SD is summarized for years 2008, 2009 and 2010 from Table 4.4 to Table 4.6 respectively. All three years data summary is tabulated in Table 4.7. In these tables measured in-situ snow depth average in between corresponding range is given in column two. The calculated snow depth average value and standard deviation in the given range was calculated and displayed in column three and four respectively. The RMSE value calculated for given range is also given in seventh column of related table. The amount of data pair used in analysis is given in column five. Relative agreement (R.A.) is calculated for given mean values via equation (4.7) as:

$$RA = \frac{SD_{\text{calculated}} - SD_{\text{measured}}}{SD_{\text{measured}}} \times 100 \quad (4.7)$$

Average measured SD versus average calculated SD is plotted in Figure 4.12 to Figure 4.15. The calculated RMSE values for 2008, 2009 and 2010 years are 23.00 cm, 19.77 cm and 16.92 cm respectively. Overall RMSE of three years 838 data pairs is 20.39 cm. RMSE distribution regarding average measured snow depth is demonstrated in Figure 4.16. The measurement counts and absolute RA are also given inside Figure 4.16 respect to average measured SD. It is obvious that RMSE values for SD in

between 0.20m to 0.80m are around average RMSE value. But RMSE values increase while depth is smaller than 0.20 m and depth is greater than 0.80 meters. RMSE and absolute RA values are smallest in between 0.40 to 0.60 m depths. The ground truth measurement count for depths greater than 0.50m is nearly half of the measurement count for depths less than 0.50 m. RA values dramatically increases for snow depths less than 0.30 m. Developed algorithm overestimated SD when compared to the measured SD which is smaller than 0.40 m. On the other hand algorithm underestimated SD when compared to the measured SD which is greater than 0.40 m.

**Table 4.4 Comparison of measured and calculated SD of 2008.**

<b>Range m</b>	<b>Meas. SD m</b>	<b>Calc. SD m</b>	<b>Stand. Dev. m</b>	<b>Data Count</b>	<b>RA %</b>	<b>RMSE m</b>
0.10-0.20	0.15	0.47	0.09	76	209.29	0.3292
0.21-0.30	0.25	0.48	0.11	59	91.74	0.2512
0.31-0.40	0.34	0.51	0.10	28	47.93	0.1924
0.41-0.50	0.43	0.45	0.09	16	4.27	0.0812
0.51-0.60	0.55	0.56	0.10	51	2.43	0.0997
0.61-0.70	0.65	0.58	0.07	23	-10.34	0.1094
0.70-0.80	0.74	0.60	0.03	32	-19.46	0.1490
0.81-0.90	0.83	0.63	0.05	33	-24.73	0.2127
0.91-1.00	0.95	0.59	0.03	8	-37.90	0.3632

**Table 4.5 Comparison of measured and calculated SD of 2009.**

<b>Range m</b>	<b>Meas. SD m</b>	<b>Calc. SD m</b>	<b>Stand. Dev. m</b>	<b>Data Count</b>	<b>RA %</b>	<b>RMSE m</b>
0.10-0.20	0.14	0.38	0.13	47	170.86	0.2731
0.21-0.30	0.26	0.41	0.13	71	54.16	0.1957
0.31-0.40	0.35	0.47	0.11	99	33.21	0.1643
0.41-0.50	0.44	0.40	0.14	85	-8.92	0.1525
0.51-0.60	0.55	0.39	0.14	21	-29.84	0.2164
0.61-0.70	0.64	0.38	0.14	10	-40.49	0.2954
0.70-0.80	0.76	0.57	0.04	7	-24.92	0.1925
0.81-0.90	0.82	0.52	0.09	5	-36.95	0.3145

**Table 4.6 Comparison of measured and calculated SD of 2010.**

<b>Range m</b>	<b>Meas. SD m</b>	<b>Calc. SD m</b>	<b>Stand. Dev. m</b>	<b>Data Count</b>	<b>RA %</b>	<b>RMSE m</b>
0.10-0.20	0.16	0.33	0.12	21	106.47	0.2157
0.21-0.30	0.25	0.33	0.13	39	34.17	0.1529
0.31-0.40	0.35	0.42	0.10	34	21.03	0.1293
0.41-0.50	0.44	0.41	0.14	35	-6.32	0.1475
0.51-0.60	0.54	0.36	0.08	7	-32.04	0.1934
0.61-0.70	0.65	0.49	0.08	17	-24.11	0.1687
0.70-0.80	0.75	0.53	0.04	10	-28.94	0.2191
0.81-0.90	0.81	0.53	0.03	4	-35.58	0.2905

**Table 4.7 Comparison of measured and calculated SD of 2008, 2009 and 2010.**

Range m	Meas. SD m	Calc. SD m	Stand. Dev. m	Data Count	RA %	RMSE m
0.10-0.20	0.15	0.42	0.12	144	181.29	0.2972
0.21-0.30	0.26	0.41	0.13	169	62.40	0.2086
0.31-0.40	0.35	0.47	0.11	161	33.14	0.1630
0.41-0.50	0.44	0.41	0.14	136	-6.70	0.1446
0.51-0.60	0.55	0.50	0.14	79	-9.19	0.1489
0.61-0.70	0.65	0.51	0.12	50	-20.97	0.1807
0.70-0.80	0.74	0.58	0.04	49	-22.20	0.1720
0.81-0.90	0.83	0.60	0.07	42	-27.19	0.2353
0.91-1.00	0.95	0.59	0.03	8	-37.90	0.3632

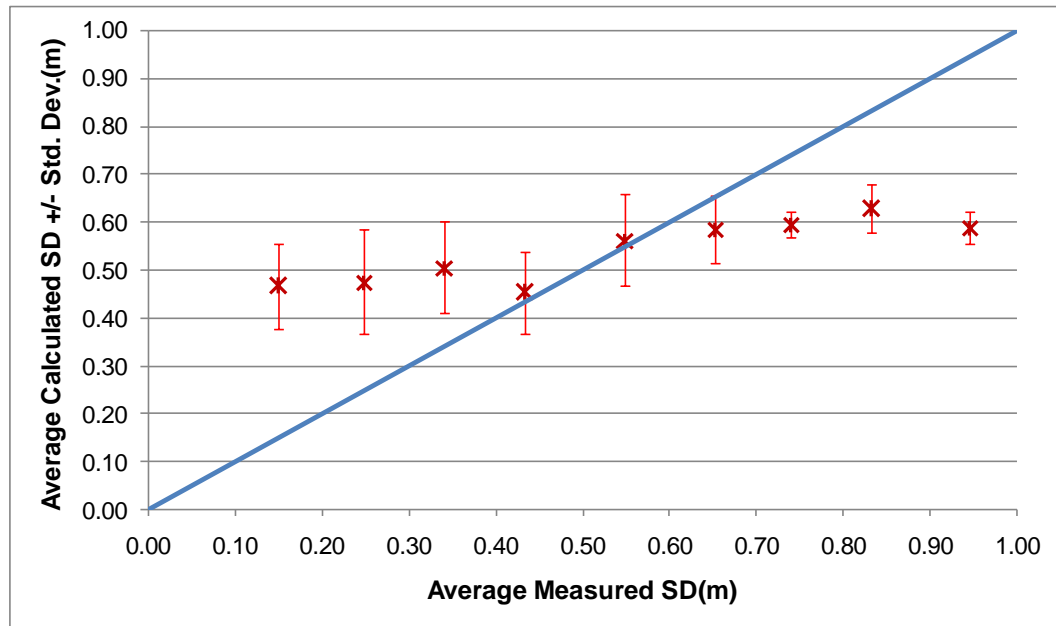


**Figure 4.12 Average calculated SD versus average measured SD of 2008**

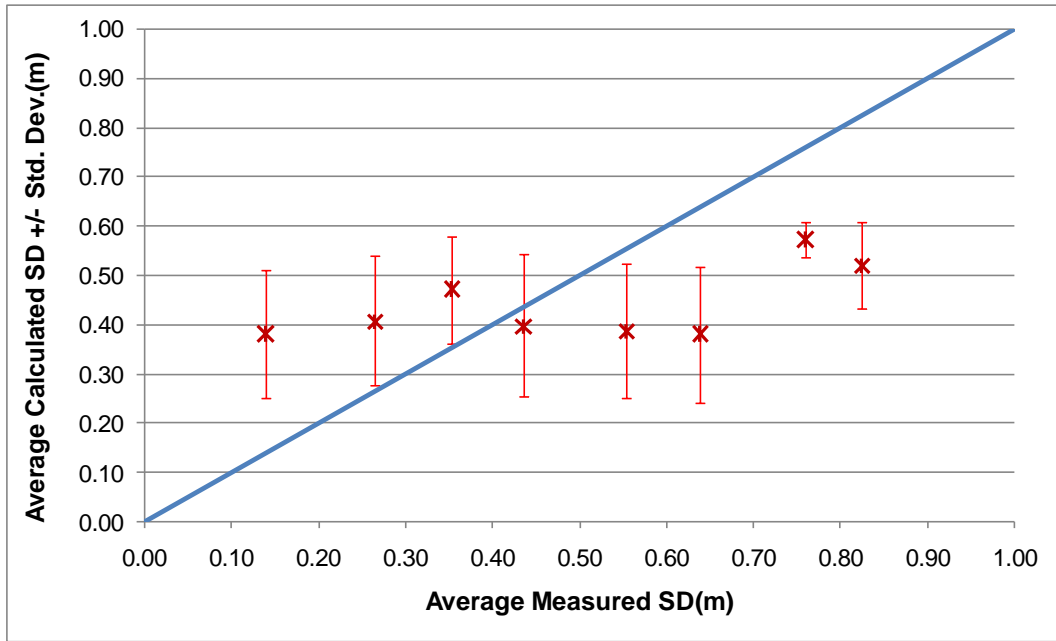


Figure 4.13 Average calculated SD versus average measured SD of 2009

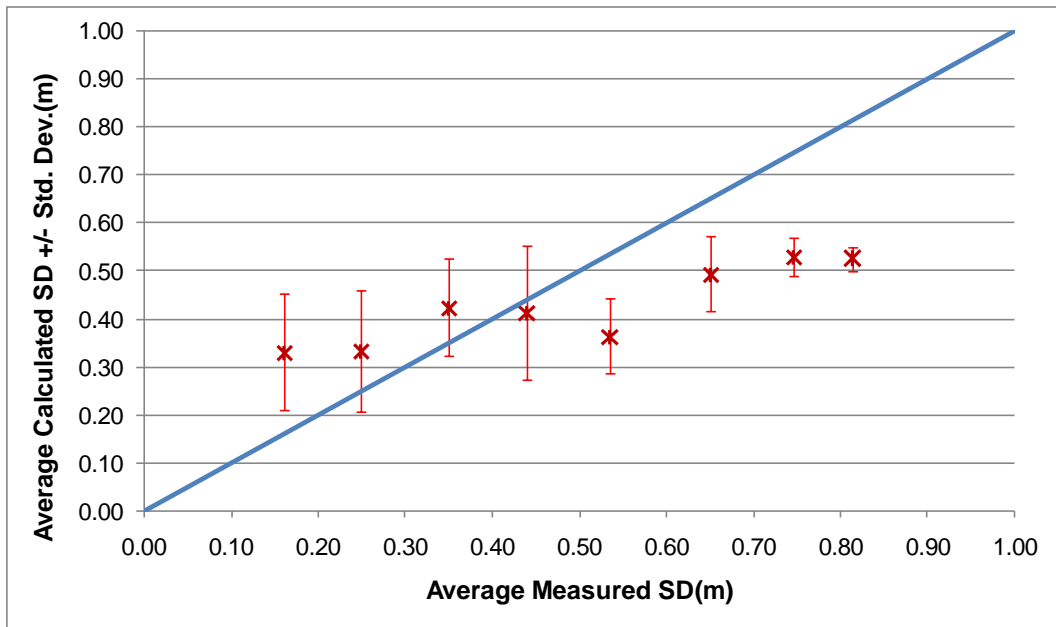


Figure 4.14 Average calculated SD versus average measured SD of 2010



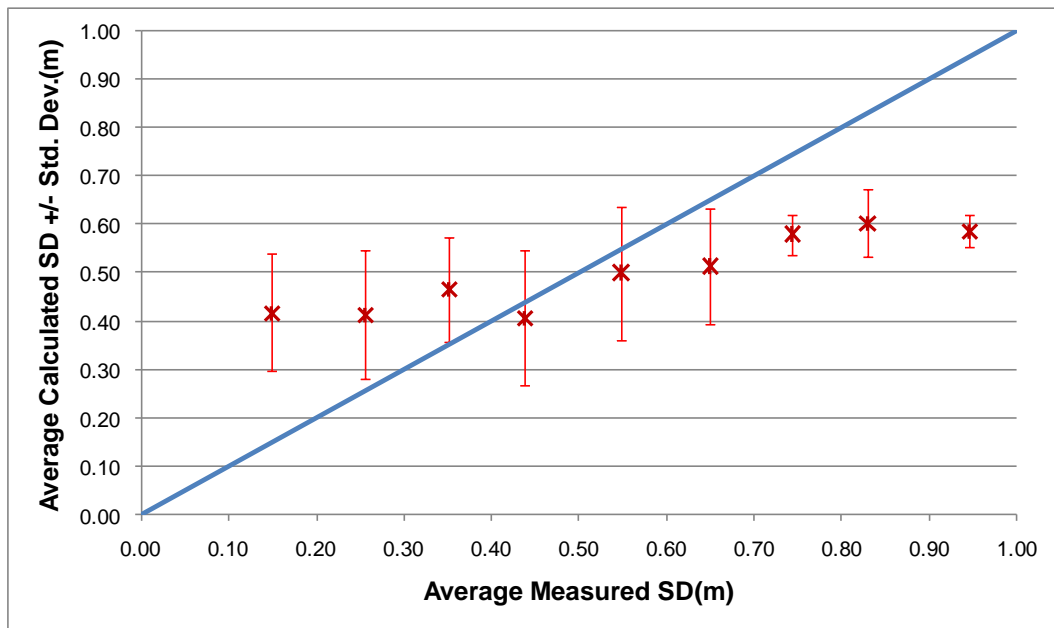


Figure 4.15 Average calculated SD versus average measured SD of 2008, 2009 and 2010.

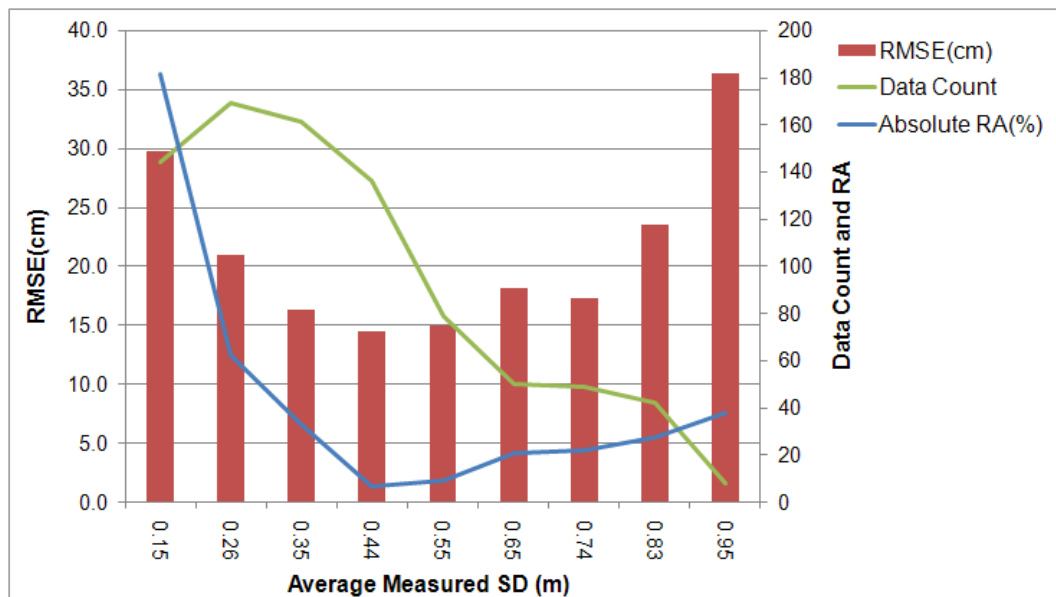


Figure 4.16 Average measured SD versus RMSE, absolute RA and data count.

Comparison of in-situ measured SWE with calculated SWE is summarized for years 2008, 2009 and 2010 in Table 4.8 to Table 4.10 respectively. All three years data summary is tabulated in Table 4.11. In these tables measured in-situ SWE average in between corresponding range is given in column two. The calculated SWE average value and standard deviation in the given range was calculated and displayed in column three and four respectively. The RMSE value calculated for given range is also given in seventh column of related table. The amount of data pair used in analysis is given in column five.

Average measured SWE versus average calculated SWE is plotted in Figure 4.17 to Figure 4.20. The calculated RMSE values for 2008, 2009 and 2010 years are 62.27 mm, 56.51 mm and 45.80 mm respectively. Overall RMSE of three years 838 data pairs is 56.94 mm. RMSE distribution regarding average measured SWE is demonstrated in Figure 4.21. The measurement counts and absolute RA are also given inside Figure 4.21 respect to average measured SWE. It is obvious that RMSE values for SWE in between 75.0 mm to 225.0 mm are under average RMSE value. But RMSE values increase while SWE is smaller than 75.0 mm and SWE is greater than 225.0 mm. RMSE and absolute RA values are smallest in between 100.0 mm to 150.00 mm SWEs. The ground truth measurement count for SWE greater than 125.0 mm is nearly half of measurement count for SWEs less than 125.0mm. RA values dramatically increases for SWE less than 50.0 mm. Developed algorithm overestimated SWE when compared with measured SWE smaller than 100 mm. On the other hand algorithm underestimated SWE when compared with measured SWE greater than 100 mm.

According to the validation results of SD, RMSE value of developed methodology for snow depths in between 0.30 m to 0.80 is 16.12 cm. RMSE values for snow depths beyond this range is 25.88 cm. Similarly

RMSE of SWE in between 75.0 mm to 200.0 mm is 45.16 mm and RMSE for SWE outside of this range is 71.13 mm.

**Table 4.8 Comparison of measured and calculated SWE of 2008.**

<b>Range mm</b>	<b>Meas. SWE mm</b>	<b>Calc. SWE mm</b>	<b>Stand. Dev. mm</b>	<b>Data Count</b>	<b>RA %</b>	<b>RMSE mm</b>
25-50	38.11	125.64	24.34	74	229.66	91.0657
50-75	60.46	125.47	31.89	47	107.52	72.0235
75-100	85.66	140.86	24.03	39	64.44	60.6643
100-125	107.86	126.76	24.07	16	17.52	29.4760
125-150	136.99	151.06	22.82	39	10.27	27.8395
150-175	161.27	156.12	23.26	34	-3.19	24.2719
175-200	192.15	154.54	11.51	31	-19.57	39.0070
200-225	207.71	164.32	12.97	37	-20.89	45.3034
>225	242.69	154.54	7.56	10	-36.32	89.3177

**Table 4.9 Comparison of measured and calculated SWE of 2009.**

<b>Range mm</b>	<b>Meas. SWE mm</b>	<b>Calc. SWE mm</b>	<b>Stand. Dev. mm</b>	<b>Data Count</b>	<b>RA %</b>	<b>RMSE mm</b>
25-50	36.06	102.34	35.96	47	183.78	75.6214
50-75	65.96	113.70	30.57	64	72.40	56.5856
75-100	88.08	122.04	35.44	104	38.56	48.9425
100-125	111.61	103.31	41.41	81	-7.43	43.4342
125-150	133.45	92.86	33.76	16	-30.42	54.2677
150-175	160.55	105.80	43.64	19	-34.11	70.2171
175-200	182.45	93.02	42.34	3	-49.02	96.4230
200-225	210.85	144.07	21.98	9	-31.67	71.0876
>225	230.95	153.91	6.14	2	-33.36	77.4678

**Table 4.10 Comparison of measured and calculated SWE of 2010**

Range mm	Meas. SWE mm	Calc. SWE mm	Stand. Dev. mm	Data Count	RA %	RMSE mm
25-50	40.96	89.23	33.77	21	117.83	60.6046
50-75	63.30	89.19	34.55	38	40.90	43.3302
75-100	87.23	116.96	26.59	30	34.09	40.6705
100-125	111.86	111.42	38.85	38	-0.39	38.9611
125-150	133.59	117.48	40.72	9	-12.06	46.8943
150-175	167.43	124.13	15.74	10	-25.86	46.3100
175-200	187.92	148.47	15.31	14	-20.99	42.6260
200-225	210.34	152.72	18.38	6	-27.39	60.2201
>225	228.69	150.94	0.00	1	-34.00	77.7548

**Table 4.11 Comparison of measured and calculated SWE values of 2008, 2009 and 2010.**

Range mm	Meas. SWE mm	Calc. SWE mm	Stand. Dev. mm	Data Count	RA %	RMSE mm
25-50	37.86	112.54	33.31	142	197.30	82.2048
50-75	63.55	111.17	34.89	149	74.94	59.0800
75-100	87.39	125.40	32.88	173	43.50	50.5614
100-125	111.23	108.37	39.75	135	-2.57	40.7697
125-150	135.63	131.79	38.33	64	-2.83	38.9587
150-175	162.03	135.86	37.70	63	-16.15	46.3175
175-200	190.31	148.92	21.95	48	-21.75	45.7570
200-225	208.56	159.48	17.47	52	-23.53	52.4732
>225	239.81	154.16	7.12	13	-35.71	86.7467

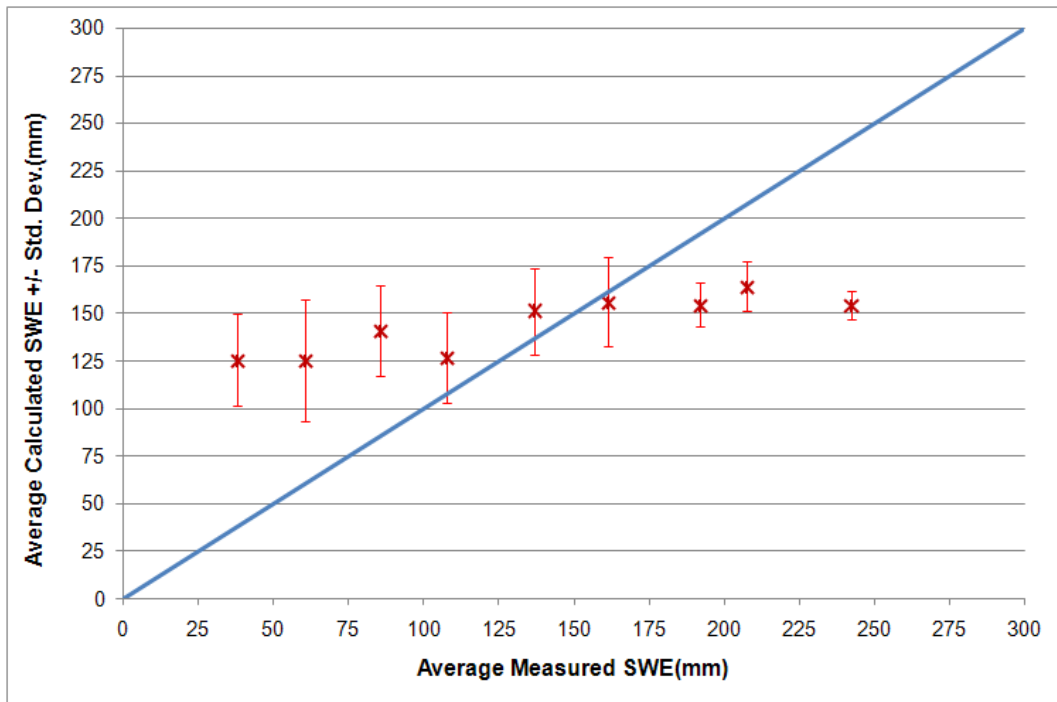


Figure 4.17 Average calculated SWE versus average measured SWE of 2008

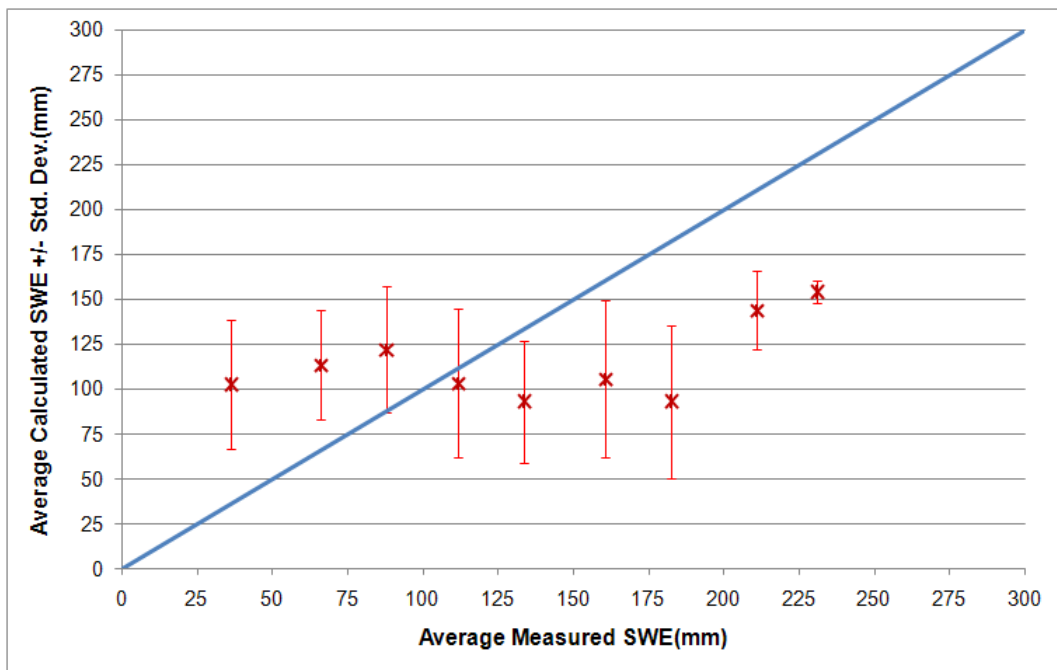
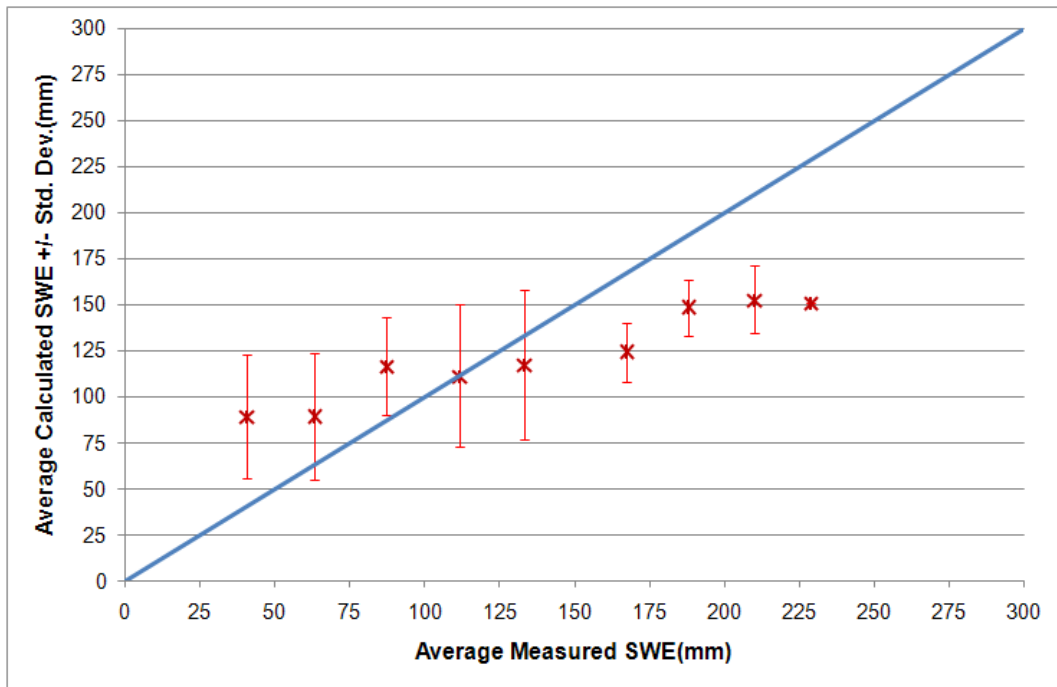
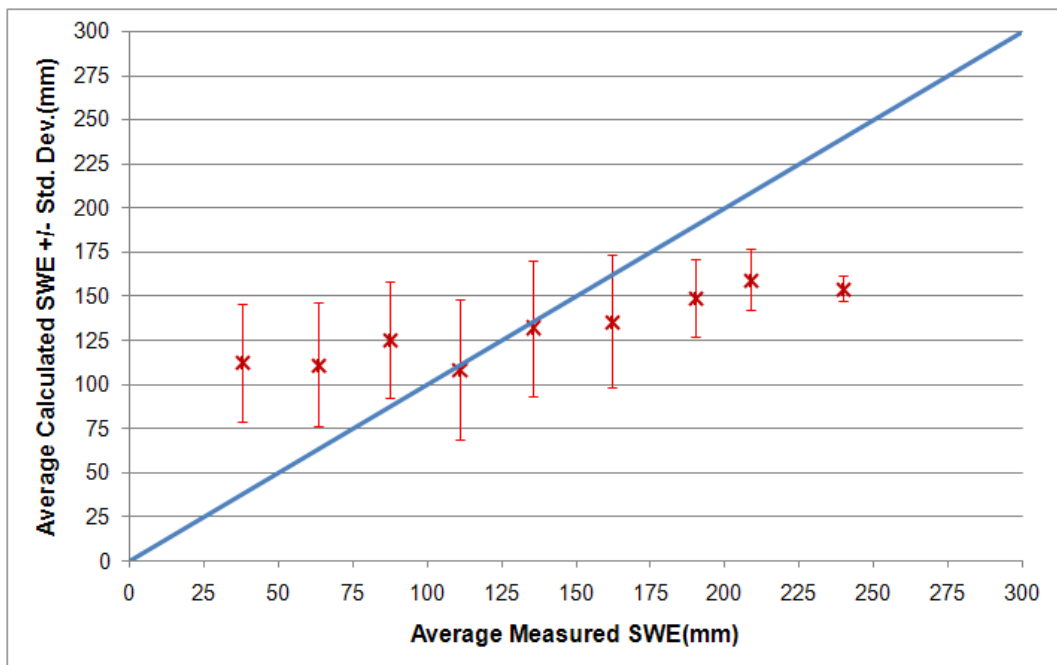


Figure 4.18 Average calculated SWE versus average measured SWE of 2009



**Figure 4.19 Average calculated SWE versus average measured SWE of 2010**



**Figure 4.20 Average calculated SWE versus average measured SWE of 2008, 2009 and 2010.**

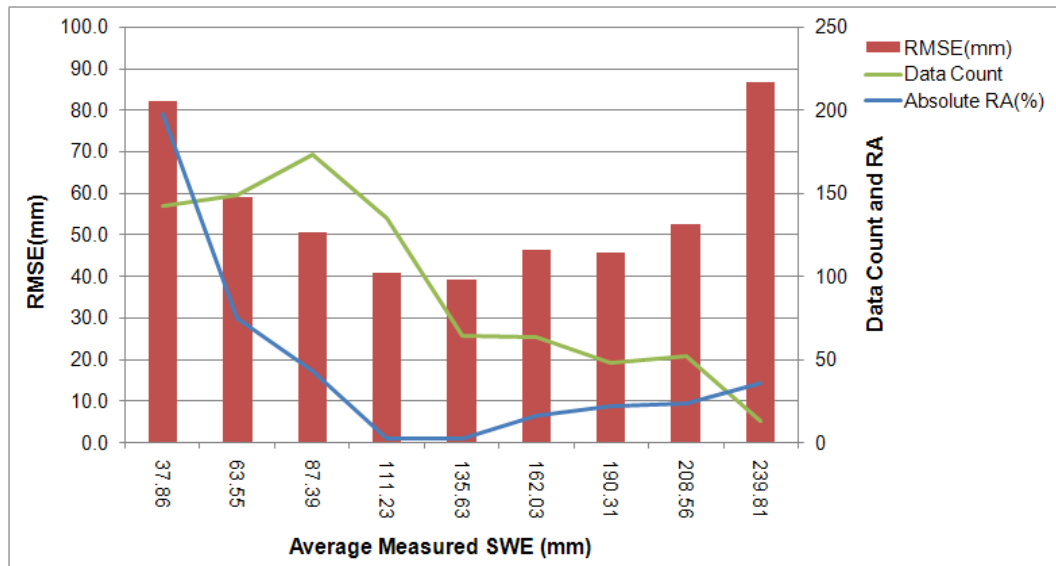


**Figure 4.21 Average measured SWE versus RMSE, absolute RA and data count.**

## CHAPTER 5

### DISCUSSION OF THE RESULTS

#### 5.1 Fine Tuning of SWE Retrieval Methodology

Validation results of SWE retrieval methodology was discussed and summarized in Table 4.7 and 4.11 in Chapter 4.3.3. It is apparent that proposed methodology validation results are less satisfactory for SWE smaller than 75.0 mm and greater than 200.0 mm.

Validation results were summarized regarding elevation ranges of reference stations for SD and SWE in Table 5.1 and Table 5.2 respectively. Elevation of stations versus RMSE, data count and absolute RA were depicted for SD and SWE in Figure 5.1 and Figure 5.2 respectively. It is obvious that RMSE and RA increase for stations that are located below 2000 m elevation. The developed methodology overestimates SWE and SD values especially for stations that are below 1750.0 m elevation. On the other hand developed methodology underestimate SD and SWE for stations located above 1750 m elevation. Underestimation amount for stations located in between 1750 m and 2500 m can be neglected regarding average of measured and calculated values.

The maximum penetration depth at 19.35 GHz can exceed 1 m, where, at 37 GHz, it generally does not exceed 0.6–0.8 m, depending on snow conditions (Tedesco, 2003). Microwave signal saturation at SWE values above 150 mm is also reported in literature (Dong et al., 2005; Derksen,



2008; Schanda et al., 1983). The saturation leads to underestimated SWE and SD levels for dense snow packs. (Pulliainen ,2006). Therefore improvement of developed methodology for SWE greater than 200 mm seems not possible with available sensors.

**Table 5.1 Comparison of measured and calculated SD values of 2008, 2009 and 2010 regarding reference station elevations.**

<b>Elev. Range m</b>	<b>Meas. SD m</b>	<b>Calc. SD m</b>	<b>Stand. Dev. m</b>	<b>Data Count</b>	<b>Station Count</b>	<b>RA %</b>	<b>RMSE m</b>
750-1000	0.13	0.30	0.05	2	2	130.77	0.1803
1000-1250	0.23	0.41	0.15	71	5	76.60	0.2333
1250-1500	0.28	0.43	0.12	260	5	49.62	0.2300
1500-1750	0.37	0.49	0.12	75	3	32.96	0.2154
1750-2000	0.51	0.49	0.13	98	6	-4.13	0.2030
2000-2250	0.49	0.48	0.14	243	9	-1.95	0.1777
2250-2500	0.44	0.43	0.12	65	2	-1.82	0.1527
2500-2750	0.81	0.60	0.05	25	1	-25.31	0.2169

**Table 5.2 Comparison of measured and calculated SWE values of 2008, 2009 and 2010 regarding reference station elevations.**

<b>Elev. Range m</b>	<b>Meas. SWE mm</b>	<b>Calc. SWE mm</b>	<b>Stand. Dev. mm</b>	<b>Data Count</b>	<b>Station Count</b>	<b>RA %</b>	<b>RMSE mm</b>
750-1000	33.70	83.13	13.95	2	2	146.68	51.7311
1000-1250	60.41	111.84	40.89	71	5	85.14	65.1697
1250-1500	73.85	115.72	33.85	260	5	56.71	63.8732
1500-1750	96.05	131.40	36.08	75	3	36.80	61.0787
1750-2000	133.35	131.85	36.91	98	6	-1.13	56.2128
2000-2250	126.39	127.30	37.69	243	9	0.72	48.9306
2250-2500	113.29	114.32	35.17	65	2	0.91	43.4532
2500-2750	202.30	158.91	12.99	25	1	-21.45	48.3687

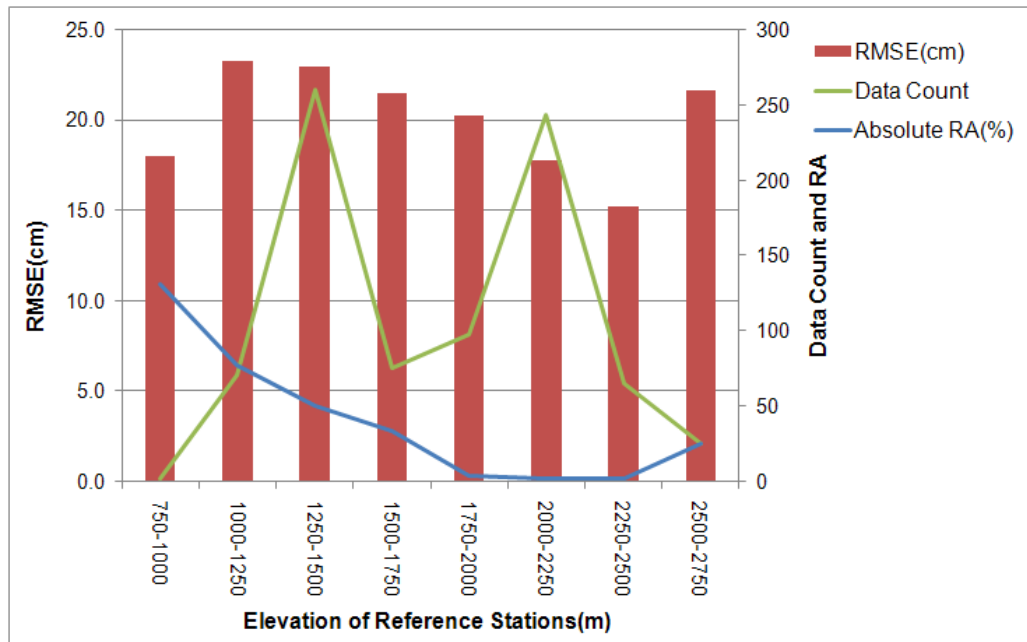


**Figure 5.1 Elevation of reference stations versus RMSE, absolute RA and data count for calculated SD.**

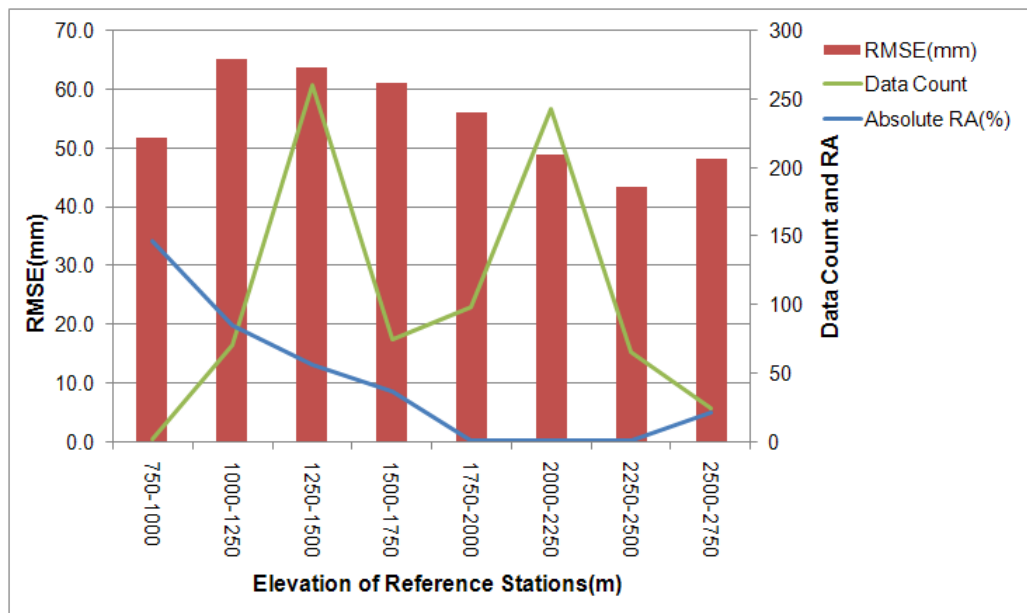


**Figure 5.2 Elevation of reference stations versus RMSE, absolute RA and data count for calculated SWE.**

Validation results indicate developed methodology based on HUT model overestimate SWE and SD for stations that are below 1750 m elevation. Hence, developed methodology should be modified to improve its performance for shallow snow depths measured at stations below 1750 m elevation. Therefore fine tuning of developed SWE retrieval methodology was done for pixels whose median elevation was below 1750 m elevation. Proposed modification approach was based on Kelly (2007) algorithm which is given in equation (5.1).

$$SD = \frac{(Tb_{10.65V} - Tb_{36.5V})}{\log(Tb_{36.5V} - Tb_{36.5H})} + \frac{(Tb_{10.65V} - Tb_{18.7V})}{\log(Tb_{18.7V} - Tb_{18.7H})} \quad (5.1)$$

where Tb is brightness temperature and subindices denote the channels.

SWE was calculated by multiplying SD with monthly average density values. Average density values based on measured values for January and February was 0.25 g/cm<sup>3</sup> and 0.27 g/cm<sup>3</sup> respectively.

Revised SWE retrieval methodology process flow chart is given in Figure 5.3. For each AMSR-E pixel in the selected domain median elevation of that pixel was checked against 1750 m elevation. If the pixel median elevation was greater than 1750 m then developed methodology based on HUT model was applied. Otherwise equation introduced in (5.1) was applied to calculate SD. SWE was calculated by multiplying SD with average monthly density values.

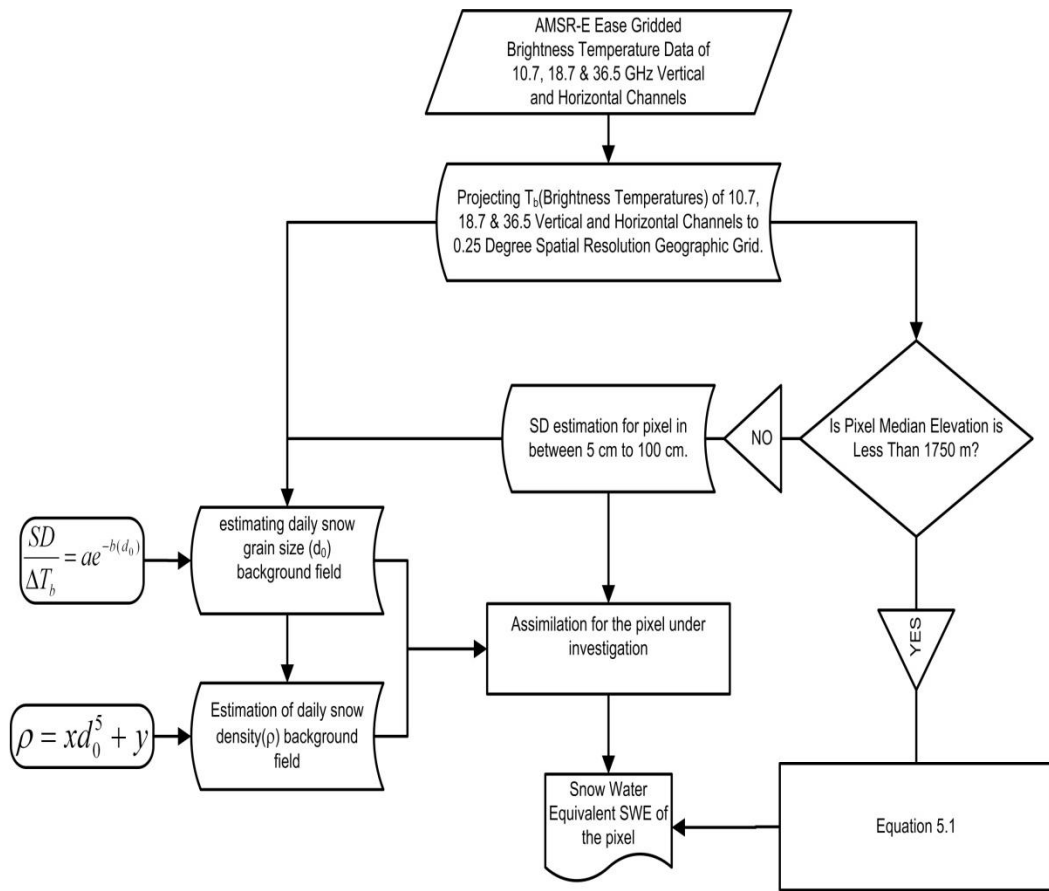


**Figure 5.3 Process flow chart of fine tuned developed methodology**

## 5.2 Validation Results of Fine Tuned Methodology

Validation studies of fine tuned developed methodology was performed with data set and methodology defined in Chapter 4.3. Summary of comparison of in-situ measured SD with re-calculated SD for all data set is given in Table 5.3. Overall RMSE of the data set was 17.38 cm which was 20.39 cm before fine tuning of the methodology. Average measured SD versus average re-calculated SD is plotted in Figure 5.4. Fine tuned algorithm decreased overall RMSE, while RMSE for SD in between 0.40 m to 0.70 m increased from 15.81 to 22.08 cm. Summary table of obtained

results grouped according to station elevation range is given in Table 5.4. Elevation range of stations versus RMSE, data count and absolute RA is plotted in Figure 5.5. The improvement of RMSE for stations located below 1750 m elevation is very obvious when Table 5.1 and Table 5.4 are compared.

**Table 5.3 Comparison of measured and re-calculated SD of 2008, 2009 and 2010.**

<b>Range m</b>	<b>Meas. SD m</b>	<b>Calc. SD m</b>	<b>Stand. Dev. m</b>	<b>Data Count</b>	<b>RA %</b>	<b>RMSE m</b>
0.10-0.20	0.15	0.25	0.09	144	65.22	0.1360
0.21-0.30	0.26	0.26	0.11	169	3.05	0.1113
0.31-0.40	0.35	0.38	0.15	161	8.52	0.1513
0.41-0.50	0.44	0.35	0.16	136	-19.07	0.1783
0.51-0.60	0.55	0.40	0.17	79	-27.69	0.2337
0.61-0.70	0.65	0.46	0.16	50	-29.31	0.2505
0.70-0.80	0.74	0.57	0.05	49	-22.92	0.1797
0.81-0.90	0.83	0.60	0.07	42	-27.19	0.2353
0.91-1.00	0.95	0.59	0.03	8	-37.90	0.3632

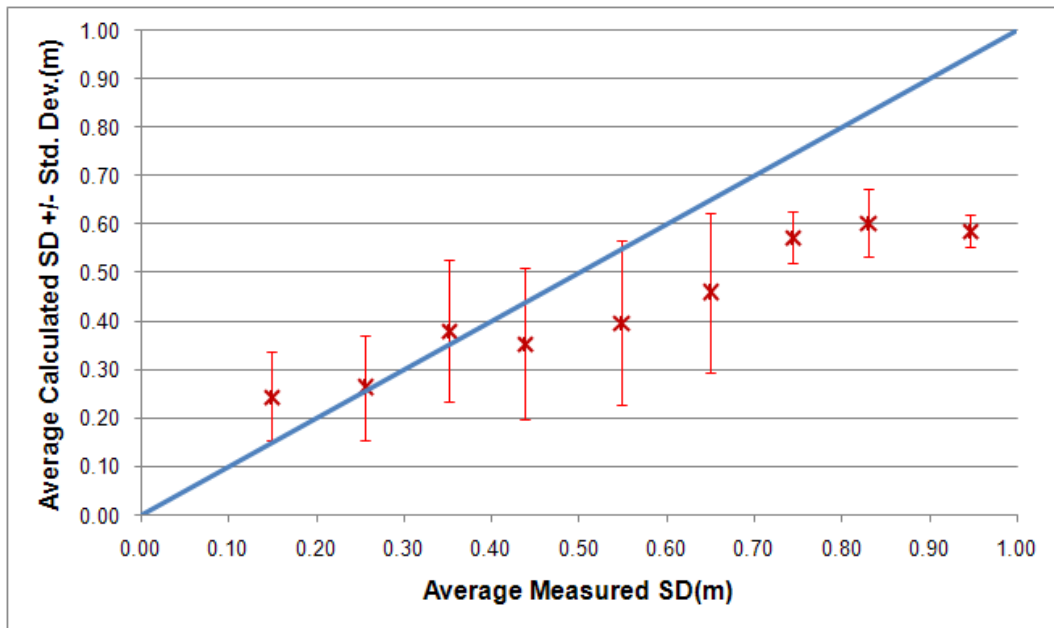


**Figure 5.4 Average re-calculated SD versus average measured SD of 2008, 2009 and 2010**

**Table 5.4 Comparison of measured and re-calculated SD values of 2008, 2009 and 2010 regarding reference station elevations**

Elev. Range m	Meas. SD m	Calc. SD m	Stand. Dev. m	Data Count	Station Count	RA %	RMSE m
750-1000	0.13	0.13	0.02	2	2	1.34	0.0256
1000-1250	0.23	0.21	0.07	71	5	-8.71	0.1115
1250-1500	0.28	0.24	0.08	260	5	-16.02	0.1663
1500-1750	0.37	0.24	0.07	75	3	-36.07	0.2059
1750-2000	0.51	0.49	0.13	98	6	-5.35	0.1951
2000-2250	0.49	0.48	0.14	243	9	-1.95	0.1777
2250-2500	0.44	0.43	0.12	65	2	-1.82	0.1527
2500-2750	0.81	0.60	0.05	25	1	-25.31	0.2169

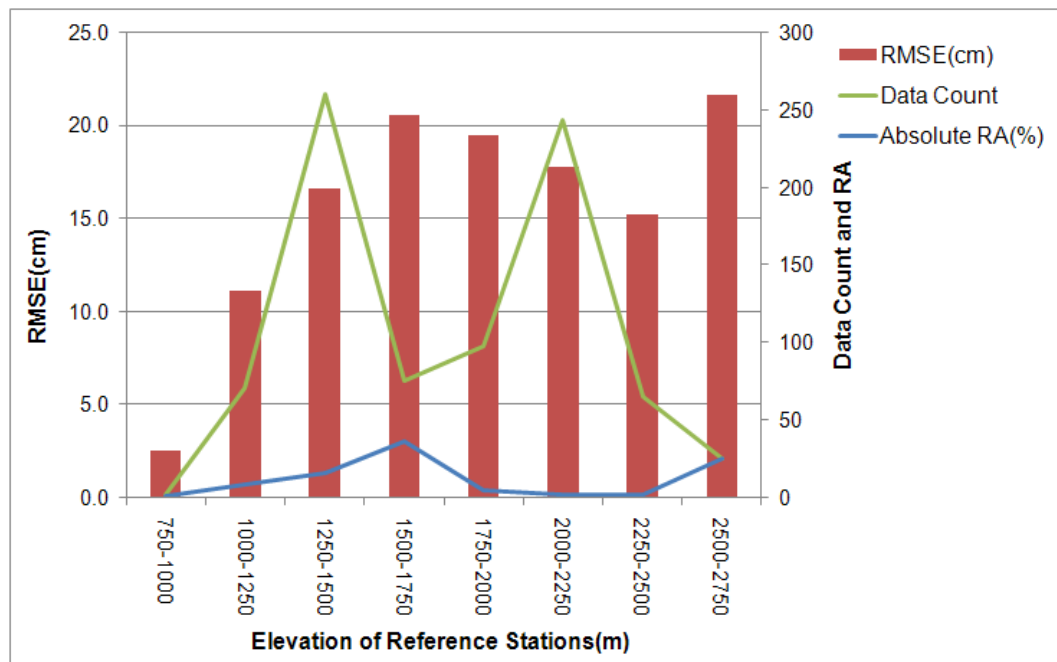


**Figure 5.5 Elevation of reference stations versus RMSE, absolute RA and data count for re-calculated SD.**

Summary of comparison of in-situ measured SWE with re-calculated SWE for all data set is given in Table 5.5. Overall RMSE of the data set was 46.92 mm which was 56.94 mm before fine tuning of the methodology. Average measured SWE versus average re-calculated SWE is plotted in Figure 5.6. While the fine tuned algorithm decreased overall RMSE, RMSE for SWE in between 100 mm to 200 mm increased from 42.95 to 57.80 mm. Summary table of obtained result grouped according to reference station elevation range is given in Table 5.6. Elevation range of stations versus RMSE, data count and absolute RA is plotted in Figure 5.7. The improvement of RMSE for stations located below 1750 m elevation is very obvious when Table 5.2 and Table 5.6 are compared.

**Table 5.5 Comparison of measured and re-calculated SWE of 2008, 2009 and 2010.**

Range mm	Meas. SWE mm	Calc. SWE mm	Stand. Dev. mm	Data Count	RA %	RMSE mm
25-50	37.86	61.85	24.82	142	63.38	34.8901
50-75	63.55	66.46	29.48	149	4.59	29.9909
75-100	87.39	96.61	41.55	173	10.55	42.5754
100-125	111.23	91.36	43.10	135	-17.87	47.8851
125-150	135.63	112.01	47.66	64	-17.41	54.8067
150-175	162.03	106.56	48.19	63	-34.23	73.0695
175-200	190.31	142.28	31.02	48	-25.24	55.4439
200-225	208.56	159.48	17.47	52	-23.53	52.4732
>225	239.81	154.16	7.12	13	-35.71	86.7467

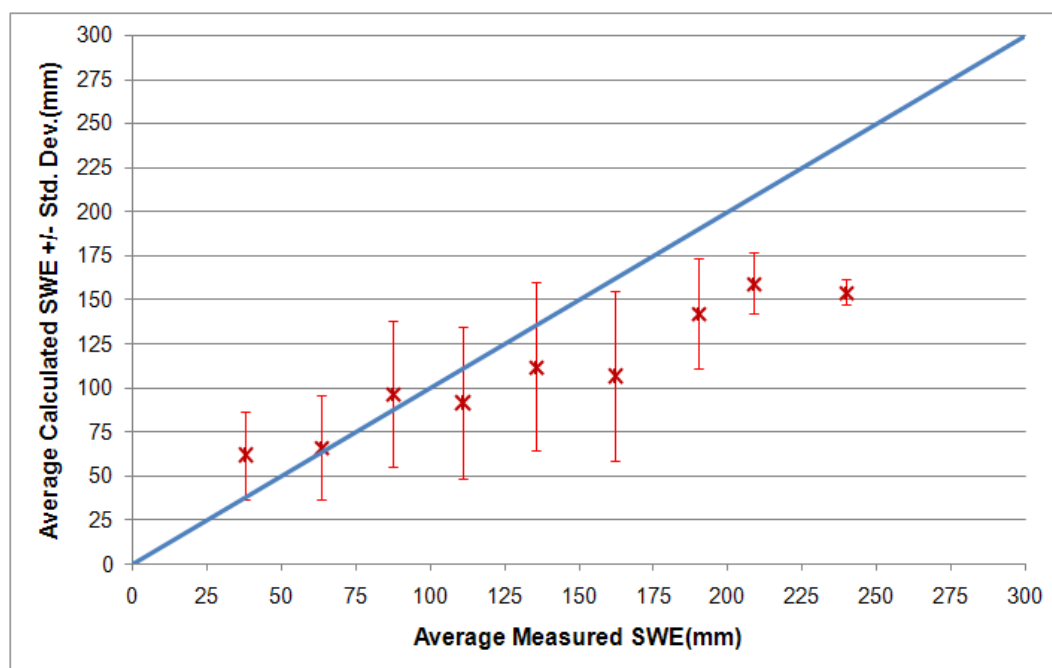


**Figure 5.6 Average re-calculated SWE versus average measured SWE of 2008, 2009 and 2010**



**Table 5.6 Comparison of measured and re-calculated SWE values of 2008, 2009 and 2010 regarding reference station elevations**

Elev. Range m	Meas. SWE mm	Calc. SWE mm	Stand. Dev. mm	Data Count	Station Count	RA %	RMSE mm
750-1000	33.70	32.67	3.87	2	2	-3.05	5.2667
1000-1250	60.41	52.46	18.03	71	5	-13.16	29.1608
1250-1500	73.85	59.35	20.49	260	5	-19.64	43.5566
1500-1750	96.05	59.05	19.43	75	3	-38.53	56.8657
1750-2000	133.35	130.15	38.00	98	6	-2.40	54.2059
2000-2250	126.39	127.30	37.69	243	9	0.72	48.9306
2250-2500	113.29	114.32	35.17	65	2	0.91	43.4532
2500-2750	202.30	158.91	12.99	25	1	-21.45	48.3687

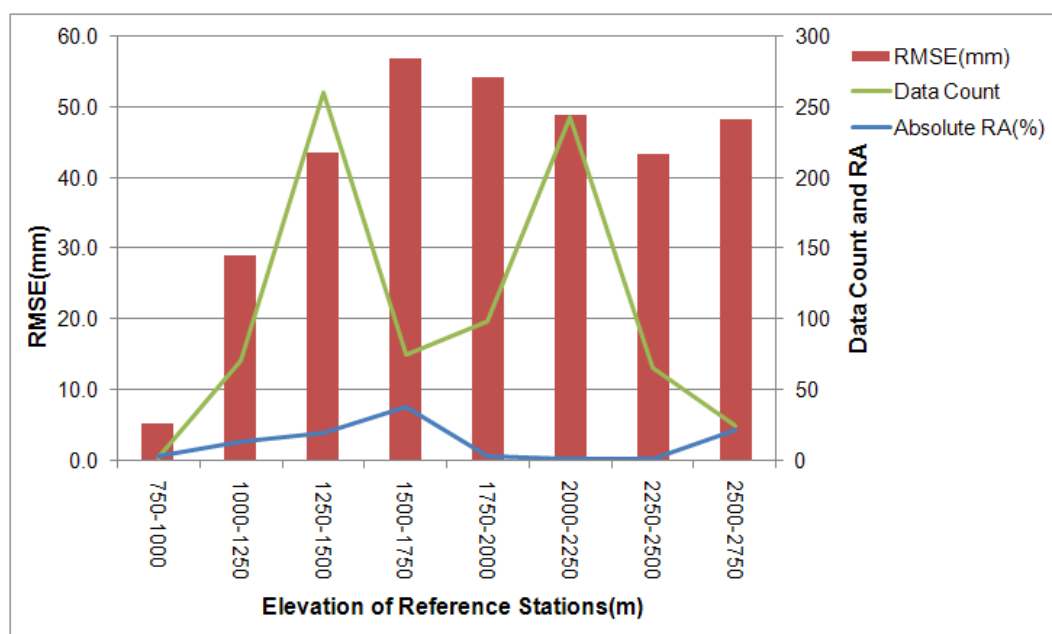


**Figure 5.7 Elevation of reference stations versus RMSE, absolute RA and data count for re-calculated SWE.**

The summary statistics of SD and SWE retrieval algorithms are tabulated and compared in Table 5.7 and Table 5.8 respectively. In these tables method based on HUT model, Kelly (2007) based approach and method

blending both technique are displayed. Developed fine tuned method improves RMSE, mean error and bias of both methods. Kelly approach underestimates SD and SWE while HUT model overestimates. Blended model bias indicates an underestimation considering overall data set. Insertion of Kelly method inside developed methodology based on HUT improves all error indicators including RMSE, mean error and bias considering all data set.

**Table 5.7 Test results summary of SD retrieval algorithms.**

	Measured	HUT	Kelly(2007)	HUT+Kelly(2007)
Mean (mm)	0.40	0.46	0.25	0.36
Standard Deviation (mm)	0.13	0.13	0.08	0.17
Minimum (mm)	0.10	0.10	0.09	0.09
Maximum (mm)	0.80	0.80	0.96	0.70
RMSE(mm)	-	0.21	0.24	0.17
Mean Error(mm)	-	0.17	0.19	0.14
Bias(mm)	-	0.06	-0.15	-0.04

**Table 5.8 Test results summary of SWE retrieval algorithms.**

	Measured	HUT	Kelly(2007)	HUT+Kelly(2007)
Mean (mm)	103.65	123.13	62.67	93.85
Standard Deviation (mm)	53.51	37.15	21.06	46.26
Minimum (mm)	25.00	18.14	21.91	21.91
Maximum (mm)	270.00	217.39	238.69	209.81
RMSE(mm)	-	56.94	64.45	46.92
Mean Error(mm)	-	48.54	49.71	38.10
Bias(mm)	-	19.48	-40.98	-9.80

## CHAPTER 6

### CONCLUSIONS AND RECOMMENDATIONS

In this thesis, the problems of modeling the electromagnetic microwave emission from dry snow covered mountainous terrain to calculate SWE by using passive microwave data have been discussed. A comprehensive review of the state of the art of the snow microwave emission has been given. The characteristics of HUT emission model have been analyzed in-depth and discussed with respects to the extinction coefficient function. A new extinction coefficient function for the HUT model has been proposed to suit model for snow over mountainous areas. Performance of the modified model have been checked against original and other modified cases against ground truth data covering 2003-2007 winter period. A methodology to calculate daily SWE products using AMSR-E data by modified HUT model was introduced and described in details. A new approach to calculate grain size and density was integrated inside proposed methodology. In order to check and test the performances of the developed methodology, an extensive validation has been successfully carried out by means of snow data measured at ground stations. It has been notified that proposed methodology validation results were less satisfactory for SWE smaller than 75.0 mm and greater than 200.0 mm. Overestimation is especially observed for stations located below 1750.0 m elevation where SWE is less than 75.0 mm. Applied methodology has been fine tuned to improve its performance for shallow snow depths measured at stations below 1750 m elevation using a relationship developed by Kelly (2007). Insertion of Kelly's approach inside developed methodology based on HUT improved all error indicators including RMSE, mean error and bias considering all validation data set. But an

underestimation for SWE values greater than 150 mm could not be resolved by discussed methods because of the passive microwave signal saturation that is observed for dense snowpack.

Consequently, a data assimilation model based on HUT emission model for mountainous areas to produce daily SWE or SD map has been developed and tested. Error statistics (RMSE and ARA) of the proposed methodology were promising compared with other studies. Based on the experience gained during this study, following recommendations can be given to be guidelines for future studies:

- HUT emission model can be used to calculate SD or SWE values over mountainous areas with modifying original extinction coefficient relationship which is dependent on grain size. But, an empirical relationship to calculate grain size dynamically without using ground data should be developed.
- Integration of 10.7 GHz channel to data assimilation schema should be evaluated especially for deep and shallow snow situations where error amounts were highest inside developed methodologies.
- New approaches for dynamic calculation of snow density should be investigated. In this study density was only related to grain size on monthly bases. But proposed equation can be also modified during accumulation stage by considering snow depth with smaller time periods (weeks).
- Snow status algorithm that is used in this study classifies snow as dry or wet. Snow status approach should be re-evaluated by considering diurnal amplitude variations. Diurnal oscillations of  $T_b$  indicate surface melt and freeze cycles in dynamic transition periods. Therefore snow status determination algorithms should also detect whether snow has undergone a metamorphism process due to melt and freeze cycles.

- Topographical effects on microwave brightness temperature should be studied in details on mountainous areas.
- Downscaling of SWE products by aid of Fractional Snow Cover Area (FSCA) products should be investigated.
- Validation studies of the SWE and SD products should be coupled with spatially distributed hydrological model outputs including runoff discharge comparisons.
- Data assimilation schema can be improved by integration of a snow hydrology model where grain size can be obtained.
- There should be more and densely located ground stations at different elevations in order to get more accurate SWE values. More spatially well distributed ground true SWE data brings more accurate satellite derived SWE values.
- Multi-layer snowpack emission models usage that takes into consideration of depth, density and grain size of each layer should be investigated.
- Wet snow problem can be solved using scatterometer data.

## REFERENCES

1. Akyürek Z., 1998, Some application of satellite remote sensing to environmental monitoring in Turkey, PhD. Thesis, Department of Civil Engineering, Middle East Technical University.
2. Armstrong R. L., Chang R; A., Rango A., and Josberger E., 1993, Snow depths and grain-size relationships with relevance for passive microwave studies, *Annals of Glaciology*. 17: pp. 171-176.
3. Aschbacher, J., 1989, Land surface studies and atmospheric effects by satellite microwave radiometry, Ph.D. Thesis, University of Innsbruck.
4. Brogioni M., 2008, Modeling microwave emission from snow covered soil, PhD. Thesis, Pisa University
5. Butt M. J. and Kelly R. E. J, 2008, Estimation of snow depth in the UK using the HUT snow emission model, *International Journal of Remote Sensing*, 29(14), pp. 4249-4267
6. Carsey F. D., 1992, Remote Sensing of Sea Ice, American Geophysical Union, pp. 30.
7. Chang A. T. C., Foster J. L. and Hall D. K., 1987, Nimbus 7 SMMR derived global snow cover patterns, *Ann. Glacial.*, vol. 9, pp. 39–44.
8. Derksen C., 2008, The contribution of AMSR-E 18.7 and 10.7 GHz measurements to improved boreal forest snow water equivalent retrievals, *Remote Sensing of Environment*, 112, pp. 2702
9. Dong J., Walker J.P., Houser P.R., 2005, Factors affecting remotely sensed snow water equivalent uncertainty, *Remote Sensing of Environment*, 97, pp. 68-82

10. Foster J.L., Chang A.T.C., Hall D.K., and Rango A., 1991, Derivation of snow water equivalent in boreal forests using microwave radiometry. *Arctic*, 44(1), pp. 147-152.
11. Foster J.L., Chang A. T. C. and Hall D., 1997, Comparison of snow mass estimates from a prototype passive microwave snow algorithm, a revised algorithm and a snow depth climatology, *Remote Sensing of Environment*, vol. 62, no. 2, pp. 132–142.
12. Foster J.L., Sun C. J., Walker J. P., Kelly R., Chang A., Dong J., Powell H., 2005, Quantifying the uncertainty in passive microwave snow water equivalent observations, *Remote Sensing of Environment*, vol. 94, no. 2, pp. 187– 203.
13. Gökdemir O., 2009, MSG-SEVIRI Uydu Görüntüleri ile Dağlık Alanlarda Kar Örtüsünün Gerçek Zamanlı Olarak Belirlenmesi ve Doğrulanması, PhD. Thesis, Department of Hydrogeology Engineering, Hacettepe University.
14. Grody, N.C., 1991, Classification of snow cover and precipitation using the Special Sensor Microwave Imager, *Journal of Geophysical Research*, 96, 7423-7435.
15. Grody N.C., and Basist A.N., 1996, Global identification of snowcover using SSM/I measurements, *IEEE Transactions on Geoscience and Remote Sensing*, 34(1), pp. 237-249.
16. Hall, D.K., Kelly, R.E.J, Riggs, G.A, Chang, A.T.C, and Foster, J.L. 2002, Assessment of the relative accuracy of hemispheric-scale snow-cover maps., *Annals of Glaciology*, 34:24–30.
17. Hallikainen M. T., Ulaby F., and Abdelrazik M.,1986, Dielectric properties of snow in the 3 to 37 GHz range, *IEEE Transaction on Antennas Propagation*., vol. AP-34, pp. 1329–1340.

18. Hallikainen M., Ulaby F.T. and Deventer T., 1987, Extinction behavior of dry snow in the 18- to 90-GHz range, *IEEE Transaction on Geoscience and Remote Sensing*, GE-25(6), pp. 737–745.
19. Hallikainen M.T. and Jolma, P.A., 1992, Comparison of algorithms for retrieval of snow water equivalent from Nimbus-7 SMMR data in Finland, *IEEE Transactions on Geoscience and Remote Sensing*, 30(1), pp.124-131
20. Hallikainen M.T., Halme P., Takala M., and Pulliainen J., 2003, Combined active and passive microwave remote sensing of snow in Finland, *Proceedings of IEEE Transaction on Geoscience and Remote Sensing Symposium, IGARSS 2003 IEEE International Volume 2*, pp. 830 – 832
21. Ishimaru A., 1978, *Wave Propagation and Scattering in Random Media*, New York: Academic, vols. I/II
22. Kelly R., Chang A. T., Tsang L, Foster J. L., 2003, A prototype AMSR-E global snow area and snow depth algorithm, *IEEE Transaction on Geoscience and Remote Sensing*, vol. 41, no. 2, pp. 230–242.
23. Kelly R., 2007, AMSR-E SWE products: status, AMSR-E Science Team Meeting Missoula, Montana, 14-16 August.
24. Matzler C., Schanda E., and Good W., 1982, Towards the definition of optimum sensor definition specification for microwave remote sensing of snow, *IEEE Transaction on Geoscience and Remote Sensing*, GE-20, pp. 57-66
25. Matzler C., 1987, Applications of the interaction of microwaves with the natural snow cover, *Remote Sensing Reviews*, 2, pp. 259–387.
26. Matzler C. and Wiesmann A., 1999, Extension of the microwave emission model of layered snowpacks to coarse-grained snow, *Remote Sensing of Environment*, 70, pp. 317–325



27. Oh Y., Sarabandi K. and Ulaby F.T., 1992, An empirical model and an inversion technique for radar scattering from bare soil surfaces, *IEEE Transactions on Geoscience and Remote Sensing*, 30(2), pp. 370-381
28. Pulliainen J., Karna, J. P. and Hallikainen, M., 1993, Development of geophysical retrieval algorithms for the MIMR. *IEEE Transactions on Geoscience and Remote Sensing*, 31, 268 -277
29. Pulliainen J. T., Grandell J. and Hallikainen M.,1999, TKK snow emission model and its applicability to snow water equivalent retrieval, *IEEE Transactions on Geoscience and Remote Sensing*, 37(3), pp. 1378–1390
30. Pulliainen J. and Hallikainen M. ,2001, Retrieval of Regional Snow Water Equivalent from Space-Borne Passive Microwave Observations, *Remote Sensing of Environment*, 75, pp. 76-85
31. Pulliainen J.,2006, Mapping of snow water equivalent and snow depth in boreal and sub-arctic zones by assimilating space-borne microwave radiometer data and ground-based observations, *Remote Sensing of Environment*, 101, pp. 257-269
32. Rees W. G., 2006, *Remote Sensing of Snow and Ice*, Taylor and Francis, pp. 47-50
33. Rott H., Nagler T., Aschbacher J., 1991, Algorithm development for monitoring global snow cover by spaceborne microwave radiometry, *Proc. 11th EARSeL Symp.*, 3-5 July 1991, Graz, Austria.
34. Roy, V., Goïta K., Royer A., Walker A. E., and Goodison B. E., 2004, Snow water equivalent retrieval in a Canadian boreal environment from microwave measurements using the TKK snow emission model, *IEEE Transaction .on Geoscience and RemoteSensing.*, 42(9), pp. 1850–1859

35. Schanda E., Matzler C., and Künzi K., 1983, Microwave remote sensing of snow cover, *Int. J. Remote Sensing*, 4, pp. 149-158.
36. Şensoy A., 2005, Physically based point snowmelt modeling and its distribution in upper Euphrates Basin, PhD. Thesis, Department of Civil Engineering, Middle East Technical University
37. Sorman A., 2005, Use of satellite observed seasonal snow cover in hydrological modeling and snowmelt runoff prediction in upper Euphrates Basin, PhD. Thesis, Department of Civil Engineering, Middle East Technical University
38. Stogryn A., 1986, A study of the microwave brightness temperature of snow from the point of view of strong fluctuation theory, *IEEE Transaction on Geoscience. and Remote Sensing*, GE-24(2), pp. 220–231
39. Sturm M., Holmgren J., Liston G. E., 1995, A seasonal snow cover classification system for local to global applications, *Journal of Climatology.*, vol. 8, no. 5, pp. 1261–1283
40. Sürer S., 2009, Real time snow cover mapping over mountainous areas of Europe using MSG-SEVIRI imagery, Msc Thesis, Department of Geodetic and Geographic Information Technologies, Middle East Technical University
41. Tateishi R., Zhu L., and Sato H.P., 2003 , The Land Cover Map for Central Asia for the Year 2000., GLC2000 database, European Commision Joint Research Centre.
42. Tedesco M.,2003, Microwave remote sensing of snow, Ph.D. Thesis ,Inst. Appl. Phys. 'Carrara', Italian Nat. Res. Council, Florence, Italy.
43. Tedesco M. and Kim E. J., 2006, Intercomparison of Electromagnetic Models for Passive Microwave Remote Sensing of Snow, *IEEE Transactions on Geoscience and Remote Sensing*, 44(10), pp. 2654.

44. Tsang L., Kong J. A., and Shin R. T., 1985, Theory of Microwave Remote Sensing, Wiley
45. Ulaby F. T., and Stiles W. H., 1980, The active and passive microwave response to snow parameters, Part II: Water equivalent of dry snow, J. Geophys. Res., 85, pp. 1045-1049.
46. Ulaby F. T., Moore R. K., and Fung A.K., 1990, Microwave remote sensing from theory to application, Artech House Publications, Vol. 2, pp. 1602-1634.
47. Wiesman A. and Mätzler C., 1999, Microwave emission model of layered snowpacks, Remote Sensing of Environment, 70, pp. 307–316

## CURRICULUM VITAE

### PERSONAL INFORMATION

Surname, Name : Beşer, Özgür  
Nationality : Turkish (TC)  
Date and Place of Birth : 07 June 1976, Aydın  
Marital Status : Married  
Email : obeser@gmail.com  
Mobile Phone : 0 533 810 47 51

### EDUCATION

1995 - 1999 METU, Ankara  
BS, Civil Engineering Department  
1999 - 2002 METU, Ankara  
MSc, Civil Engineering Department  
2002-2011 METU, Ankara  
PhD, Civil Engineering Department

### WORK EXPERIENCE

Year	Place	Enrollment
1999 May	Tubitak Bilten	Software Engineer
1999 September	Ünal Construction Ltd	Design Engineer
2000 June	Intergraph Ltd	GIS Engineer
2000 September	Prokon Engineering	Design Engineer
2002 December	Turuncu Systems	Design Engineer
2004 January	YPA Engineering	Design Engineer
2006 December	Birim Engineering	Design Engineer
2008 January- Present	Beray Engineering	Design Engineer

## QUALIFICATIONS

**Programming Languages:** (c, c++, c#, java, visual basic, asp.net, matlab, idl, fortran).

**GIS Software:** (Geomedia, Mapinfo, Arcgis, Idrisi, Envi, TNT Mips, Erdas).

**Cad Software:** (Autocad, Microstation, Netcad).

**Engineering Software:** (Haestad Methods, HEC-RAS, HEC-HMS, Eagle Point, Inroads).

## PUBLICATIONS

- Şorman A.Ü., **Beşer Ö.**, 2008, Determination of Snow Water Equivalent Over Mountainous Areas Using Microwave Satellite Images in Türkiye, *8th International Congress on Advances in Civil Engineering*.
- Sürer S. Gökdemir O., Akyürek Z., Şorman A.Ü., **Beşer Ö.**, 2008, Real time snow recognition from MSG satellite for mountainous areas, *düzeltilme, EARSeLe Proceedings*.
- Sürer S. Gökdemir O., Akyürek Z., Şorman A.Ü., **Beşer Ö.**, 2009, MSG-SEVIRI verisi kullanılarak Avrupa üzerindeki dağlık alanlarda gerçek zamanlı kar kaplı alanürünü üretilmesi, Erzurum 3. Kar Kongresi.
- Akyurek, Z., Surer, S. and Beser, Ö. (2011), Investigation of the snow-cover dynamics in the Upper Euphrates Basin of Turkey using remotely sensed snow-cover products and hydrometeorological data. *Hydrological Processes*. doi:10.1002/hyp.8090

## RESEARCH AND DEVELOPMENT PROJECTS

TÜBİTAK 1507 Teydeb Project – National Satellite Based Data Archive Project – NASABADA (Software and Product Development Director) 2009-2011, [www.nasabada.com](http://www.nasabada.com)